HIGH-THROUGHPUT, CONTINUOUS NANOPATTERNING TECHNOLOGIES FOR DISPLAY AND ENERGY APPLICATIONS

by

Se Hyun Ahn

A dissertation submitted in partial fulfillment
of the requirements for the degree of
Doctor of Philosophy
(Mechanical Engineering)
in The University of Michigan
2010

Doctoral Committee:

Associate Professor L Jay Guo, Co-Chair
Associate Professor Katsuo Kurabayashi, Co-Chair
Associate Professor Jinsang Kim
Assistant Professor Kevin Patrick Pipe

© Se Hyun Ahn

2010

To my family: Your love and dedication made this possible

Acknowledgements

It is a great pleasure to thank those who made this thesis possible. First and foremost, I would like to show my gratitude to my advisor, Prof. L. Jay Guo, who has supported me throughout Ph. D study with his patience, encouragement and guidance. Without his supports, this thesis would not have been possible, and I can not thank him enough for what he has done for me in the past five years.

I would like to appreciate my co-advisor, Prof. Katsuo Kurabayash, who has provided me many kind advices on my research.

I am also highly thankful to my committee members, Prof. Jinsang Kim, Prof. Kevin Pipe for their valuable suggestions throughout this study.

I would like to acknowledge all current and past nanogroup members, Dr. Philip Choi, Brandon, Dr. Myung-Gyu Kang, Dr. Carlos Pina-Hernandez, Tao, Yi-Hao, Sung-Liang, Hyoung Won, Abram, Hui Joon, Yazeed, Alex, Yi-Kuei, Jong Girl, Liangjin, Dr. Shi, Ting, Mihee, Dr. Jin-Sung Kim, Dr. Chung-Yen Chao, Prof. Dawen Li and Dr. Larry Cheng for their kindness and help for my study. I would also like to acknowledge the staff and student members of Lurie Nanofabrication Facility and Solid State Laboratory for their kind help during my study. It was a great luck for me to work with wonderful facility and people.

I am greatly indebted to my parents for their love and supports throughout my life. I also wish to thank my wife, Young Hee for her love and sacrifice; and my beloved

daughter, Kristin. Without my family's love and dedication, this thesis would not have been possible.

Lastly, I offer my regards and blessings to all of those who supported me in any respect during the completion of Ph. D study.

Table of Contents

Dedication .... **ii**

Acknowledgements .... **iii**

List of Figures .... **ix**

List of Tables .... **xv**

Abstract .... **xvi**

Chapter 1. Introduction **1**

1.1 Nanogratings and their applications **2**

1.1.1 Optical and electrical applications 2

1.1.2 Bio-sensor applications 2

1.1.3 Other various applications 3

1.2 Nanofabrication technologies for nanogratings **3**

1.2.1 Nanoimprint lithography 3

1.2.2 Other nanopatterning technologies 5

1.3 Goal of research **7**

1.4 Organization of thesis **8**

Chapter 2. High-Speed Roll-to-Roll Nanoimprint Lithography on Flexible Plastic Substrates **9**

2.1 Introduction **9**

2.2 Experimental details **11**

2.2.1 Material requirements for high-speed R2RNIL 11

2.2.2 R2RNIL apparatus (Model I) for thermal and UV imprinting 13

2.2.3 Method 17

2.3 Results and discussion **20**

2.4 Fabrication of metal wire-grid polarizers as an application of R2RNIL **24**

2.4.1 Introduction to metal wire-grid polarizers 24
2.4.2 Fabrication of metal wire-grid polarizers by R2RNIL..... 25
2.5 Summary..... 26

Chapter 3. Scaled-up Roll-to-Roll / Roll-to-Plate Nanoimprint Lithography for Large-Area Nanopatterning 28
3.1 Introduction..... 28
3.2 Experimental details 30
3.2.1 Design parameters for scaled-up R2RNIL apparatus 30
3.2.2 Scaled-up R2R/R2P NIL apparatus 31
3.3 Results and discussion 34
3.3.1 Large-area nanoimprinting by R2RNIL / R2PNIL..... 34
3.3.2 Analytical models for RLT estimation in R2RNIL 36
3.3.3 Mold separation analysis..... 41
3.3.3.1 Introduction..... 41
3.3.3.2 Theoretical background 42
3.3.3.3 Modeling and analysis 44
3.3.4 Large-area semi-transparent metal electrode for organic solar cell application 48
3.3.5 Roll-to-roll fabrication of morphology-optimized bulk heterojunction polymer solar cells 51
3.4 Summary..... 52

Chapter 4. Direct Metal Imprinting (DMI)..... 53
4.1 Introduction..... 53
4.2 Principle of DMI 54
4.3 Results and discussion 56
4.4 Summary..... 60

Chapter 5. Dynamic Nano-Inscribing for Continuous and Seamless Metal and Polymer Nanogratings..... 62
5.1 Introduction..... 62
5.2 Principle of DNI 63
5.3 Experimental details..... 66

5.4 Results and discussion 67
5.4.1 DNI on metals 67
5.4.2 DNI on plastics 68
5.4.3 Localized heating assisted DNI (LH-DNI) 72
5.4.4 LH-DNI of functional materials 77
5.4.5 Fabrication of split-ring resonator (SRR) using DNI 79
5.5 Summary 81

Chapter 6. Continuous Formation of Nano-scale Periodic Patterns by Localized Dynamic Wrinkling 82
6.1 Introduction 82
6.2 Principle of LDW 84
6.3 Results and discussion 87
6.3.1 Large-area continuous grating generation by LDW 87
6.3.2 Controllable period and geometry in LDW patterning 88
6.3.3 Easy pattern transferring 94
6.3.4 High-speed patterning with constant period regardless of speed 95
6.3.5 Large-opening nanowires for semi-transparent metal electrode application ... 96
6.4 Summary 99

Chapter 7. Continuous Fabrication of Nanogratings with Real-Time Period Modulation using High-Frequency Sequential Indentations 100
7.1 Introduction 100
7.2 Principle of Dynamic Nano-Cutting (DNC) 102
7.3 Experimental details 103
7.4 Results and discussion 105
7.5 Summary 111

Chapter 8. Conclusion 112
8.1 Summary of thesis 112
8.2 Summary of specific achievements 115
8.3 Future works 117
8.3.1 Multiple-layer DNI 117

8.3.2 Nanowire/ nano particle fabrication by DNI 118
8.3.3 DNI on a free-curved surface 118
8.3.4 Pattern writing based on liquid DNI 120
8.3.5 Si mold fabrication using LDW process 121
8.3.6 LDW combined with DNI 122
Bibliography 124

List of Figures

Figure 1.1 The schematics of NIL. (a)Thermal NIL (b) UV NIL (S-FIL).......................... 4

Figure 2.1 A flexible ETFE mold fabricated from an original Si mold. The ETFE mold assembly is prepared as shown in (b) and attached to a 60 mm diameter stain steel roller. A soft cushion layer is placed between the ETFE mold assembly and the roller surface for conformal contact during imprinting... 12

Figure 2.2 Schematic of the R2RNIL process, and the continuous fabrication of metal wire grid polarizer as one of its applications (the metal deposition is carried out in a separate evaporator in this study). 14

Figure 2.3 (a) Photograph of R2RNIL apparatus (Model I). Inset shows operation system (backside). (b) The coating unit and (c) the Imprint unit of the R2RNIL apparatus. 16

Figure 2.4 Schematic of UV curing test of epoxysilicone. UV curable epoxysilicone resist is sandwiched by two sheets of PET film, as in the actual R2RNIL process. *H* is distance between the light source and the sample, and *D* is the diameter of fully solidified area after curing. 19

Figure 2.5 Thermal R2RNIL results: (a) Photograph of a 700 nm period, 300 nm line width PDMS grating pattern imprinted on PET strip by using the thermal R2RNIL and (b) the SEM micrograph of the replicated grating structure. UV R2RNIL results: (c), (d) Photographs of 700 nm period, 300 nm line width epoxysilicone grating pattern imprinted on PET strip by the UV R2RNIL, showing bright light diffraction and (e) the SEM of the replicated grating structure. Total length is 570 mm........... 21

Figure 2.6 (a) The original Si mold. (b), (c) the epoxysilicone gratings replicated from the ETFE mold. (d), (e) SEM pictures of 200 nm period, 70 nm line width epoxysilicone pattern and (f) a 100 nm period, 70 nm line width epoxysilicone pattern fabricated by UV R2RNIL.. 23

Figure 2.7 (a) Schematic of the metal wire grid polarizer by depositing metal on top of the roller imprinted polymer grating. (b) SEM picture of a 200 nm period grating with 50 nm Al on top. (c) Spectral transmittance (TM, TE mode) and extinction ratio (TM/TE) of metal wire-grid polarizer fabricated by R2RNIL................................. 26

Figure 3.1 Prototype design of R2R/R2P NIL (Model II) which enables 6” wide patterning. (a) Side view (b) Front view 31

Figure 3.2 Schematics of R2RNIL(a) and (b) R2PNIL process. (c) A Photograph of 6”-capable R2R/R2PNIL apparatus. 33

Figure 3.3 (a) A 4” wide, 12” long 700 nm period epoxysilicone patterns on flexible PET substrate by R2RNIL process and (b) a 4” wide, 10.5” long 700 nm period patterns on glass substrate. (c), (d) SEM images of the patterned grating structure. 35

Figure 3.4 Schematic diagram of the liquid resist being squeezed by the contact rollers in (a) *the solid plane squeeze model*, (b) *the elastic roller contact model* and (c) *the dynamic elastic roller contact model*. 38

Figure 3.5 The comparison of three models (Solid / Elastic / Dynamic model) for R2PNIL and experimental data (average value of three time measurement). (a) RLT as a function of web speed with keeping maximum rolling force, 220 N. (b) RLT as a function of maximum rolling force with keeping web speed, 7.94 mm/s. SEM images of (b): (c) 2.58 μm RLT for 50 N force, (d) 1.3 μm RLT for 180 N force, (e) 1.15 μm RLT for 240 N force. 40

Figure 3.6 Schematic of two different mold separation methods; (a) peeling parallel to the grating orientation and (b) peeling perpendicular to the grating orientation. Right pictures show that “peeling parallel to the grating orientation” provides better pattern quality for 200 nm period grating pattern. 42

Figure3.7 (a) Schematic illustration of imprinted system used in modeling and (b) the mold separation model 43

Figure 3.8 Schematic illustration of the perpendicular peeling method. 45

Figure 3.9 Energy release rate of each 4 step in the perpendicular peeling process when pulling force of 0.01 N is applied on 20 mm wide sample. (a) $\theta \leq 90°$ (b) $\theta \geq 90°$. Red line in each graph represents minimum energy release rate (46.1 mJ/m^2) required to successfully separate mold under the given force condition. 46

Figure 3.10 FEM illustration of stress distribution in the perpendicular peeling method. Stress is concentrated on each corner during the mold separation in which case the upper right corner is raised by 20 nm. 48

Figure 3.11 (a) Schematic of R2R NIL process. SEM images of (b) epoxysilicone mold and (c) transferred Au nanograting on PET substrate. (d) Photograph of large area (32 mm x 184 mm) Au nanogratings on PET substrate. Inset photograph shows the transparency of Au nanogratings fabricated. 50

Figure 3.12 (a) A photograph of the roll_to_roll apparatus and (b) the resultant flexible polymer solar cell before electrode deposition. 52

Figure 4.1 Schematics of Direct Metal Imprint (DMI) process. Optional metal transferring process to the second substrate can be done after DMI. 55

Figure 4.2 Figure 4.2 Effect of the modulus of polymer cushion layer on DMI patterning. (a) Polydimethylsiloxane (PDMS, E = 2.4 MPa), (b) Polyurethane (PU, E = 500 MPa), (c) Polycarbonate (PC, E = 2.0 GPa), (d) Poly(methyl methacrylate) (PMMA, E = 3.0 GPa) as a cushion layer, respectively. 50 nm thick gold is coated on each polymer layer on the Si substrate. 20 MPa pressure. 57

Figure 4.3 SEM images of the Si molds with different tip-geometries (a, b) and the resulting 700 nm period, 50 nm thick gold nano patterns by DMI (a-1, b-1) using each mold respectively. Applied pressure is 20 Mpa. (a-2, b-2) Finite element analysis supporting each DMI result under the same pressure condition but using different geometry of mold (a, b). 58

Figure 4.4 (a) Schematics of the space enlarging process, DMI followed by bending with heating. (b) SEM image of 700 nm period DMI pattern after space enlarging process showing 250 % increase in space (186 nm). 60

Figure 5.1 (a) Schematics of the DNI process for creating metal nano gratings. (1) Initial contacting point, (2) Gradual imprinting region, (3) Edge point responsible for plastic deformation and (4) Elastic recovery region. (b, c) SEM images of the Si molds with two different tip geometries (flat end, sharp tip) and the resulting silver nano gratings inscribed by each mold respectively. 65

Figure 5.2 (a) Experimental setup for DNI. (b) Inscription part composed of heater attached tool holder, thermocouple and force sensor. (c) Temperature controller and web speed controller 66

Figure 5.3 SEM images of (a) continuous 200 nm period gold gratings by DNI with sharp turns, (b) Square shaped gold nanopatterns fabricated by two sequential DNIs in orthogonal directions, and (c) 700 nm period grating directly fabricated on ITO surface. 68

Figure 5.4 (a) A 22 inch long, half inch wide, 700 nm period, continuous nano-grating pattern directly created on a polycarbonate strip by roll-to-roll DNI process and (b) its SEM image. (c) Concentric nano-gratings on ethylene-tetrafluoroethylene (ETFE) film fabricated by a rotating DNI process. Outer diameter is 2 inch. (d) 700 nm period gratings inscribed in crosslinked photoresist SU8 on curved surfaces. (e) A 46 mm by 88 mm, large area 700 nm period grating pattern on ETFE film fabricated by DNI. 70

Figure 5.5 (a) Micro/nano combined structure fabricated by single step DNI process. (b) Micro scale bumps having ideally smooth top surface fabricated by DNI. 71

Figure 5.6 (a) A schematic of the localized heating assisted DNI (LH-DNI) process. (b) Inscribed depth in the polycarbonate film versus temperature. (c) 700 nm period polycarbonate gratings fabricated by room-temperature DNI (RT-DNI). (d) The polycarbonate sample fabricated at 140 °C showing sharper and more faithful pattern formation. The inset (e) shows the deep Si mold used to produce (c) and (d). (f) RT-DNI and (g) LH-DNI (140 °C) on polycarbonate using a low aspect-ratio (1:1, 150 nm thick), 500 nm period Si mold (h).. 74

Figure 5.7 (a) Inscribed depth corresponding to the web speed for RT_DNI (20 °C) and LH_DNI (140 °C). (b) Simplified heat transfer model for LH_DNI. (c) The temperature distribution from (b) corresponding to the web speed and measured point. In this plot, the surface temperature (T_s) is 140 °C and the initial temperature (T_i) is 20 °C. 76

Figure 5.8 700 nm period gratings created by LH_DNI on (a) conductive polymer PEDOT and (b) semiconducting polymer P3HT coated on PET substrate (90 °C) and their corresponding AFM images shown in the insets, respectively. (c) 700 nm period gratings generated on proton exchange polymer, Nafion by LH-DNI (80 °C). 78

Figure 5.9 (a) 200 nm period silver gratings fabricated by DNI. 20 nm thick silver is thermally deposited on polycarbonate film and simply inscribed using a 200 nm period Si mold. (b) Transmittance spectra of sample (a) showing valleys at 430 and 590 nm which are due to electrical and magnetic resonances, respectively. 80

Figure 6.1 (a) Schematic of LDW system. (b) LDW process to create discrete metal gratings. (c) Finite element analysis (ABAQUS software) representing localized wrinkle formation by LDW on thin gold layer on PET substrate, which is contrast to the bulk wrinkling, (d), when compressive stress is evenly distributed. 86

Figure 6.2 SEM image of 970 nm period gold grating pattern fabricated by LDW process 88

Figure 6.3 (a) A schematic of double layer system used in winkling analysis [110]. (b) Graphical illustration of three representative patterns of wrinkles: stripes, labyrinths and herringbones. (Reprinted from Ref.[110]. Copyright 2005 ELSEVIER Publication)... 89

Figure 6.4 (a) Pattern period as a function of stiff layer (gold) thickness. Solid line: theoretical model from eq. (1), Dots: experimental data from LDW process. (b) Corresponding SEM images of LDW grating pattern on different gold thicknesses (10 nm, 50 nm and 100 nm) on PET substrate at 160 °C representing different periods (200 nm, 1.2 µm and 2.3 µm, respectively). Room temperature LDW produces smaller period (900 nm) pattern for the same thickness (50 nm) of gold. 91

Figure 6.5 (a) Room temperature LDW of 50 nm gold on a bare PET substrate produces 900 nm period patterns on both gold and PET layers, and (b) the same process but on a fluoro_silane surface treated PET shows much larger period (3 μm) and different shape. 93

Figure 6.6 (a) Schematic of pattern transferring step after LDW using UV curable epoxysilicone as an adhesive layer (b) Initial LDW gold pattern on fluoro-silane surface treated PET (from Figure 6.5b), (c) Transferred pattern on glass substrate showing inverse profile of initial pattern (a). 95

Figure 6.7 Periodic pattern by LDW at different sliding speed (from 24 μm/sec to 5 mm/sec) showing identical pattern period, 1.5~1,6 μm, regardless of speed (contacting time) for the same thickness (100 nm) of gold layer on PET at ambient temperature. 96

Figure 6.8 (a) Uniaxial stretching with heat (T > Tg) to enlarge openings between metal wires. (b) SEM of LDW pattern in 50 nm gold coated PET. (c) 20% strained LDW pattern. (d) 30% strained LDW pattern. (e) 20% strained 50nm gold coated PET without patterns (for comparison). (f) Transmittance of each sample listed. 98

Figure 7.1 Graphical illustration of Dynamic Nano_Cutting (DNC) to generate periodic grating pattern. 103

Figure 7.2 Experimental setup for Dynamic Nano-Cutting (DNC). 104

Figure 7.3 Micro / Nano gratings directly fabricated on PET substrate by DNC using different vibration frequency. (a) 70 Hz vibration with 250 μm/s feeding speed generates 3.5 μm period pattern. (b) The same speed with 325 Hz vibration yields 780 nm period pattern. 106

Figure 7.4 Micro scale gratings fabricated on various substrates by DNC. (a) On 100 nm gold coated PET, (b) on 50 nm Aluminum coated Polycarbonate, (c) on Kapton film (polyimide), (d) on PEDOT coated PET. 108

Figure 7.5 Grating patterns having decreasing (and increasing) period from micro to nano scale. (a) DNC on PET at feeding speed of 100 μm/s but increasing vibration frequency from 80 Hz to 200 Hz yielding 1.2 μm to 500 nm period. (b) Keeping the frequency 200 Hz but decreasing feeding speed from 100 μm/s to 10 μm/s generates down to 126 nm periodic gratings. 110

Figure 8.1 Schematic of multilayer DNI. 117

Figure 8.2 DNI followed by lift_off (polymer layer removal) can produce nano metal wires (single DNI) or dots (double DNI). 118

Figure 8.3 (a) Tool fabrication steps for free_surface DNI. A Si stamp is molded into PDMS/Si substrate and backside of the stamp is etched away to fabricate Si fingers. (b) DNI on any free-curved surface including spherical surface. 120

Figure 8.4 Schematic of pattern writing based on DNI 121

Figure 8.5 Schematics of a hard mold fabrication process from LDW pattern on a flexible substrate. (1) LDW to generate metal gratings on plastic substrate. (2, 3) Transfer metal gratings to Si substrate using adhesion layer (e.g. UV curable resist) (4) Etch down to the Si substrate. (5) Lift-off to remove metal/resist layer. 122

Figure 8.6 Combination of DNI and LDW can produce nanoscale metal dot arrays in a simple single step. 123

List of Tables

Table 2.1 Cured area of epoxysilicone as a function of the curing time, the iris opening ratio and the distance from UV light source. (a) Iris opening ratio. (b) UV exposure time. (c) Distance between UV source and sample. 19

Table 3.1 Work of adhesion at the interface of two solid materials................................. 43

Table 3.2 Energy release rate in each step of the perpendicular peeling method 45

Table 8.1 Patterning characteristics of each proposed process. NIL is for comparison.. 113

ABSTRACT

The motivation of this work is to enable continuous patterning of nanostructures on flexible substrates to push nanoscale lithography to an entirely new level with drastically increased throughput.

The Roll-to-Roll Nanoimprint Lithography (R2RNIL) technology presented in this work retains the high-resolution feature capabilities of traditional NIL, but with an increase in throughput by at least one or two orders of magnitude. We demonstrated large-area (4” wide) continuous imprinting of nanogratings by using a newly developed apparatus capable of roll-to-roll imprinting on flexible substrates (R2RNIL) and roll-to-plate imprinting on rigid substrates (R2PNIL). In addition, analytical models were developed to predict the residual layer thickness in dynamic R2RNIL. As a potential application, high-performance metal wire-grid polarizers have also been fabricated utilizing R2RNIL.

Another research focus involved Direct Metal Imprinting (DMI) to create discrete nano-scale metal gratings. DMI uses a polymer cushion layer between a thin metal layer and a hard substrate, which enables room-temperature nanoimprinting of the metal by overcoming troublesome hard-to-hard surface contact issues while preserving the Si mold.

We also introduced a novel nanofabrication technique, Dynamic Nano-Inscribing (DNI) for creating truly continuous nanograting patterns by using the sharp edge of a

tilted Si mold on a variety of metals or polymer materials, creating linewidths down to 50 nm at extremely high speeds (~100 mm/sec) under ambient conditions.

Additionally, a new nanograting fabrication method, Localized Dynamic Wrinkling (LDW) has been developed. LDW enables the continuous formation of micro/nano-scale gratings by simply sliding a flat edge of a cleaved Si wafer over the metal film. LDW shares the same basic principle as the buckling (wrinkling) phenomenon but the moving edge of the tilted Si wafer exerts stress on a metal coated polymer and sequentially generates localized winkles in the metal film in a dynamic fashion. The period in LDW can be controlled by several processing parameters and shows good agreement with a theoretical model.

Finally, we developed a Dynamic Nano-Cutting (DNC) process using high-frequency indentations on a moving substrate to sequentially create nanograting patterns. DNC provides perfectly straight lines with real-time period modulation, which is difficult to achieve by other nanomanufacturing techniques.

Chapter 1

Introduction

Entering the nano-world, where the minimum structural dimension is on the order of 100 nm or smaller, we encounter many interesting phenomena in electronics, optics and biophysics which cannot be observed in larger dimensions. For instance, localized surface plasmon resonance (LSPR) found in nano-metallic structures has been contributing a great deal to the development of near-field scanning optical microscopy[1], biological sensors[2] and light-emitting diodes with enhanced functionality[3]. Nanograting patterns in the form of ordered periodic line structures with nano-scale lateral dimensions are the most fundamental and important components in many practical applications due to their electrical and optical characteristics. In that sense, increased effort has been stimulated in the last couple of decades to develop new fabrication technologies which allow nano-scale structuring with enhanced geometrical complexity. However, most nanomanufacturing processes are still facing the bottleneck of stepping toward commercialized production due to their fundamental limitation of low throughput and high processing costs.

1.1 Nanogratings and their applications

1.1.1 Optical and electrical applications

Grating nanostructures with periods smaller than optical wavelengths have been extensively used in many optical applications. Anti-reflection (AR) patterns, in the form of ordered nanogratings or moth-eye structures, are a potential replacement for AR thin-film coating due to their enhanced performance in the visible and near infrared spectrum[4]. Subwavelength metal wires on transparent substrates show polarizing effects with a high extinction ratio. Metal wire-grid polarizers have many advantages such as low insertion loss with a wide incident angle range and broad wavelength bandwidth[5-7]. Ordered metal gratings pattern can also be used as transparent electrodes in organic electronics applications, which can potentially replace expensive Indium Tin-Oxide (ITO) layers [8, 9].

1.1.2 Bio-sensor applications

Surface plasmon resonance (SPR) induced bio-sensors have been extensively explored for biomedical, food and environmental applications due to their label-free and real-time sensing capability with very high sensitivity[10]. Periodic nanograting structures or nano island patterns in metal produce SPR, and various technologies such as nanoimprint lithography[11] or electron-beam lithography[12] are involved in the fabrication.

1.1.3 Other various applications

In addition to optical and electrical applications, nanogratings can be utilized in various fields of science and engineering. Submicron grating structures can be used as a measurement tool of residual strain/stress in MEMS and NEMS (micro/nano-electro-mechanical-systems)[13]. High aspect ratio Si nanogratings can even act as a deep UV-blocking particle filter for space engineering applications[14]. Nanogratings can also serve as a medium filter: Micro/nano particles having different sizes are simply separated by flowing over a micro/nano buckled surface[15].

1.2 Nanofabrication technologies for nanogratings

1.2.1 Nanoimprint lithography

Among the emerging techniques, Nanoimprint Lithography (NIL) clearly stands out as a promising technology for high throughput nanoscale patterning[16, 17] which can achieve resolutions beyond the limitations set by light diffraction or beam scattering that are encountered in other traditional techniques. The development in this area has enjoyed great momentum in the past decade, and numerous applications such as in Si electronics[18, 19], organic electronic and photonics[20, 21], magnetics[22, 23], and biology[24-27] have been exploited by many researchers.

The principle of nanoimprinting is very simple. Figure 1.1 shows the schematics of originally proposed NIL processes that use thermal softening[17] and UV curing [28], respectively. For thermal NIL (Figure 1.1a), a hard mold is placed in intimate contact with a substrate where a thermal plastic resist is uniformly coated. The mold is then

pressed into the resist material that is softened by heating (> Tg) to form the thickness contrast of the resist. Demolding after cooling followed by anisotropic etching finalizes the nano-structuring on the substrate. For UV NIL, which is also called Step and Flash Imprint Lithography (S-FIL), a UV curable low-viscosity liquid resist is molded by a transparent mold such as Quartz. The resist is then quickly cured by UV exposure. Demolding followed by anisotropic etching generates residual-free nano features.

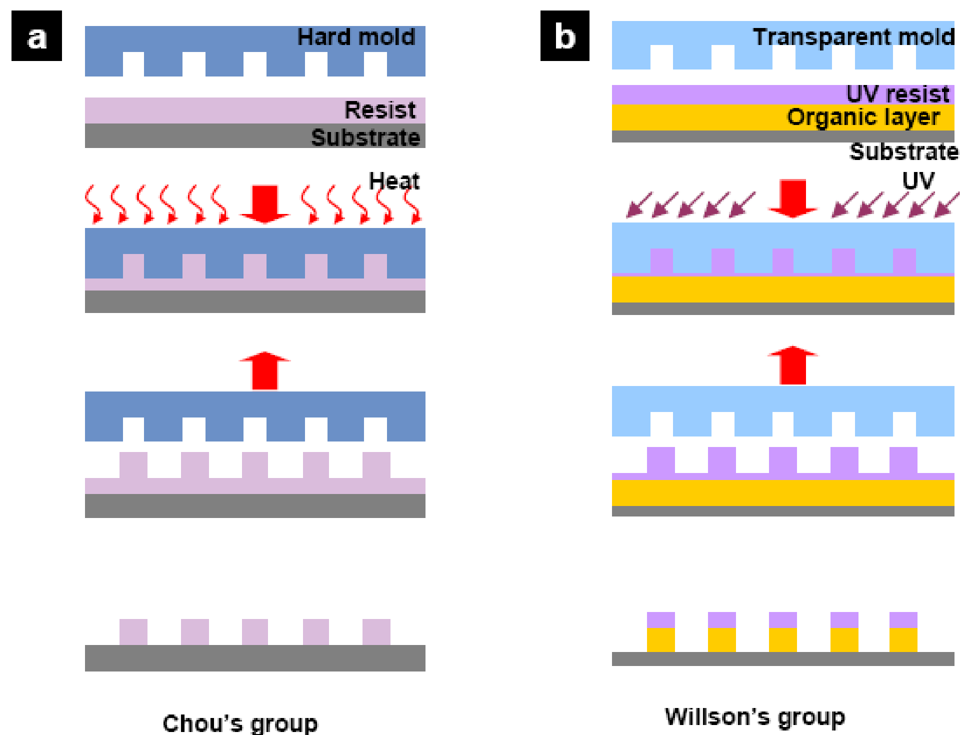

Figure 1.1 The schematics of NIL. (a)Thermal NIL (b) UV NIL (S-FIL)

For successive imprinting, there are stringent requirements for the mold and resist materials. Since the mold trench size is very small and has a much larger contact area, especially for high aspect ratio structures, compared to a flat surface, very strong adhesion acts on the mold-resist interface. Therefore, we occasionally observe resist stuck in the mold unless a special surfactant treatment is used. The most widely used approach

is to form a self-assembled monolayer of fluoro-silane surfactant (e.g., 1*H*,1*H*,2*H*,2*H*-perfluorodecyl-trichlorosilane), either by a solution-phase or a vapor-phase reaction[18]. Alternatively, fluoro-copolymer materials that have inherent low surface energy are used as a flexible mold[29, 30]. Proper choice of the resist material in NIL is a key to successful nanopatterning. The material should have a low modulus and viscosity at the moment of pressing for faithful filling, but should become hard enough after cooling (or curing in UV-NIL) to retain the patterned features. Low free energy at the surface is another criterion of the NIL resist for clean mold separation. Many applications require nanostructures on hard substrates (Si or glass) rather than on the polymer resist itself. Therefore, good etching selectivity is highly recommended for good NIL resist.

Current NIL enables the fabrication of sub-10 nm size features with complex geometries. Three-dimensional nanostructures by successively stacking several layers using NIL has also been demonstrated[31]. Stepping over simple 2-D patterning, NIL is now broadening its range to flat-panel displays[32] and even CMOS[33] industries as a strong candidate to replace current photolithography in the near future.

1.2.2 Other nanopatterning technologies

Laser interference lithography (LIL) is a very powerful method to form periodic patterns without use of pre-patterned masks or stamps. LIL is based on the interference of coherent laser beams to selectively expose a photosensitive material thereby creating periodic patterns after development[34]. Using additional beams in an exposure, 3D periodic structures can also be fabricated[35]. LIL has many advantages over conventional photolithography; it is maskless and a low-cost process. Moreover, if a high

power laser is used, large-area subwavelength gratings can be achieved with high throughput.

Electron-beam (e-beam) lithography (EBL) uses an electron beam (typically 10-100 eV) to expose an electron-sensitive resist, such as PMMA[35]. EBL provides excellent patterning resolution, down to 10 nm, with free-drawing capability on demand. However, due to its extremely low throughput, EBL is commonly used in small-area patterning or prototype fabrications.

An ion beam can be used as a nanomachining tool to directly remove material in a vacuum environment[36]. Focused ion beam (FIB) allows for the fabrication of 3-D structures by moving (or rotating) a specimen with very high resolution. However, similar to EBL, the milling speed of FIB is very slow, therefore, only a limited area can be patterned efficiently.

A new approach based on the phase separation of self-assembled block copolymers can also form nano-scale periodic structures. The spatial resolution in block copolymer assembly is between 10 to 100 nm, which is determined by the chain dimension[37]. Patterning using the block copolymer method does not require expensive optical devices and provides large-area nano patterning. However, uniform morphology control with good repeatability is still a challenge.

1.3 Goal of research

Many of the emerging technologies addressed above have given rise to many beneficial changes providing subwavelength patterning of periodic lines, complex 2-D shapes and even 3-D structures on demand. However, most of nanopatterning processes have been struggling to overcome the inherent low productivity.

The work proposed here pursues high-throughput and continuous processes that maintain nanoscale patterning resolution. Roll-to-roll nanoimprint lithography (R2RNIL) enables continuous patterning of nanostructures on flexible substrates with at least an order of magnitude higher processing speed than that of conventional NIL. Direct Metal Imprinting (DMI) can be a solution to create discrete metal gratings in a simple way. Nanograting fabrication technologies such as Dynamic Nano-Inscribing (DNI), Localized Dynamic Wrinkling (LDW) and Dynamic Nano-Cutting (DNC), provide high-speed patterning of nanogratings relying on each a novel method that has not been introduced by other researchers. We are certain that these proposed nanopatterning technologies can contribute to nano-science in stepping toward high-throughput applications, especially in the display and energy industries.

1.4 Organization of thesis

The organization of the thesis is as follows: Chapter 2 introduces the Roll-to-Roll Nanoimprint Lithography (R2RNIL) apparatus, process and its application to bilayer metal wire-grid polarizers. Chapter 3 presents scaled-up 6" capable Roll-to-Roll, Roll-to-Plate Nanoimprint Lithography (R2R/R2PNIL) for large-area, high-speed nanopatterning. New analytical models for predicting residual layer thickness (RLT) in the dynamic R2RNIL process have been developed. Chapter 4 describes the Direct Metal Imprinting (DMI) technique that enables direct metal grating fabrication using a polymer cushion layer to enhance pattern fidelity with lowered imprinting pressure. Chapter 5 introduces a novel nano-patterning technology, Dynamic Nano-Inscribing (DNI) for continuous and seamless gratings at very high speed (up to 10 cm/sec). The simple fabrication of split ring resonator (SRR) has been demonstrated as the application of DNI. Chapter 6 describes the newly developed Localized Dynamic Wrinkling (LDW) process that allows sequential generation of metal nanogratings utilizing the flat edge of a Si mold. Pattern period and geometry are controlled by several processing parameters. Chapter 7 introduces Dynamic Nano-Cutting (DNC) based on high-frequency indentation for nanograting patterns on various materials with real-time period modulation. Chapter 8 summarizes all of the work done so far and discusses the future experiments to be done.

Chapter 2

High-Speed Roll-to-Roll Nanoimprint Lithography on Flexible Plastic Substrates

2.1 Introduction

The ability of micro- to nanoscale patterning on flexible substrate can enable many new applications in the area of photonics and organic electronics. A major roadblock has remained for many practical applications of patterned nanostructures, which is the throughput of nanopattern replication and the associated cost issues. Among the emerging techniques, Nanoimprint Lithography (NIL) clearly stands out as a promising technology for high throughput and high-resolution nanoscale patterning[16, 17], which can achieve resolutions beyond the limitations set by light diffraction or beam scattering that are encountered in other traditional techniques. The development in this area has enjoyed great momentum in the past decade, and numerous applications such as in Si electronics[18, 19], organic electronic and photonics[20, 21], magnetics[22, 23], and biology[24-27] have been exploited by many researchers. On the other hand, the current process and throughput in NIL (~few min or longer per wafer) is still far from meeting the demands of many practical applications, especially in photonics, biotechnology and organic optoelectronics. The concept of roller imprinting has been pursued by previous investigators as a means to improve speed[38]. However, the procedure was to imprint a

small piece of Si mold onto a Si substrate, which is not too different from that of conventional NIL except a rod is used to apply pressure rather than a flat platen. Reverse Nanoimprinting[31] or Nanotransfer printing method[39] produce positive tone polymer or metal patterns, which in principle can also be applied to roll-to-roll printing process. In addition, Lee et al. proposed a bilayer transfer process from a 'rigiflex' mold to a Si wafer[40], and pointed out that the process can potentially be extended to a roller bilayer transfer process. However, these are yet to be demonstrated.

The Roll-to-Roll Nanoimprint Lithography (R2RNIL) technology presented in this paper inherits the high-resolution feature of the traditional NIL because it is also based on a mechanical embossing approach, but with a speed of nanopatterning increased by at least one or two orders of magnitude[29]. R2RNIL process primarily targets large area patterning of nanostructures. In the conventional approach, embossing a large area requires very large force. Huge contact area between the mold surface and the imprinted nanostructures also produce significant adhesion force, making the mold-sample separation difficult or even impossible without damaging the substrates. In thermal NIL, if the mold and substrate are made of materials with different thermal expansion coefficients such as Si mold and polymer substrate, stress can build up during a thermal cycle with such a magnitude that even destroys the Si mold during mold releasing. R2RNIL provides a unique solution to these challenges encountered in the conventional wafer-scale NIL process, because imprinting in R2RNIL proceeds in a narrow region transverse to the web moving direction, thus requires much smaller force to replicate the patterns. Also since the mold used in R2RNIL is in the form of a roller, the mold-sample

separation proceeds in a “peeling” fashion, which requires much less force and reduces the probability of defect generation.

2.2 Experimental details

2.2.1 Material requirements for high-speed R2RNIL

True roll-to-roll nanoimprinting has been a challenge to the community because it requires a complete set of solutions to address a number of interrelated material issues. First of all, a special roller mold is required for continuous roll-to-roll imprinting of nanostructures. Molds used in R2RNIL should be flexible enough to wrap on a roller surface, and they should also have sufficient modulus and strength to imprint other materials. Low surface energy is essential for clean mold releasing. In addition, the roller mold should be durable under continuous imprinting. In this study, a flexible fluoropolymer, ethylene-tetrafluoroethylene (ETFE), is used as mold material. ETFE has a high modulus (~1.2 GPa) at room temperature but can be softened at elevated temperature. Therefore, a ETFE mold can be easily replicated (Figure 2.1a) from the original Si mold by a thermal NIL process at 220 °C[18], where the original large area Si mold can be fabricated by laser interference lithography[41, 42]. Moreover, the exceptional anti-sticking property of ETFE (surface energy of 15.6 dyn/cm, cf. PDMS ~19.6 dyn/cm) makes it easy to de-mold after imprinting without any mold surface treatment and without deterioration in surface properties over many imprinting cycles. In our experiment, several pieces of ETFE molds of proper size were replicated, wrapped and fixed to a 60 mm diameter stainless steel roller (Figure 2.1b).

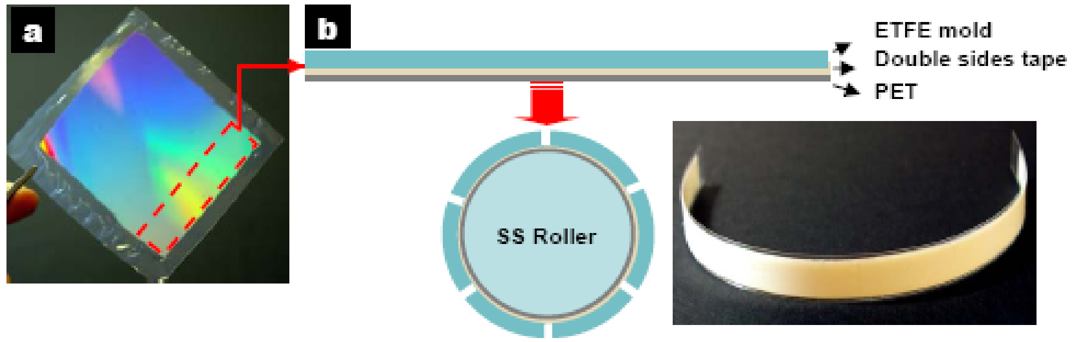

Figure 2.1 A flexible ETFE mold fabricated from an original Si mold. The ETFE mold assembly is prepared as shown in (b) and attached to a 60 mm diameter stain steel roller. A soft cushion layer is placed between the ETFE mold assembly and the roller surface for conformal contact during imprinting.

For a fast roll-to-roll process, there are several stringent requirements for the resist materials. First, liquid resists having good coating property are preferred because they can be continuously and uniformly coated on plastic substrates and be easily imprinted with low pressure. Second, such liquid resists `should have low viscosity before curing for fast imprinting. Third, resists used in R2RNIL need to be quickly cured and with minimum shrinkage after curing. Therefore, conventional resist materials dissolved in solvents and require additional baking process are not suitable for the R2RNIL process. Thermoplastic materials that are typically used in conventional NIL are also not adequate for R2RNIL because they require very high pressure and relatively long processing time to complete the imprinting. In our experiment, two types of liquid resists were exploited for R2RNIL application. For thermal R2RNIL, a fast, thermal-curable liquid resist[43] based on a modified Poly(dimethylsiloxane) (PDMS) was used. The resist consists of four basic chemical components: a vinyl terminated polydimethylsiloxane polymer, a silyl-hydride (Si-H) based dimethylsiloxane crosslinker, a platinum catalyst, and an inhibitor. The inhibitor is an unsaturated organic ester that

keeps the catalyst inactive until the application of heat, which quickly deactivates the inhibitor and releases the catalyst in its active form. The low-viscosity liquid resist can quickly fill into the cavity features on the mold surface by the web tension and the pressure from the backup rollers. The material can be cross-linked within a few second at a temperature of 120 ^{o}C because of the rapid deactivation of the inhibitor. The fast crosslinking ensures high-speed patterning required for R2RNIL.

For even higher speed R2RNIL, we used a UV curable low viscosity liquid epoxysilicone[44] as imprint resist material. Different from acrylate-based resists often used in UV-assisted NIL process such as Step-and Flash Imprint Lithography (S-FIL)[28], epoxysilicone is cured via cationic curing mechanism, thereby free from the oxygen sensitivity issue when exposed in air. So no special vacuum environment is required, which is convenient for the roll-to-roll process. Furthermore, its very low shrinkage after curing (only a fraction of the acrylate system) allows a faithful pattern replication. Due to its low-viscosity, the resist precursor can be imprinted with low pressure and cured within a second by focused UV light. The low pressure and room temperature imprinting characteristics are advantageous for R2RNIL.

2.2.2 R2RNIL apparatus (Model I) for thermal and UV imprinting

Figure 2.2 shows the overall configuration of a continuous R2RNIL nanomanufacturing process, which consists of three separate processing steps: 1) the coating process, 2) the imprinting and the separating process, 3) any of the subsequent processes, which in this work is a film deposition over the imprinted nanostructures to make wire-grid polarizers. Material deposition is carried out in a separate machine.

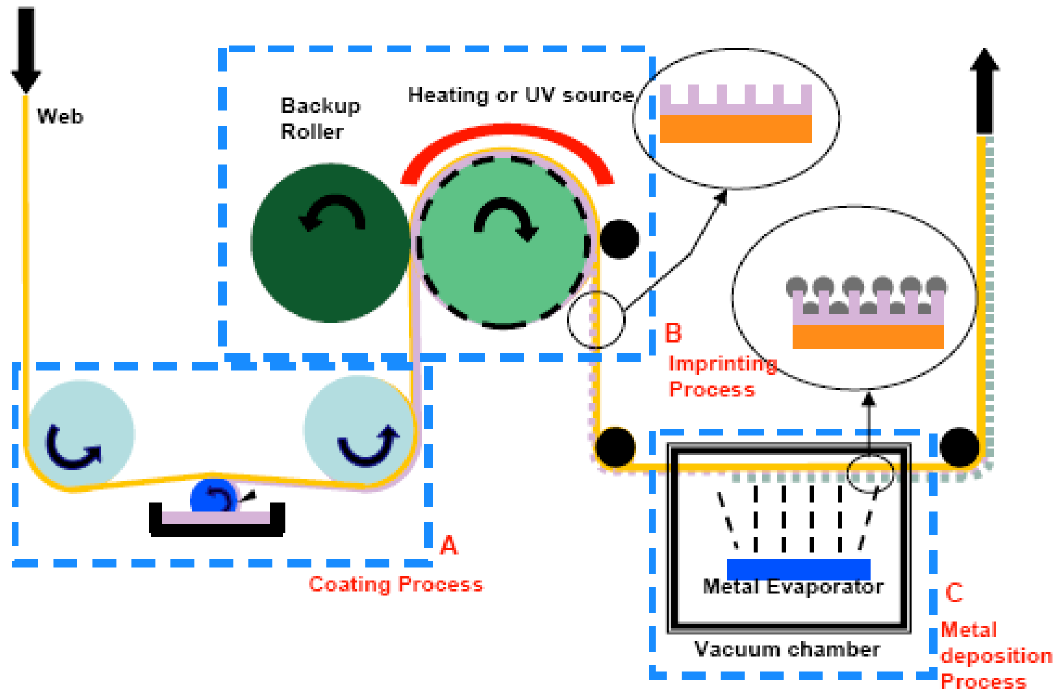

Figure 2.2 Schematic of the R2RNIL process, and the continuous fabrication of metal wire-grid polarizer as one of its applications (the metal deposition is carried out in a separate evaporator in this study).

Figure 2.3a shows the R2RNIL apparatus (Model I) which enables continuous nano imprinting of UV or thermal curable resist materials. This is the initial pilot model producing 10 mm wide patterns on a flexible strip, but all processes including coating, imprinting and mold separation steps are done continuously and synchronized by an AC motor.

The resist film uniformity on the flexible web and the resist thickness are important from both pattern quality and economic point of view. Too thin a film may cause insufficient filling of resist into certain mold regions or cause film fracture during mold releasing. Too thick a resist not only results in accumulation of resist from successive rolling cycles that hampers further imprinting, but also squeezes out excess

materials resulting in resist waste. In our experiment, two types of coating methods, reverse and forward web coating, are used. Reverse coating in which web direction is opposite to rolling direction provides uniform coating profile by eliminating film separation. However, such coating tends to be rather thick. Forward coating provides thinner film layer but slightly lower surface uniformity. In our R2RNIL system, we can easily select either the forward or the reverse coating (Figure 2.3c), and adjust the speed ratio of the moving web and the coating roller that determines the film thickness. Liquid resist is transferred from a resist-container to the flexible PET substrate by the coating roller and its final thickness controlled by a doctor blade.

The Imprint section is the most important part in the R2RNIL system because pattern quality mostly depends on the pressure of the imprint roller and curing conditions. Our Imprint module is composed of an imprint roller, two backup rollers, a release roller and a curing section (Figure 2.3b). Under the web tension and the pressure from the backup roller, low-viscosity monomer resist quickly fills into mold cavity by. Moreover, the two backup rollers with spring system also guarantee non-slip motion in the rolling process, which is very important for successful pattern replication. In the next step, resist precursor is cured either by convection heating (Steinel heat gun) or UV irradiation (Omnicure1000 high-power UV source, EXFO). A box-shaped radiation shield is used to limit the UV exposure only in the curing region, preventing premature curing of the resist before reaching the imprinting zone. Finally, PET substrate with roller-imprinted nanostructures continuously separates from the roller mold via the release roller.

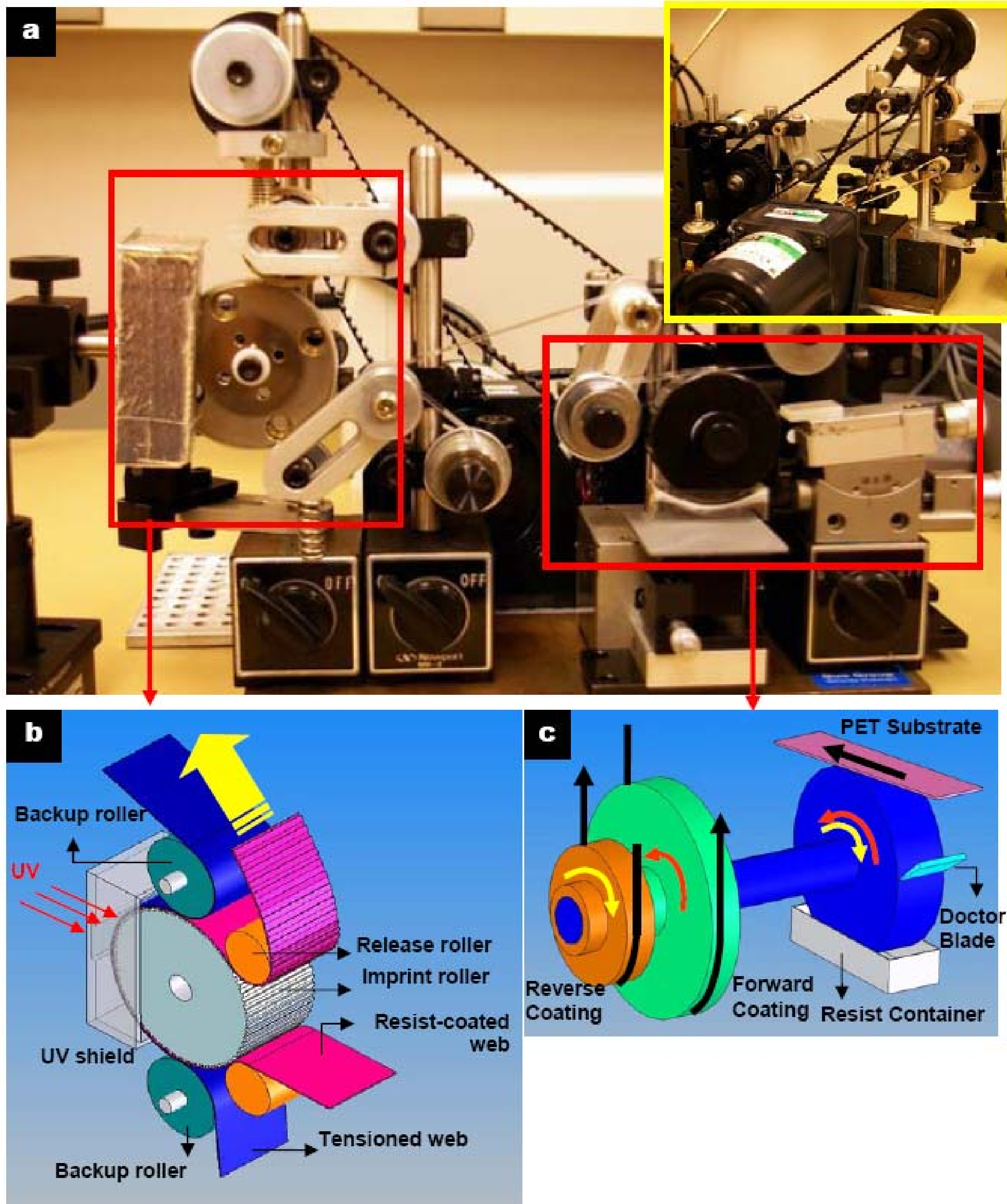

Figure 2.3 (a) Photograph of R2RNIL apparatus (Model I). Inset shows operation system (backside). (b) The coating unit and (c) the Imprint unit of the R2RNIL apparatus.

2.2.3 Method

Fabrication of Si mold: SiO_2 of 200-nm thickness was thermally grown on a Si wafer, and then chrome (Cr) of 10-nm thickness was deposited on the SiO_2 layer by using a radiofrequency (RF) sputter. The Cr layer was used for the improvement of adhesion properties between the photoresist (PR) and the SiO_2 layer as well as for an etch mask to the SiO_2 layer, and PR of 90-nm thickness was spin-coated on the Cr layer. Laser interference lithography using a 325nm wavelength He-Cd laser was performed to form a grating pattern of 200-nm pitch on the PR. The Cr layer was etched with Cl_2 and O_2 RIE, and then SiO_2 layer with CHF_3 RIE. After etching the SiO_2, the Cr mask was removed by Cr wet etchant. The fabricated stamp was pretreated by an anti-sticking layer (1H, 1H, 2H, 2H Perfluorodecyl trichlorosilane) to prevent the stamp from adhering to the imprint pattern for the demolding step.

Fabrication of ETFE mold: A 200 ㎛ thick ETFE film (SAINT- GOBAIN) was sandwiched between a Si mold containing grating structures and a Si substrate, and pressed by a pressure machine with a temperature controller. A temperature of 220℃ and an imprint pressure of 2 MPa were used. After 5-minute hot embossing, the sample was cooled to ambient temperature while keeping the pressure at 2 MPa. Then, the ETFE film was released from the Si mold by manual peeling.

Surface treatment of PET substrate: To improve the adhesion of the PET substrate with the resist pattern, especially for the high aspect-ratio (>5) or small pitch(200 nm/100 nm period) grating structures, the PET substrate was pretreated by

Oxygen plasma (100 W, 250 mTorr, 10 min) followed by thermal deposition of adhesion promoter, Silquest187 (GE Advance Materials, 100 ℃, 15 min).

Roll-to-roll imprint: A flexible ETFE mold was wrapped on a stainless steel imprint roller (diameter = 60 mm, width = 10 mm) using a double-sided adhesion tape. A 1 mm thick rubber cushion layer was placed between the roller and the ETFE mold to ensure adequate conformal contact. Liquid resist material was continuously coated on the flexible PET substrate in the coating module. The amount of resist material was adjusted by the doctor blade fixed in the two-DOF (linear, tilting) stage. The PDMS resist precursor was cured by convention heating (hot-air gun, Steinel) and epoxysilicone resist by UV exposure (7.2 W/cm^2, EXFO Inc.). For the UV curing, light intensity depends on the opening ratio of iris and the distance from the source. To determine the curing time and the cured area in relation to the iris opening ratio and distance from UV source, an epoxysilicone resist (10 % crosslinker formulation)[44] sandwiched by two PET films was cured by UV irradiation (Figure 2.4). The test results are shown in Table 2.1. When the gap was 5 mm, 15 mm diameter area of epoxysilicone was cured within 0.2 sec for both 90% and 40% opening. In the actual R2RNIL process, the resist was cured by the UV light source placed 15 mm away and at 40 % opening. Web speed (1.3 ~ 23.5 mm/s) was controlled by an AC motor controller.

Al deposition for the wire-grid polarizer: Al film of various thicknesses (50 nm, 70nm, 100 nm) was thermally deposited on the grating structures in a separate evaporator.

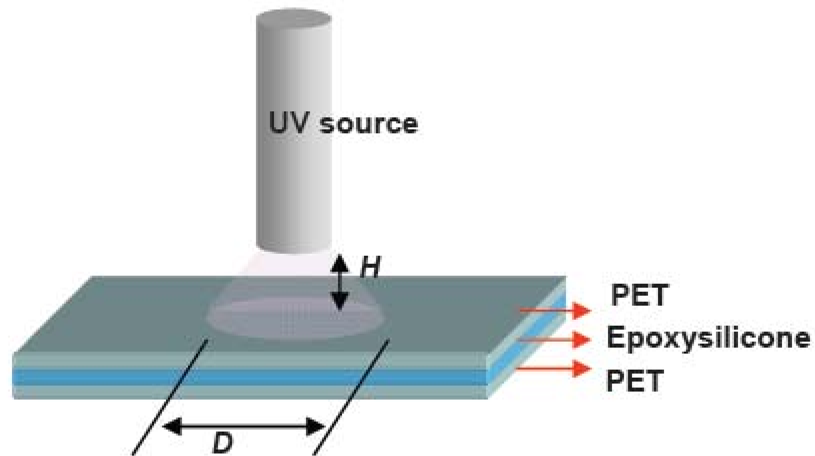

Figure 2.4 Schematic of UV curing test of epoxysilicone. UV curable epoxysilicone resist is sandwiched by two sheets of PET film, as in the actual R2RNIL process. *H* is distance between the light source and the sample, and *D* is the diameter of fully solidified area after curing.

Iris Opening (a)	Time (b) / H (c)	1 sec	0.5 sec	0.2 sec
90 %	15 mm	D= 20 mm	D= 15 mm	D=12 mm
	5 mm	D=12 mm	D=10 mm	D=10 mm
40 %	15 mm	D= 15 mm	D= 15 mm	D=15 mm
	5 mm	D= 10 mm	D= 10 mm	D=10 mm

Table 2.1 Cured area of epoxysilicone as a function of the curing time, the iris opening ratio and the distance from UV light source. (a) Iris opening ratio. (b) UV exposure time. (c) Distance between UV source and sample.

2.3 Results and discussion

For easy visualization of the imprinting results, we chose a grating pattern of 700nm period in our initial experiment, because well-replicated grating structure should show strong light diffraction and therefore the pattern quality can be easily examined by eye. We first performed continuous nanoimprint on flexible plastic substrate by using thermal curable liquid resist. A 200 mm long, 300 nm linewidth and 700 nm period gratings imprinted using the thermally cured PDMS on PET substrate are shown in Figure 2.5a and 2.5b. Curing of PDMS liquid resist was done by convection heating using a heat gun. Next we experimented with UV curable epoxysilicone liquid resist. Figure 2.5c ~ 2.5d show UV R2RNIL results of a 570 mm long (width of 10 mm), 700 nm period grating structure created on PET substrate. Scanning electron microscopy (SEM) shows that the UV cured epoxysilicone resist pattern has higher quality than the thermal-cured PDMS, which can be attributed to the lower viscosity of the epoxysilicone material that facilitates the fast filling of the mold cavity. Printing speed can be adjusted depending on the period of grating pattern and its aspect ratio. The fast curing of the resist material allow us to achieve a web speed of ~ 1 m/min.

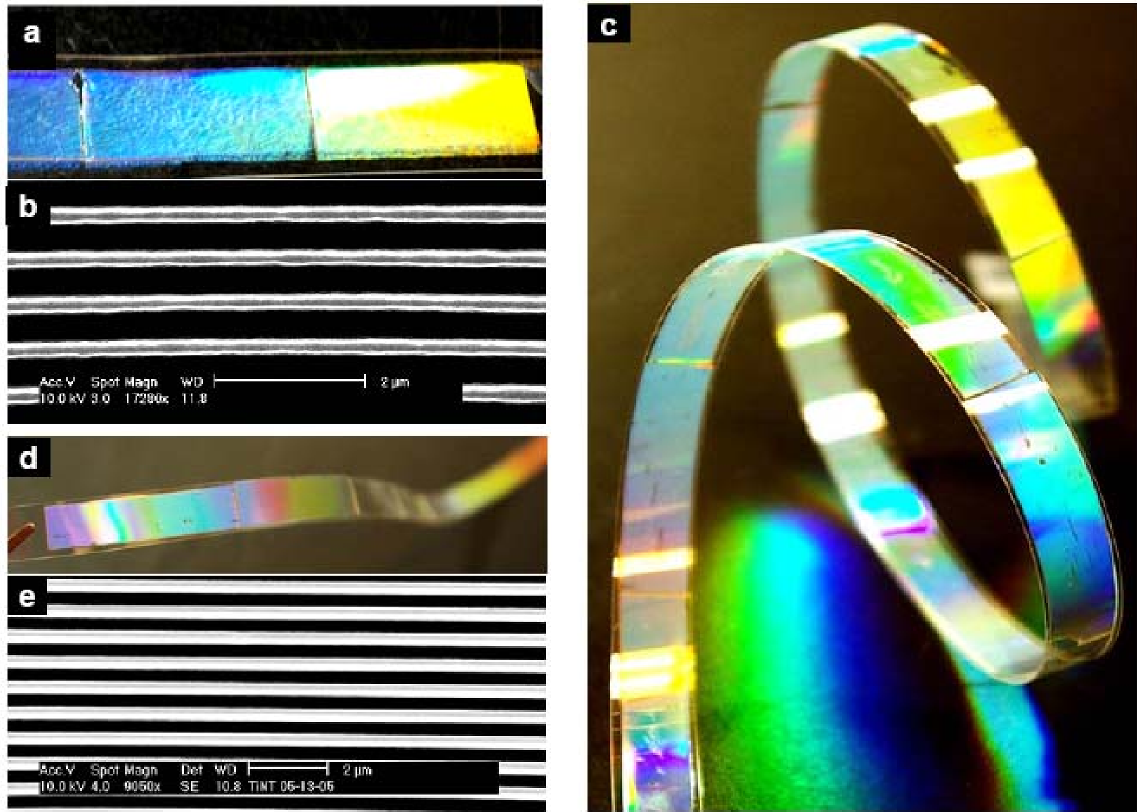

Figure 2.5 Thermal R2RNIL results: (a) Photograph of a 700 nm period, 300 nm line width PDMS grating pattern imprinted on PET strip by using the thermal R2RNIL and (b) the SEM micrograph of the replicated grating structure. UV R2RNIL results: (c), (d) Photographs of 700 nm period, 300 nm line width epoxysilicone grating pattern imprinted on PET strip by the UV R2RNIL, showing bright light diffraction and (e) the SEM of the replicated grating structure. Total length is 570 mm.

High aspect ratio (AR = 5.4) grating structures with very sharp pattern definition fabricated by R2RNIL are shown in Figure 2.6b and 2.6c. Faithfully replicated epoxysilicone pattern should have the same geometry as in the original Si mold (Figure 2.6a) because the ETFE mold, replicated from the Si mold, has the exact inverse patterns of the Si mold. Comparing the grating structure on the original Si mold (Figure 2.6a) and the imprinted epoxysilicone pattern (Figure 2.6c), we observe excellent pattern replication even for the very fine details at the bottom of the grating trenches. Residual

layer thickness in this result is about 2 μm, but can be controlled by web tension and backup roller pressure. Even though the ETFE mold has good anti-sticking property, such a high aspect ratio imprinted structure tends to show significant sticking to the ETFE mold due to the much larger contact area with the grating sidewalls on the mold. To achieve successful pattern transfer, we performed oxygen plasma treatment followed by thermal deposition of Silquest A187 adhesion promoter (GE Advance Materials) on PET substrate before imprinting, which improves the adhesion of the resist pattern to the PET substrate. Additionally, a few drops of fluorosurfactant were added to the epoxysilicone resist to further reduce the adhesion between the imprinted pattern and the ETFE mold surface.

Continuous roll-to-roll imprinting of thinner and denser grating structure is more challenging because such patterns are mechanically fragile, and tend to collapse during demolding if the trench is very small. This requires the cured resist to have sufficient modulus and yield strength. Good adhesion of the resist to the substrate is also very important for such denser structures, which was achieved by using the aforementioned adhesion promoter. Figure 2.6d and 2.6e show 200 nm period, 70 nm linewidth epoxysilicone patterns by the UV R2RNIL process. SEM photograph of 100 nm period grating structure is also replicated successfully and shown in Figure 2.6f.

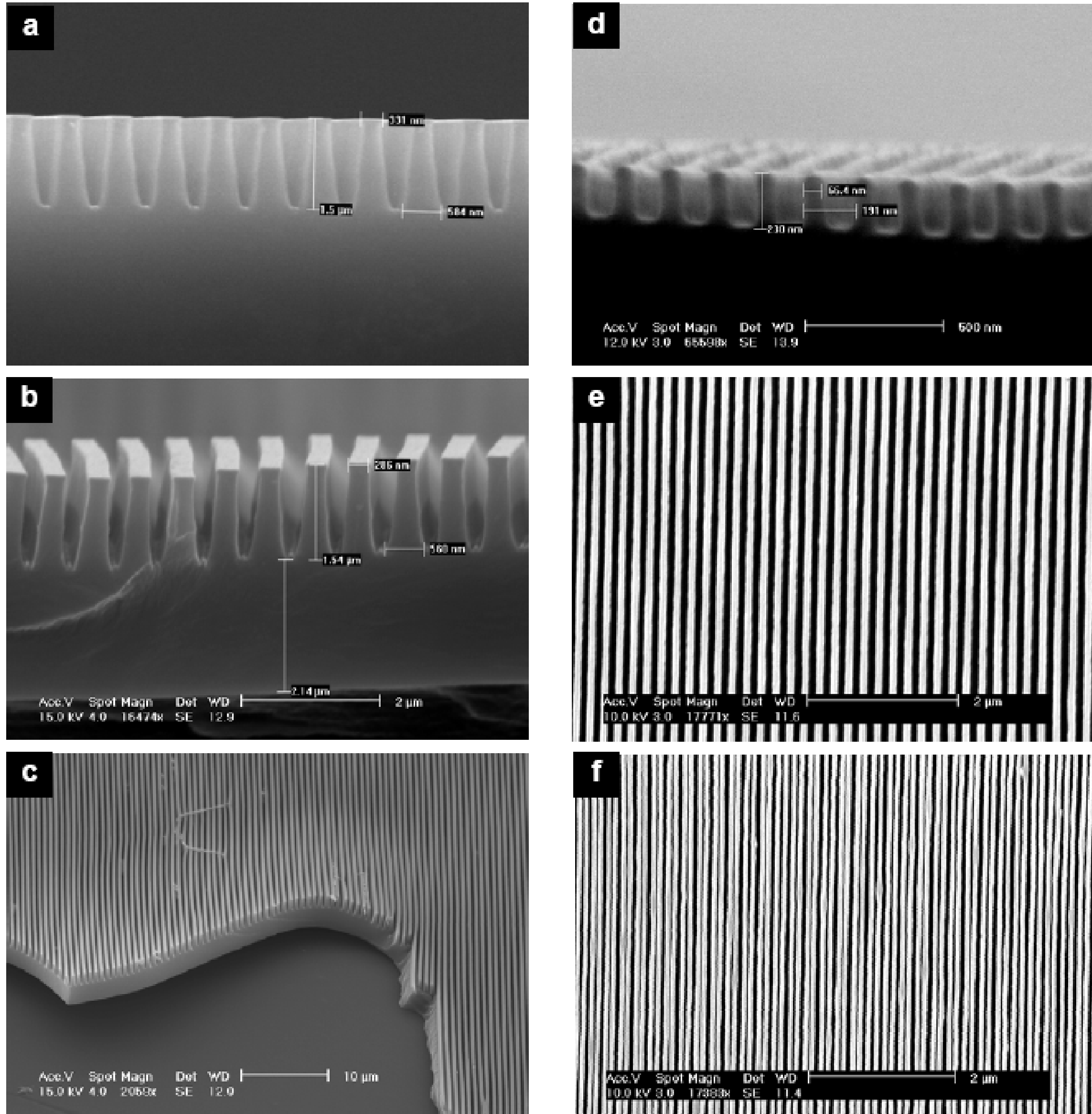

Figure 2.6 (a) The original Si mold. (b), (c) the epoxysilicone gratings replicated from the ETFE mold. (d), (e) SEM pictures of 200 nm period, 70 nm line width epoxysilicone pattern and (f) a 100 nm period, 70 nm line width epoxysilicone pattern fabricated by UV R2RNIL.

2.4 Fabrication of metal wire-grid polarizers as an application of R2RNIL

2.4.1 Introduction to metal wire-grid polarizers

The polarizer is an important optical element used in a variety of applications. Wire grid polarizers in the form of sub-wavelength metallic gratings are an attractive alternative to conventional polarizers, because it provides high extinction ratio between the transmitted TM-polarized light and the reflected TE-polarized light over a wide wavelength range and incident angle with long term stability[6, 45]. In addition, they are thin and planar structures and can be easily integrated with other thin film optical elements. Ekinci et al. have recently demonstrated a new bilayer metal wire-grid polarizer with superb performance[6]. The bilayer metal wire-grids can be considered as two metal gratings separated by a certain distance. Not only does this type of new polarizer show very high extinction ratio between the lights of two orthogonal polarizations, but also it offers the advantage of easy fabrication and defect tolerance.

To create subwavelength grating structure required for wire-grid polarizer, several nano- fabrication techniques can be used. Electron beam lithography can provide high resolution, but its throughput is very low. Liquid immersion or achromatic interference lithography can be used to fabricate 100 nm pitch grating patterns, but they have a limited field size and require a precise process control[46]. Furthermore, fabrication of nanoscale metallic wire-grids on an optically transparent substrate mostly involves reactive ion etching or special sidewall deposition processes[6]. Nanoimprint lithography is an emerging technology that enables low-cost and high throughput nano-fabrication of sub-wavelength structures[16, 47]. Chen et al. demonstrated high efficiency flexible metal

wire-grid polarizer using nanoimprint lithography and shadow metal evaporation technique[48]. For many practical applications of metal wire grid polarizers, it is essential to have a high-speed fabrication process.

2.4.2 Fabrication of metal wire-grid polarizers by R2RNIL

To demonstrate an application of the R2RNIL process, we fabricated a metal wire-grid polarizer. By depositing a thin metal (Al) layer over the imprinted grating structures, high-efficiency polarizer in the form of bilayer metal wire grating can be achieved[6, 7]. In our initial experiment, a 200 nm and 100 nm period grating pattern (Figure 2.6d ~ f) were prepared by the R2RNIL process and various thickness of aluminum was thermally deposited on top of the grating as well as at the bottom of the trench (Fig. 2.7a, 2.7b). To quantify the polarization effect, spectral transmittance was measured using UV/Vis spectrometer. Figure 2.7c shows the transmittance of the TM, TE polarized light through the fabricated metal wire-grid polarizer. The best polarizer result was obtained from the 100 nm period grating with 50 nm Al layer, with transmittance ~ 30 % at 800 nm wavelength and extinction ratio (transmittance of TM / transmittance of TE) over 2,000 at 700 ~ 800 nm wavelength and 2,500 maximum extinction ratio at 770 nm. We would like to point out that in these preliminary experiments, many parameters such as grating period, line width and metal thickness have not yet been optimized.

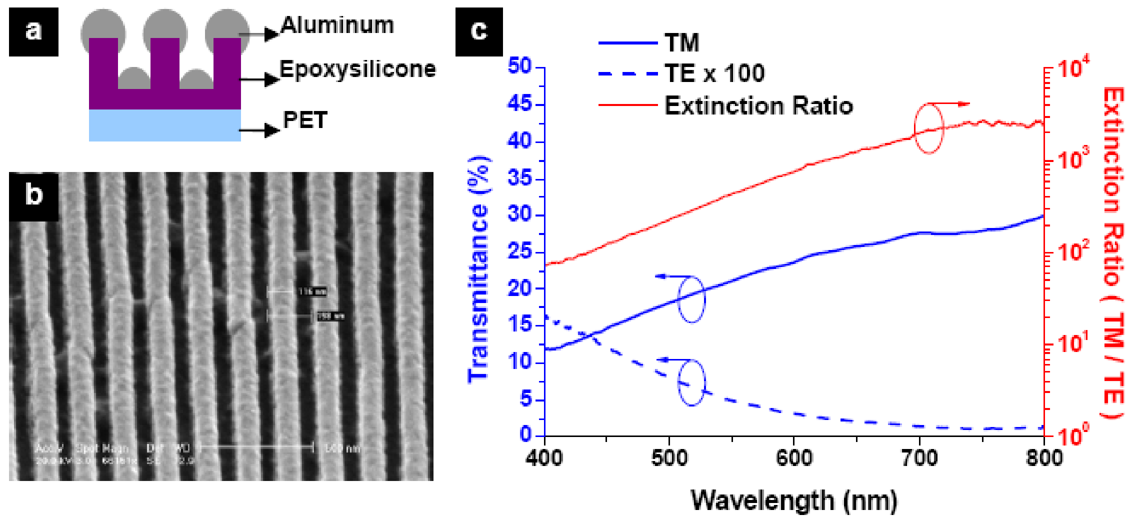

Figure 2.7 (a) Schematic of the metal wire-grid polarizer by depositing metal on top of the roller imprinted polymer grating. (b) SEM picture of a 200 nm period grating with 50 nm Al on top. (c) Spectral transmittance (TM, TE mode) and extinction ratio (TM/TE) of metal wire-grid polarizer fabricated by R2RNIL.

2.5 Summary

In this work, we developed an initial model of R2RNIL apparatus and demonstrated a true R2RNIL process in which polymer patterns down to 70 nm feature size were continuously imprinted on a flexible web. In this process, both thermal R2RNIL and UV NIL have been explored, and material requirement for high-speed R2RNIL has been addressed. As one of many applications, we demonstrated a fabrication of flexible metal wire-grid polarizer by a continuous R2RNIL process followed by metal deposition. A bilayer polarizer fabricated by R2RNIL process provides high extinction ratio, and could find attractive applications in LCD displays to double the brightness by utilizing the reflected light. Furthermore, from the manufacturing point of view, it has great advantages such as simple fabrication process and defect tolerance. R2RNIL may

provide a drastic increase in the process throughput, which addresses one of the bottlenecks in nanopatterning for many practical applications.

Chapter 3

Scaled-up Roll-to-Roll / Roll-to-Plate Nanoimprint Lithography for Large-Area Nanopatterning

3.1 Introduction

A continuous roll-to-roll nanoimprint lithography (NIL) technique can provide a solution for high-speed large-area nanoscale patterning with greatly improved throughput; furthermore, it can overcome the challenges faced by conventional NIL in maintaining pressure uniformity and successful demolding in large area printing. In the previous chapter[7, 29], we presented fabrication of metal wire-grid polarizers done by continuous roll-to-roll imprinting of nanoscale structures (70 nm and 300nm linewidth gratings) on a narrow flexible plastic substrate (10 mm width) using a flexible fluoropolymer mold and a fast thermal curable PDMS[43] and a liquid UV curable epoxysilicone resist[44]. On the other hand, truly large area continuous imprinting is yet to be demonstrated. Also in many applications such as flat panel displays, rigid substrates such as glass plate are preferred over plastic substrates. In addition to the pattern quality and large-area printability, residual layer thickness (RLT) of the imprinted pattern is an important factor in NIL, especially for subsequent etching process and for the patterned film to be used in optical applications. In this respect, the RLT in terms of initial resist thickness[49] and applied pressure[50] in conventional imprinting process have been

studied. The filling of viscoelastic thermoplastic resist material into the mold cavity in hot embossing process has been investigated [51-54], and its dependency on polymer properties[55] and cavity geometry [56] also have been exploited. In addition, the mold filling mechanism in a continuous imprinting process using flexible mold has been explored[57]. However, the model assumed squeezing action of two parallel plates is not very realistic in a dynamic roll-to-roll process. Apart from nano patterning, flow property based on hydrodynamics and contact mechanics also has been studied by many researchers. Squeezing flow properties between two plates[58], hard sphere to hard plane contact[59], hard cylinder to elastic body contact[60] and elastic sphere and hard plate contact[61] have been investigated.

In this work, we demonstrated large-area (4” wide) continuous imprinting of nanoscale structures by using a newly developed 6”-capable roll-to-roll (R2RNIL) / roll-to-plate (R2PNIL) apparatus, which can be potentially applied to many practical applications[30]. 300 nm linewidth grating patterns are imprinted continuously on either rigid glass substrate (R2PNIL mode) or flexible plastic substrate (R2RNIL mode) with greatly enhanced productivity. In addition, the residual layer thickness, which is critical in optical applications, as a function of several imprinting parameters such as the roller pressure and roller speed, has been thoroughly investigated. An analytical model was developed to predict the RLT and the results are consistent with the experimental values. For successful patterning in large-area R2RNIL process, we also performed an analytical study in mold separation in terms of demolding directions based on fracture mechanics.

3.2 Experimental details

3.2.1 Design parameters for scaled-up R2RNIL apparatus

Our initial R2RNIL apparatus (Model I) provides continuous nanoimprinting on 10 mm wide flexible plastic strip at high speed (Chapter 2, [29]). However, to meet the demands from many actual applications, new apparatus that enables larger size continuous patterning is required. Followings are the design parameters that new apparatus (Model II) should possess. First, it should provide continuous NIL process from coating to demolding. Second, the minimum pattern width is 4 inches (c.a. 100 mm). Third, it should keep high processing speed (1 m/min) as previous model. Finally, it should provide nanoimprintings on both flexible plastic substrates (R2RNIL) and hard substrates (R2PNIL) without major change in the apparatus. Figure 3.1 is the prototype design for 6” capable R2R/R2P NIL apparatus.

To scale up the apparatus, we may also face some challenges: Fabrication of large-size flexible mold to minimize seams in patterned area is difficult because it also requires the same size original Si mold. Uniform coating over large area may be challenging. As the inertia of the roller gets larger, slip motion becomes more significant. This requires very tight control on the roller and the web to have an identical linear speed. Probability of the defect generation is likely to increase unless tighter defect control. Additionally, as each axis longer, more precise alignment of roller axis is required.

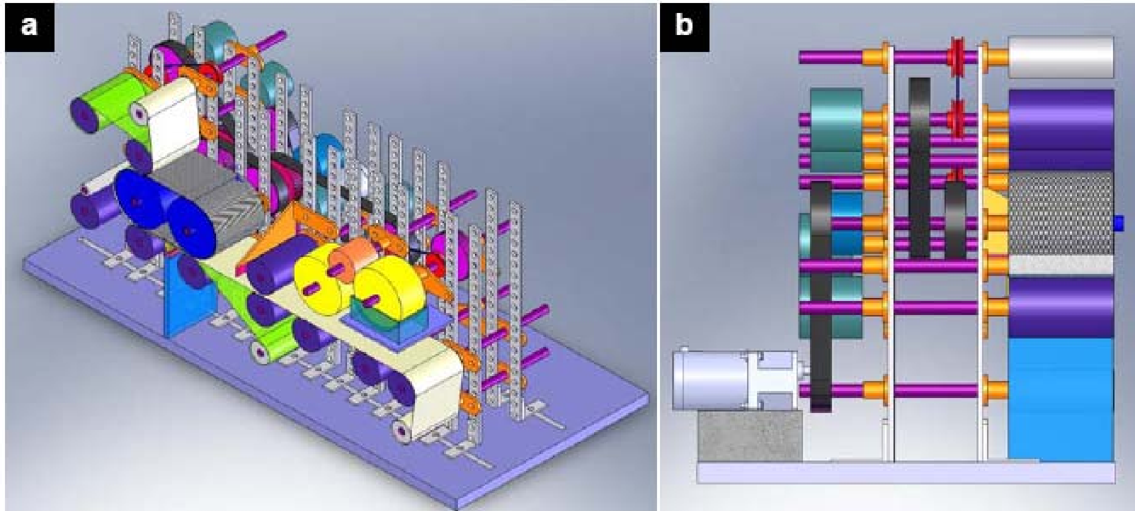

Figure 3.1 Prototype design of R2R/R2P NIL (Model II) which enables 6” wide patterning. (a) Side view (b) Front view

3.2.2 Scaled-up R2R/R2P NIL apparatus

Figure 3.2 shows the overall configuration of a continuous (a) R2RNIL and (b) R2PNIL nanomanufacturing process, which consists of two processing steps: 1) the coating process and 2) the imprinting-curing process. First, liquid phase UV curable resist material is continuously coated on either flexible PET in R2RNIL or glass substrate in R2PNIL by a 3-step roller coating system. The coating system is synchronized with the main imprinting roller to guarantee uniform coating thickness regardless of web speed. In our system, dual imprint-rollers and a tensioned belt supported by the two rollers are used to allow large curing area and to maintain constant pressure during the curing process for fast patterning speed. The pressure between the imprint roller and the back-up roller is controlled by a clamping device and a force sensor. In this study, a flexible fluoropolymer, ethylene-tetrafluoroethylene (ETFE), is used as a mold material. For

R2RNIL (Figure 3.2a) process, the resist material is imprinted by the dual rollers and the tensioned belt and then, cured by a high-power UV source (Omnicure1000, EXPO) under the web tension at the second roller. On the other hand, in the R2PNIL (Figure 3.2b) process, UV curing of the imprinted resist material takes place between the two rollers under the pressure provided by the belt tension. Even though the normal component of the belt tension is smaller than that of the roller pressure, it is sufficient to maintain the resist film thickness after passing through the first roller. Through this process, nano grating patterns are continuously created either on PET or glass substrate as the ETFE mold continuously detaches from the imprinted resist on the substrate.

For a fast roll-to-roll process, we used a UV-curable low viscosity liquid epoxysilicone[44] as the imprint resist material. Different from the acrylate-based resists often used in UV-assisted NIL process such as step-and flash imprint lithography (S-FIL)[28], epoxysilicone is cured via a cationic curing mechanism, thereby free from the oxygen inhibition issue when exposed in air. Thus no special vacuum environment is required, which is convenient for the roll-to-roll process. Furthermore, its very low shrinkage after curing (only a fraction of the acrylate system) allows a faithful pattern replication. Owing to its low viscosity, the resist precursor can be imprinted at low pressures and cured within a second by focused UV light. The low pressure and the room temperature imprinting characteristics are advantageous for R2RNIL.

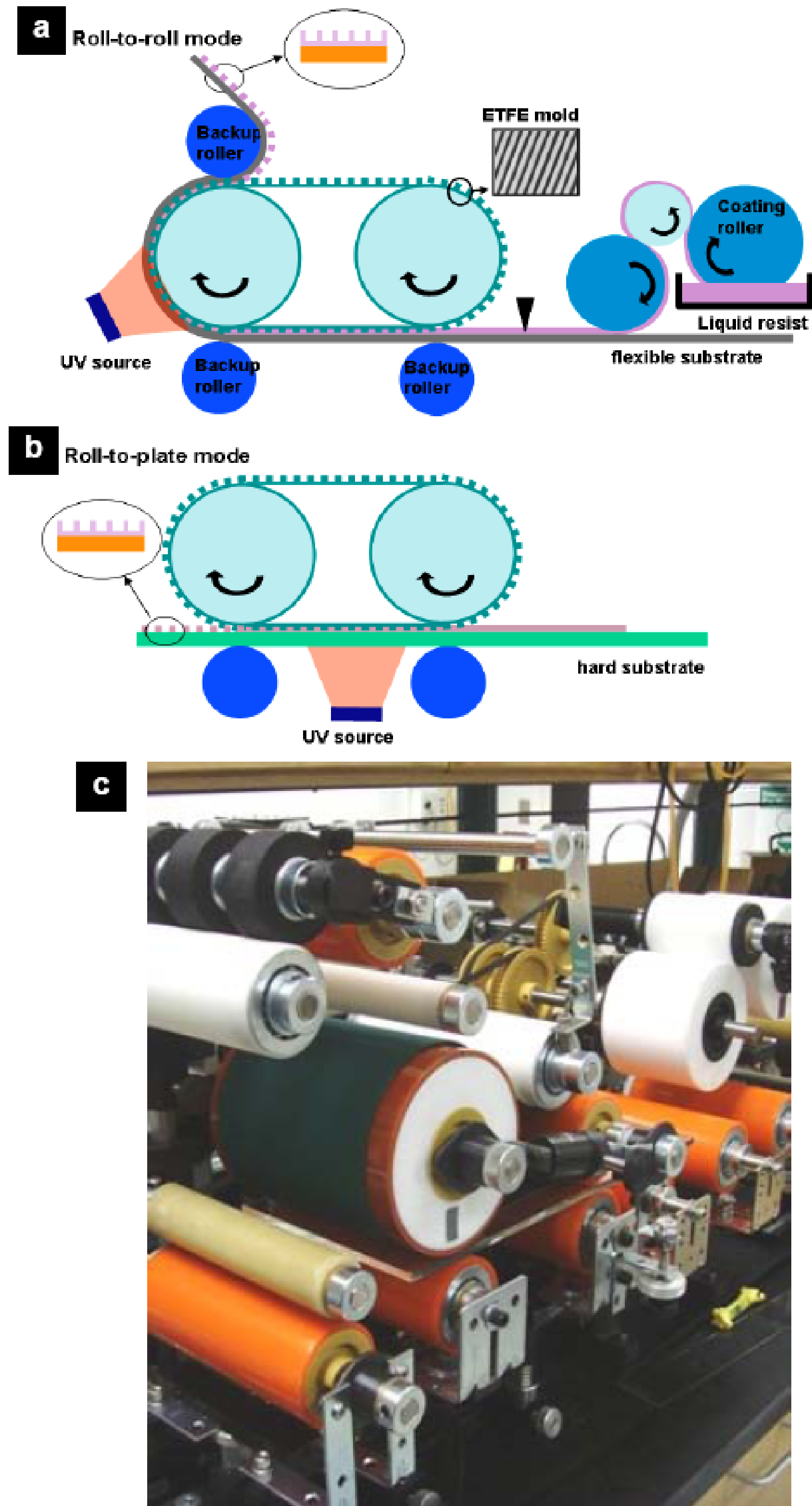

Figure 3.2 Schematics of (a) R2RNIL and (b) R2PNIL process. (c) A Photograph of 6”-capable R2R/R2PNIL apparatus.

3.3 Results and discussion

3.3.1 Large-area nanoimprinting by R2RNIL / R2PNIL

Figure 3.3a represents large area (4” by 12”) nanograting patterns produced on a flexible PET plastic substrate by the R2RNIL process. Figure 3.3b shows the imprinted nanograting patterns on glass substrate by R2PNIL. The strong light diffraction from the 700 nm periodic grating structures can be clearly observed. As described earlier, several pieces of ETFE molds were attached to the tensioned belt and the separation between them produces the seams that can be seen between the square-shape patterned areas. SEM images (Figure 3.3c, 3.3d) show that 300 nm linewidth, 600 nm height gratings are faithfully replicated onto the substrate. The light intensity used for UV curing is 110.8 mW/cm^2 in the central part. The fast curing of the epoxysilicone resist results in a web speed of 1 m/min, a 20 fold increase in imprinting speed as compared with that reported in [62]. A requirement for achieving such a large-area nano-pattern is that the resist material needs to have low adhesion to the mold and high adhesion to the substrate. For R2PNIL, we found that the epoxysilicone resist has relatively lower adhesion to the bare glass substrate and so it tends to peel off from the substrate during the de-molding process despite the low surface energy of the ETFE mold. To overcome this problem, the glass substrate is pre-treated by oxygen plasma followed by the thermal deposition of an adhesion promoter (Silquest A187, GE Advance Materials).

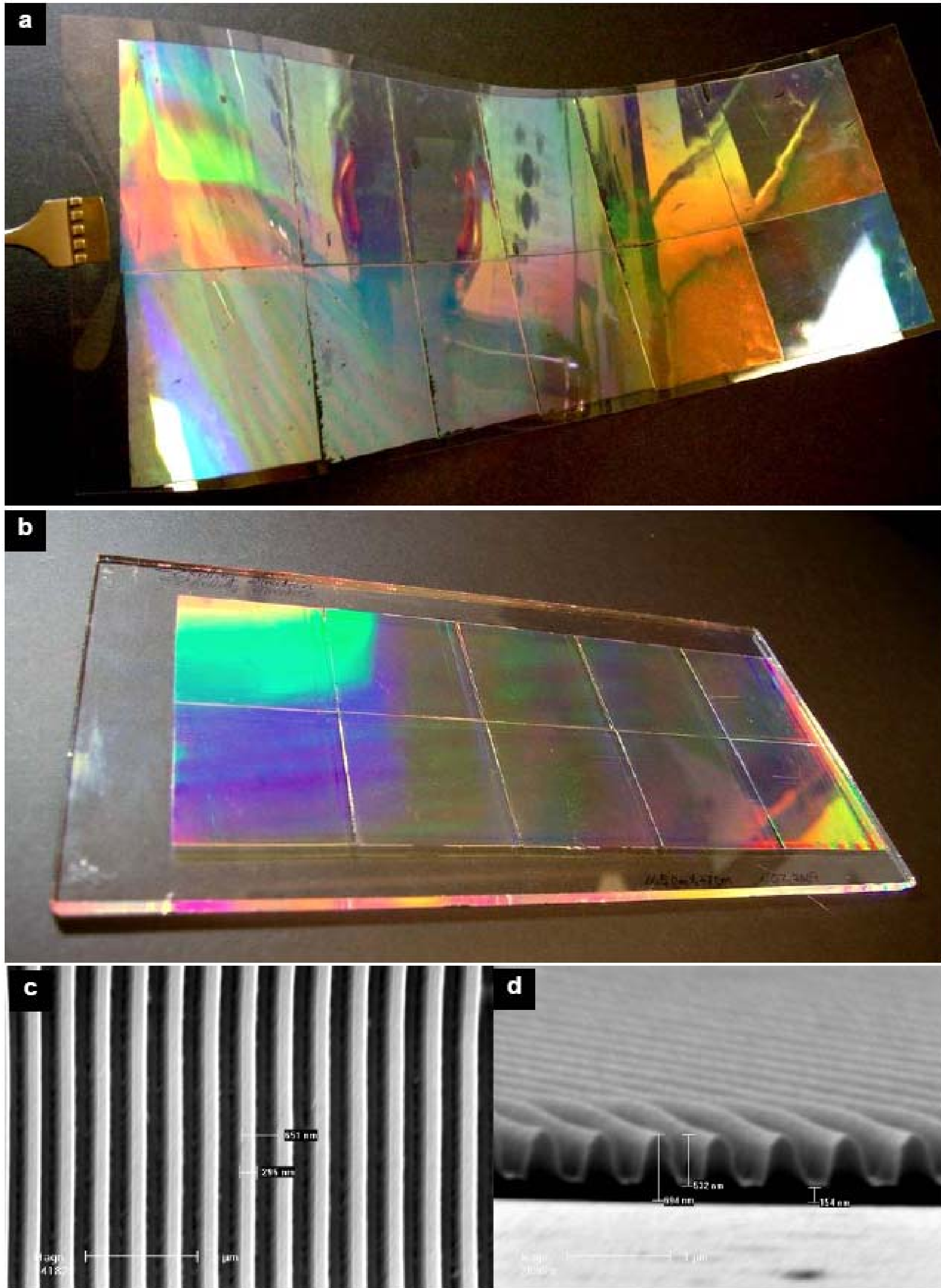

Figure 3.3 (a) A 4” wide, 12” long 700 nm period epoxysilicone patterns on flexible PET substrate by R2RNIL process and (b) a 4” wide, 10.5” long 700 nm period patterns on glass substrate. (c), (d) SEM images of the patterned grating structure.

3.3.2 Analytical models for RLT estimation in R2RNIL

In some optical applications such as metal wire-grid polarizers and solar cells, the overall film thickness or the RLT of imprinted structure is very important due to light absorption or film birefringence. Moreover, most of semiconductor applications prefer thinner RLT to minimize the impact on the pattern profile during the residual layer removal by the following plasma etching process. We will compare several analytical models to predict the RLT in a typical R2RNIL process.

Figure 2.4a depicts a process where the liquid resist is squeezed by two planar plates. In *the solid plane squeeze model*, the time (t) to reach the final film thickness (h_f) can be expressed as following[53].

$$t = \frac{\mu a^2}{2P}\left(\frac{1}{h_f^{\,2}} - \frac{1}{h_0^{\,2}}\right) = \frac{\mu a^3 L}{2F}\left(\frac{1}{h_f^{\,2}} - \frac{1}{h_0^{\,2}}\right)$$

where, μ is the dynamic viscosity, h_0 the initial film thickness, L the width of the panel, F the force applied to the plates, and $\boldsymbol{a}$ the contacting length where resist gets squeezed by rollers (Figure 3.4a). From this equation, we can get the final RLT in terms of the applied force (F) and the web speed (V).

$$h_f = \left(\frac{2F}{\mu a^2 LV} + \frac{1}{h_0^{\,2}} \right)^{-\frac{1}{2}} \qquad (3\text{-}1)$$

However, in practical roll-to-roll imprinting (R2RNIL), rather than two parallel plates, the resist is pressed by two cylindrical rollers that are wrapped with elastic cushion layers. In this case, the pressure distribution from the rollers is given by Hertz contact solution [63] as (*elastic roller contact model,* Figure 3.4b):

$$P = \frac{8F}{\pi a^2 L}\left((\frac{a}{2})^2 - x^2 \right)^{\frac{1}{2}} \tag{3-2}$$

where, F is the applied force.

By combining Equation (3-2) with the Navier-Stokes equation the final RLT at the center of contacted region from *the elastic roller contact model* becomes,

$$h_f = \left(\frac{8F}{\pi \mu a^2 LV} + \frac{1}{h_0^2} \right)^{-\frac{1}{2}} \tag{3-3}$$

For more realistic modeling of the dynamic roll-to-roll imprinting where the liquid resist is squeezed between two rotating elastic rollers, we can consider time dependant parabolic pressure distribution, or *the dynamic elastic roller contact model* as shown in Figure 3.4c). In this model, every small element in the liquid resist experiences a pressure distribution as a function of time, *t*, as the roller moves. I.e.,

$$P(t) = \frac{8F}{\pi a^2 L}\left((\frac{a}{2})^2 - \left(-\frac{a}{2} + V \cdot t \right)^2 \right)^{\frac{1}{2}} \tag{3-4}$$

By equating it with the Navier-Stokes equation, the final RLT in *the dynamic elastic roller contact model* yields a simple expression,

$$\therefore h_f = \left(\frac{F}{\mu a^2 LV} + \frac{1}{h_0^2} \right)^{-\frac{1}{2}} \tag{3-5}$$

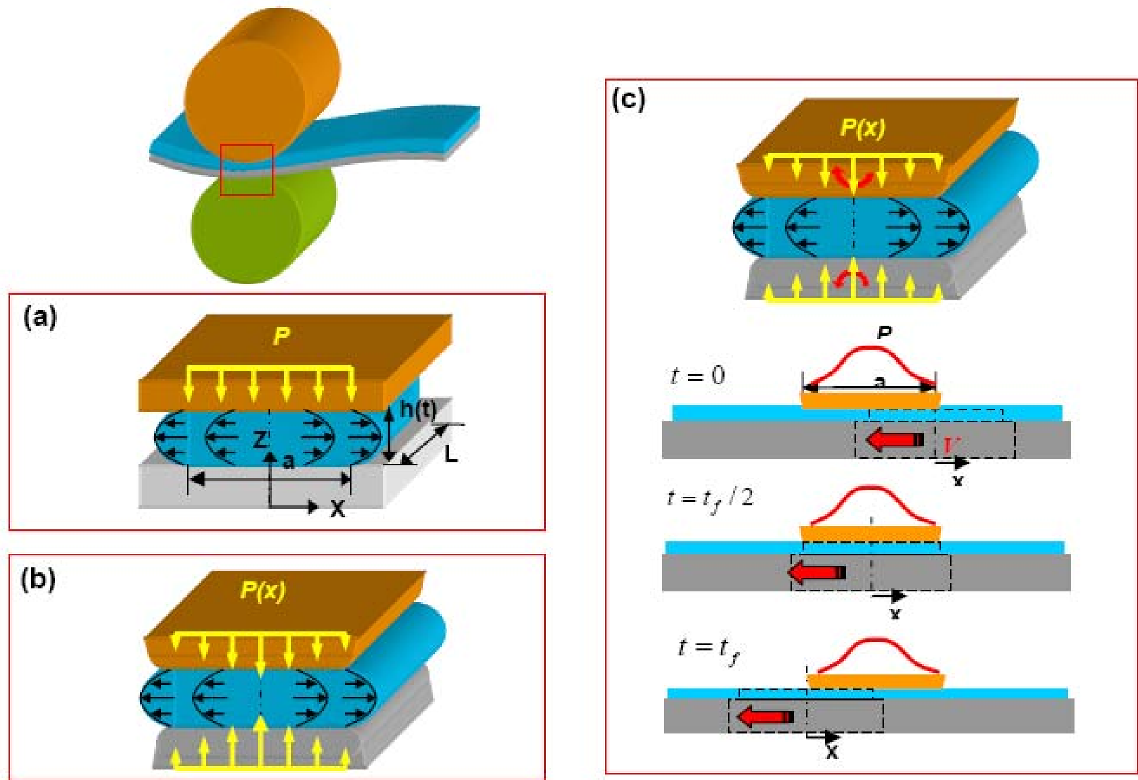

Figure 3.4 Schematic diagram of the liquid resist being squeezed by the contact rollers in (a) *the solid plane squeeze model*, (b) *the elastic roller contact model* and (c) *the dynamic elastic roller contact model*.

To evaluate the three models and to compare with the experimental data, several assumptions will be made. First, in the modeling, we assume 2-D symmetric squeezed flow in z- and x-directions since the sample width, *L,* is much larger than contacting length, ***a***. Second, the initial resist thickness (h_0) is set to 50 µm, which is close to the actual measurement data in our coating system. This assumption is reasonable because the dependence of RLT on the initial film thickness is negligibly small for the force range (50 to 300 N) used in our experiment. In addition, the accumulation of resist material (i.e. increase of h_0) by back-squeezing as a roller moves also has negligible effect on the final

RLT. Because for large h_0, the second term ($\frac{1}{h_0^2}$) in each model in Equations (3-1), (3-3) and (3-5), is negligibly smaller than the first term in the force range used in our experiment. Third, for simple analysis, the contacting length between a roller and backing plate, ***a***, is assumed to be a constant value, 6.5 mm, which is the average measured value corresponding to the force range used in our experiment. Here, ***a*** is measured by the pressure sensing film (Tekscan, Inc.) under stationary condition. Although ***a*** is the function of applied rolling force, its deviation (± 0.3 mm) in the force range of 50 to 300 N is small enough to be neglected. Finally, in each model, we consider 3 % volumetric shrinkage of epoxysilicone resist after UV curing[44] to compare it with the experimental RLT data measured after crosslinking by UV curing. The dynamic viscosity (μ) of epoxysilicone resist is 0.032 $Pa \cdot s$ and sample width, *L*, is 25 mm.

Figure 3.5 shows RLT in each model (*the solid plane squeeze, the elastic roller contact and the dynamic elastic roller contact model*) and the experimental data as a function of web speed (a) and applied rolling force (b). As shown in Figure 3.5a, RLT gets thicker as web speed increases because the pressure engaging time gets shorter. Figure 3.5b shows the expected result that the RLT decreases with increasing rolling force. In both graphs, all three models have similar trends but, *the dynamic elastic roller contact model* has an almost perfect match to the experimental data while the other two static models underestimate the RLTs. This implies that in dynamic R2RNIL process it is important to consider the time-dependant force gradient in predicting the final residual layer thickness. Figure 3.5c, 3.5d, 3.5e show RLT 700 nm period grating pattern in terms of applied roller force of 50 N, 180 N and 240 N, respectively.

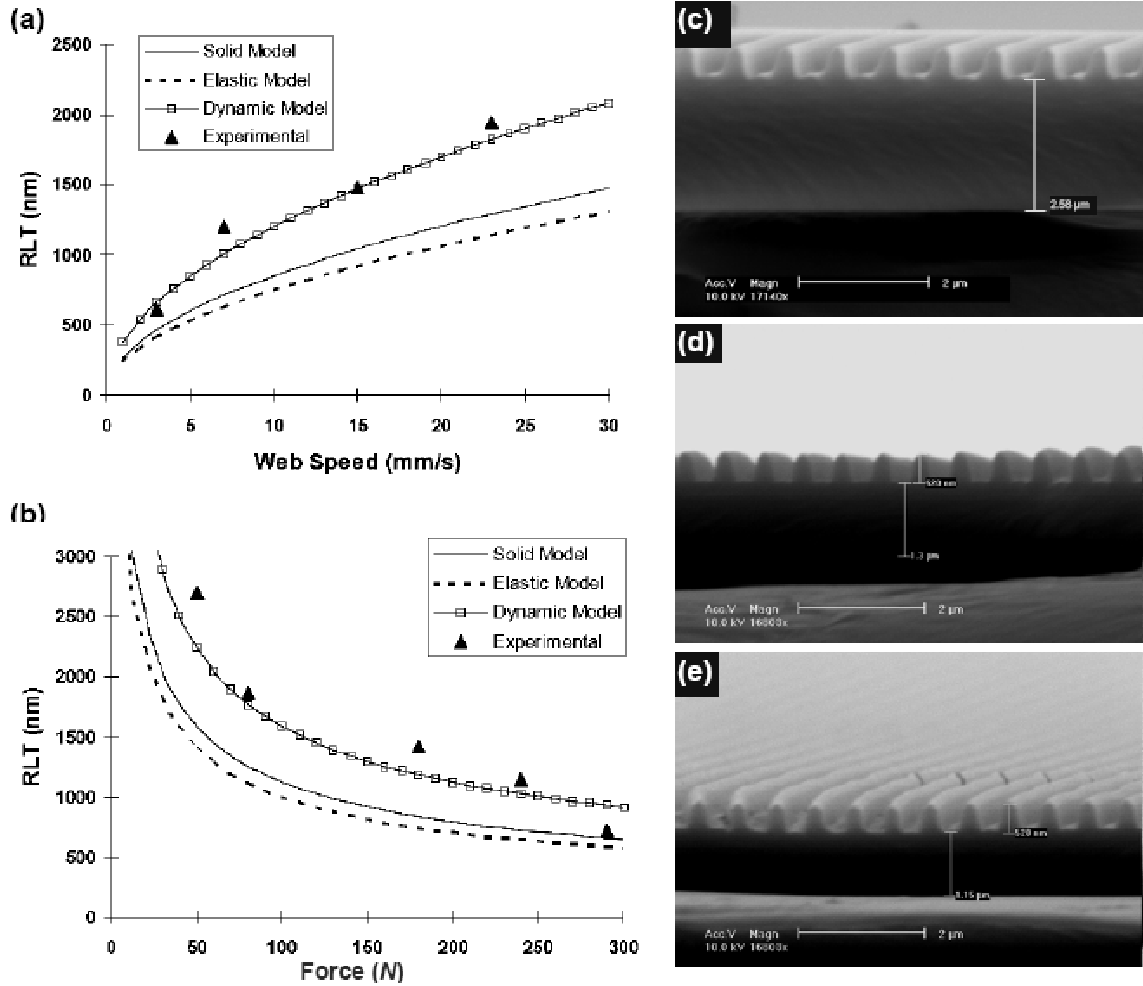

Figure 3.5 The comparison of three models (Solid / Elastic / Dynamic model) for R2PNIL and experimental data (average value of three-time measurement). (a) RLT as a function of web speed with keeping maximum rolling force, 220 N. (b) RLT as a function of maximum rolling force with keeping web speed, 7.94 mm/s. SEM images of (b): (c) 2.58 *µm* RLT for 50 *N* force, (d) 1.3 *µm* RLT for 180 *N* force, (e) 1.15 *µm* RLT for 240 *N* force.

3.3.3 Mold separation analysis

3.3.3.1 Introduction

In R2RNIL process, the imprinted pattern is separated from the flexible mold in a continuous "peeling" manner, which allows much lower separation force to be used as compared to the conventional wafer based NIL. However, in high speed R2RNIL process especially for high aspect-ratio or small trench structures, nano patterns occasionally stick to mold cavity, resulting in demolding failure. Therefore, for high quality nano patterning in continuous R2RNIL process, mold-separation step is very important. As illustrated in Figure 3.6, two different mold pealing methods, that parallel to the gratings and that perpendicular to the gratings, have been tested. It is observed that mold peeling has different aspects according to mold-separation directions with respect to the grating orientation. For the imprinting of 200 nm period grating pattern in R2RNIL process, we observed that "peeling parallel to the grating orientation" provides better pattern quality than "peeling perpendicular to the grating orientation".

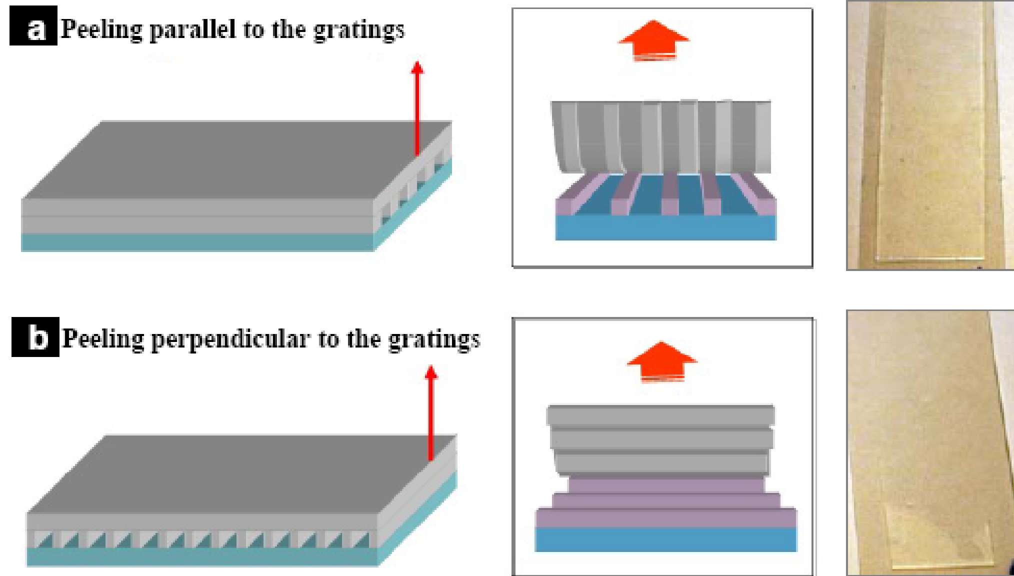

Figure 3.6 Schematic of two different mold separation methods; (a) peeling parallel to the grating orientation and (b) peeling perpendicular to the grating orientation. Right pictures show that "peeling parallel to the grating orientation" provides better pattern quality for 200 nm period grating pattern.

3.3.3.2 Theoretical background

From the point of view of contact mechanics, the mold-substrate separation can be evaluated by considering the interfacial energy between a mold and a polymer resist and the work of adhesion between the two surfaces. The interfacial energy between two materials (1 and 2) can be expressed as,

$$\gamma_{12} = \gamma_1 + \gamma_2 - 2\sqrt{\gamma_1 * \gamma_2} \qquad (3\text{-}6)$$

$$\gamma_1 = \gamma_1^d + \gamma_1^p,\ \gamma_2 = \gamma_2^d + \gamma_2^p \qquad (3\text{-}7)$$

where, γ^d and γ^p are specific type of intermolecular force of disperse and polar components, respectively. i.e. γ^d for the long distance (>0.4 nm) dispersive (non-polar) Lifschitz–Van der Waals interactions and γ^p for the short distance (<0.4 nm) Lewis

acid–base (polar) interactions[64]. The work of adhesion between two surfaces is given by

$$W_{1,2} = \gamma_1 + \gamma_2 - \gamma_{12} = 2\sqrt{\gamma_1 * \gamma_2} \qquad (3\text{-}8)$$

Considering 200 nm period grating pattern in PDMS on the PET substrate that is imprinted by the ETFE mold as illustrated in Figure 3.7, the work of adhesion of each interface has been calculated and summarized in Table 3.1.

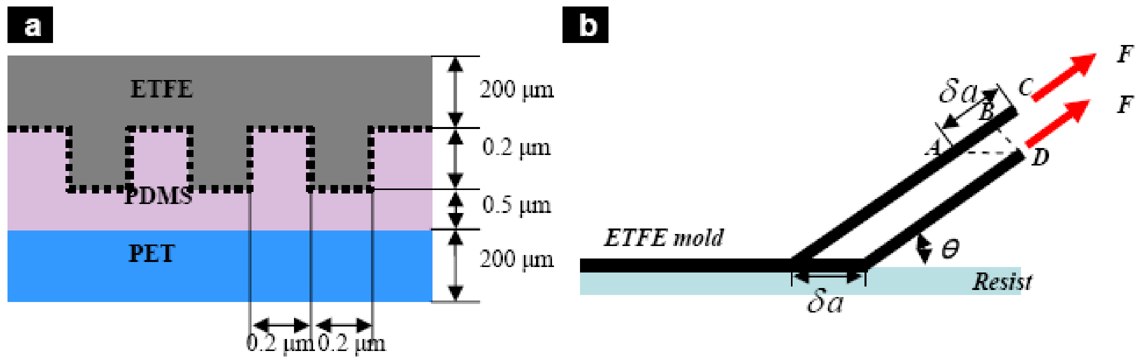

Figure3.7 (a) Schematic illustration of imprinted system used in modeling and (b) the mold separation model

Materials	W(mJ/m^2)
PDMS / ETFE	46.1
PDMS / PET (Untreated)	66.1
PDMS / PET (Air plasma treated, 10 min)	82.8

Table 3.1 Work of adhesion at the interface of two solid materials

3.3.3.3 Modeling and analysis

Assuming inextensible film (ETFE mold) in which strain energy in the film can be ignored, parallel peeling can be modeled as shown in Figure 3.7b. In this configuration the mold separation direction is parallel to the grating orientation, the energy release rate, G, can be denoted as follows.

$$G = \frac{F}{l} \cdot (1 - \cos(\theta)) \qquad (3\text{-}9)$$

where, F is pulling force, l the sample width and the peeling angle.

Since the energy release rate in the parallel peeling method is constant if the puling force and the peeling angle are fixed. Therefore, the mold can be separated from the substrate under smooth peeling action only if the energy release rate is higher than the work of adhesion of ETFE mold and PDMS interface (i.e., 46.1 mJ/m^2).

On the other hand, if the mold separating direction is perpendicular to the grating orientation, the energy release rate, G, varies according to each step of the mold separation from different surfaces of the imprinted patterns because the peeling process can be modeled as crack propagation between the ETFE mold and the PDMS along the rectangular-shape patterned surfaces where the peeling angle varies (Figure 3.8). The calculated energy release rate in each separation step is summarized in Table 3.2.

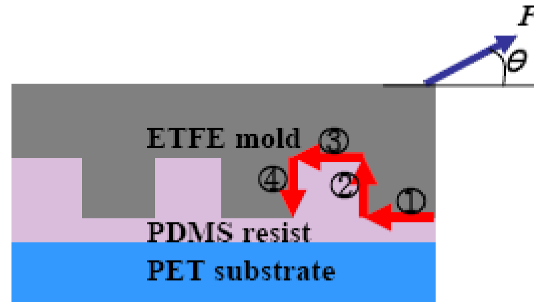

Figure 3.8 Schematic illustration of the perpendicular peeling method.

Step	**G (energy release rate)** [mJ/m^2] ($\theta \le 90°$)	**G (energy release rate)** [mJ/m^2] ($\theta \ge 90°$)
1	$G_1 = P \cdot (1-\cos(\theta)) = \frac{F}{l} \cdot (1-\cos(\theta))$	$G_1 = P \cdot (1-\cos(\theta)) = \frac{F}{l} \cdot (1-\cos(\theta))$
2	$G_2 = P \cdot (1-\cos(\theta+90)) = \frac{F}{l} \cdot (1-\cos(\theta+90))$	$G_2 = \frac{1}{2}\frac{P^2 \sin^2(\theta)}{\overline{E}h} = \frac{1}{2}\frac{F^2 \sin^2(\theta)}{\overline{E}hl^2}$
3	$G_3 = P \cdot (1-\cos(\theta)) = \frac{F}{l} \cdot (1-\cos(\theta))$	$G_3 = P \cdot (1-\cos(\theta)) = \frac{F}{l} \cdot (1-\cos(\theta)$
4	$G_4 = \frac{1}{2}\frac{P^2 \sin^2(\theta)}{\overline{E}h} = \frac{1}{2}\frac{F^2 \sin^2(\theta)}{\overline{E}hl^2}$	$G_4 = P \cdot (1-\cos(\theta-90)) = \frac{F}{l} \cdot (1-\cos(\theta-90))$

Table 3.2 Energy release rate in each step of the perpendicular peeling method

For example, when 20 mm wide ETFE mold is pulled with 0.01 N while keeping the peeling angle at = 30° and 60° respectively, the energy release rate in the perpendicular peeling method is shown in Table 3.2. Clearly the energy release rate is not continuous but has discrete values in each step. For $\theta \le 90°$, step ④ has the lowest energy release rate level, which is smaller than the work of adhesion of the two materials,

indicating no separation between the surfaces. In addition, for $\theta \geq 90°$, step ② has the lowest energy release rate resulting in no pattern generation.

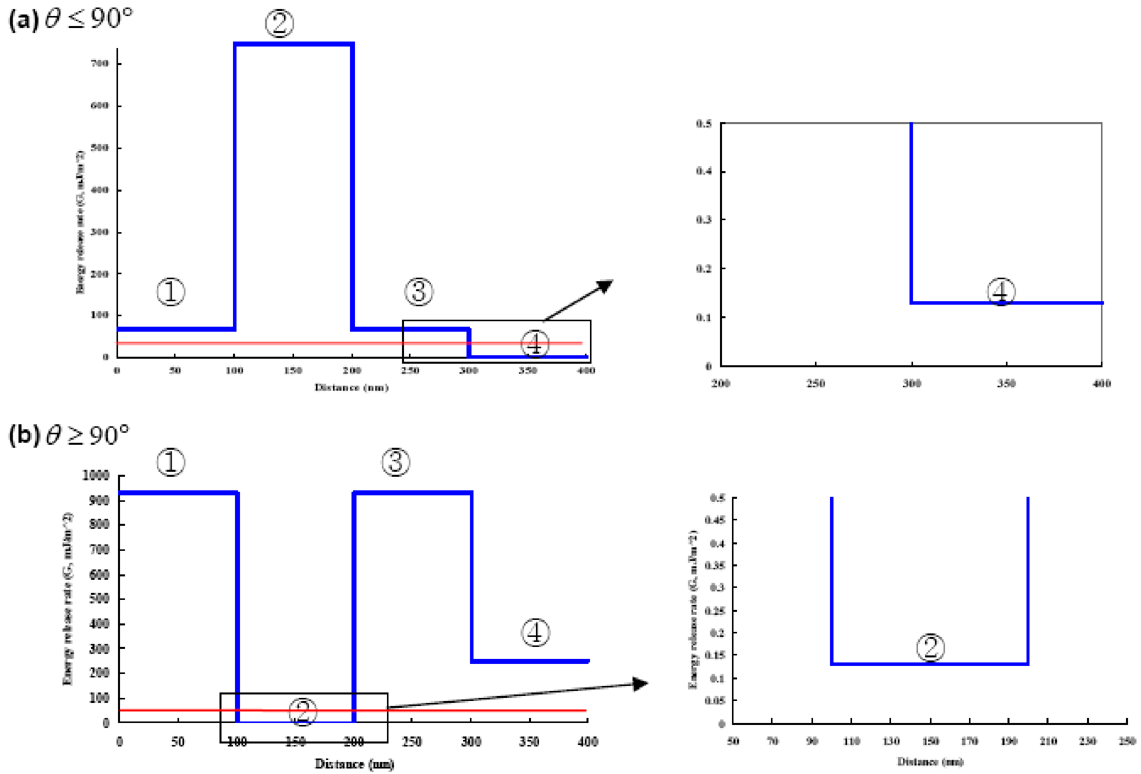

Figure 3.9 Energy release rate of each 4 step in the perpendicular peeling process when pulling force of 0.01 N is applied on 20 mm wide sample. (a) $\theta \leq 90°$ (b) $\theta \geq 90°$. Red line in each graph represents minimum energy release rate (46.1 mJ/m^2) required to successfully separate mold under the given force condition.

To ensure successful separation, higher pulling force can be applied to increase the energy release rate so that it is greater than the work of adhesion between ETFE and PDMS. However, excessive pulling force during the peeling process may generate stress concentration on each corner of the PDMS pattern that is higher than the ultimate yield strength of PDMS, which results in patterning failure. Figure 3.10 shows the finite

element analysis result representing stress distribution in the perpendicular peeling. In this analysis, the right upper corner of the mold is raised by 20 nm to separate from resist. As in Figure 3.9a, the energy release rate in step (4) is very low, therefore, it requires higher pulling force. However, as shown in Figure 3.10, the maximum stress higher than the fracture stress of resist material (2.24 Mpa) may be applied in step (4-1), (1-2) and (2-3) which causes fracture of the resist material (PDMS) before mold separation. Therefore, for successful demolding in the perpendicular peeling configuration, the pulling force should be higher than the critical force to ensure that the energy release rate is larger than the toughness of the material, but should be kept within certain level to avoid the fracture of the imprinted resist patterns. In summary, different from the peeling parallel to the gratings where the energy release rate is constant, the perpendicular peeling has discrete energy release rate in each step, which should be carefully considered to prevent failure in mold-sample separation.

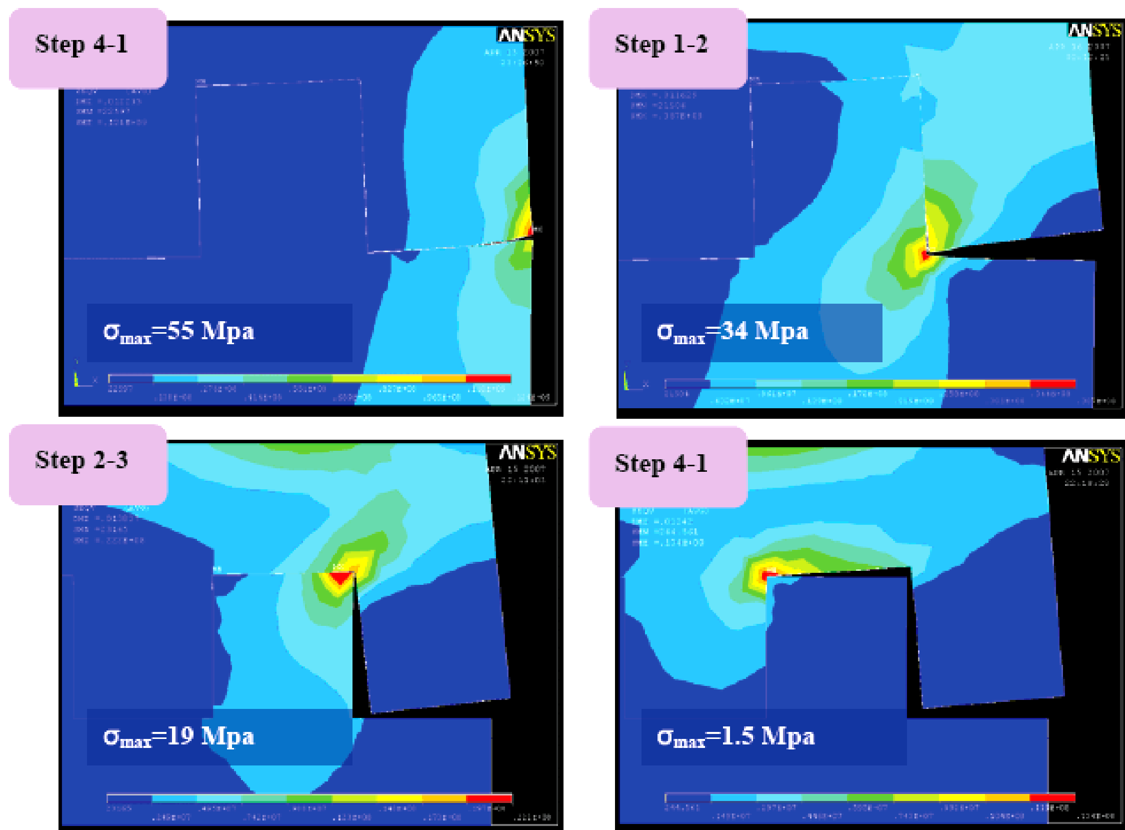

Figure 3.10 FEM illustration of stress distribution in the perpendicular peeling method. Stress is concentrated on each corner during the mold separation in which case the upper right corner is raised by 20 nm.

3.3.4 Large-area semi-transparent metal electrode for organic solar cell application

As an application of large-area R2RNIL, we demonstrated the fabrication of semi-transparent metal electrode that can potentially replace current ITO layer in organic solar cells[8, 65]. To demonstrate this possibility, an attempt was made to fabricate nanoscale metal (e.g. Au) gratings on large area PET substrates using roll-to-roll process. Figure 3.11a shows the schematic of a continuous R2RNIL process. For this work, surfactant treated UV curable epoxysilicone patterns[44] with a period of 700 nm and duty cycle of

about 50 % on PET substrate were used as a flexible mold (3.11b) and then 40 nm thick Au film were deposited on them. Au films on protrusions of the mold were transferred onto half cured UV epoxy layer on PET substrates as shown in Figure 3.11a. Figure 3.11a and 3.11b shows the SEM image and the photograph of Au nanogratings on PET substrate fabricated by R2R NIL process. As shown in Figure 3.11d, large area (32 mm x 184 mm) Au nanogratings were successfully fabricated. This result implies that the fabrication of the nanopatterned metal electrode can be easily extended to R2RNIL process, which would help realize low cost, large area transparent electrode.

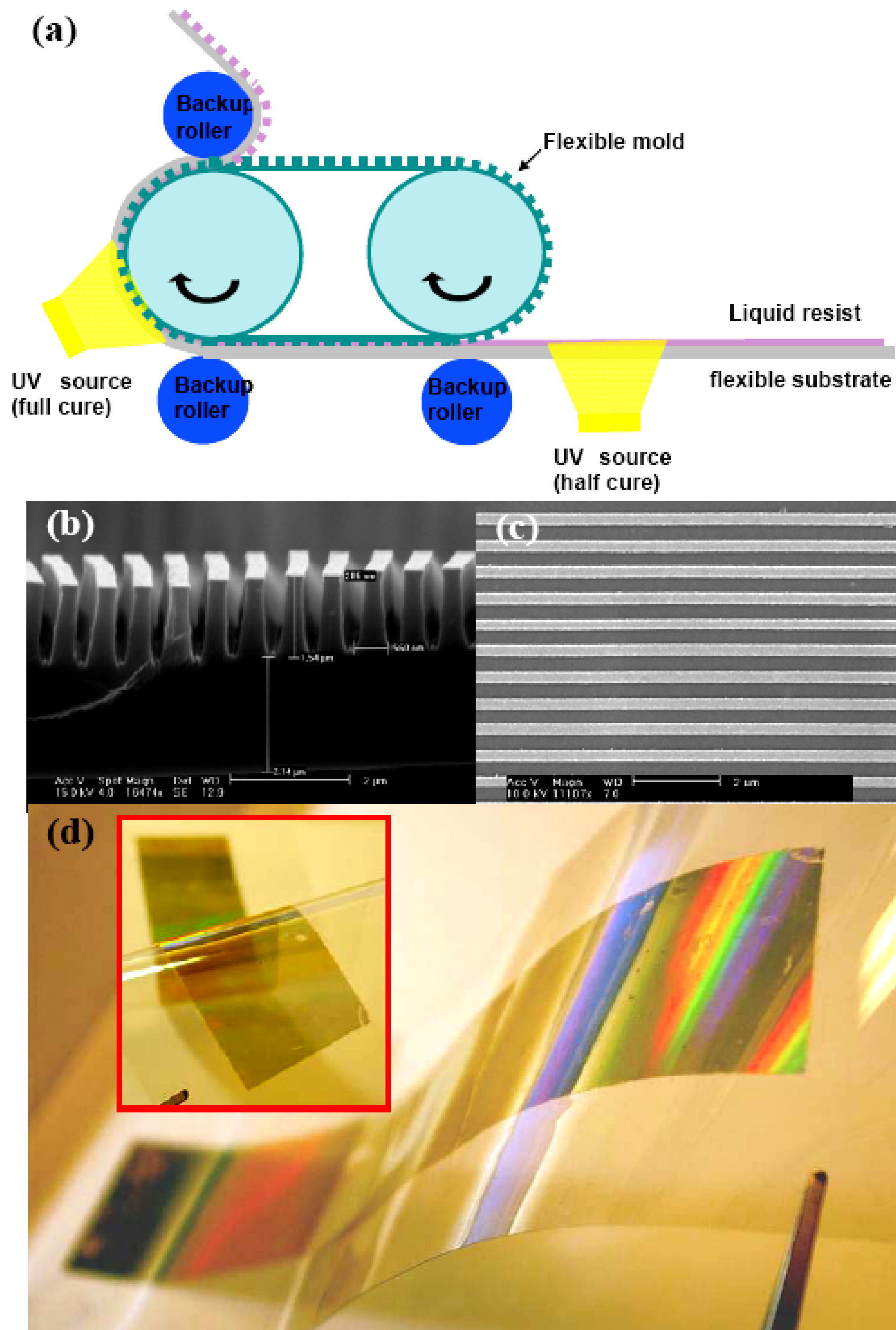

Figure 3.11 (a) Schematic of R2R NIL process. SEM images of (b) epoxysilicone mold and (c) transferred Au nanograting on PET substrate. (d) Photograph of large area (32 mm x 184 mm) Au nanogratings on PET substrate. Inset photograph shows the transparency of Au nanogratings fabricated.

3.3.5 Roll-to-roll fabrication of morphology-optimized bulk heterojunction polymer solar cells

Recently, we introduced a novel route to fabricate polymer solar cells that allows high-throughput roll-to-roll process [66, 67]. The essence of this approach is to utilize a gas-permeable cover layer for solvent evaporation that simultaneously protect the otherwise free surface and induce shear flow of the blend solution by an applied pressure. This process not only leads to optimized morphology having more uniform distribution and high crystallinity of the components favorable for charge generation and transportation that cannot be achieved by conventional thermal annealing (TA) and solvent-assisted annealing (SAA) methods[68, 69], but also is applicable to high-speed dynamic process which is ultimately demonstrated in a roll-to-roll process while preserving high device performances

In the part of polymer solar cell fabrication, we used a roll-to-roll NIL apparatus[30] to coat P3HT:PCBM polymer blend with uniform thickness and fast solvent evaporation in a continuous fashion (Figure 3.12a). In this work, a gas-permeable silicone film is covered on a tensioned belt, instead of EFTE flexible mold used in R2RNIL[30]. Figure 3.12b shows 3 inches wide uniform BHJ active layer film made of P3HT:PCBM blend on ITO coated PET substrate using the continuous roll-to-roll process. After 1 min baking, the deposition of LiF and Al cathode complete final devices.

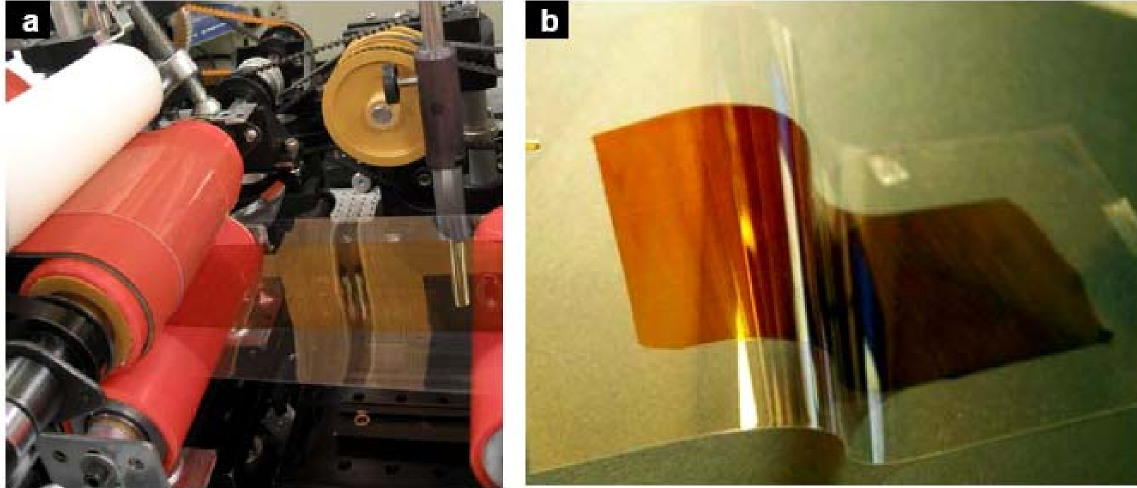

Figure 3.12 (a) A photograph of the roll-to-roll apparatus and (b) the resultant flexible polymer solar cell before electrode deposition.

3.4 Summary

We have demonstrated large-area (4” wide) imprinting of 300 nm linewidth grating structures on either hard or flexible substrate by developing a new apparatus capable of both R2RNIL and R2PNIL process with greatly enhanced throughput. In addition, we developed a more accurate model by taking into account the time-dependent pressure distribution for predicting the residual layer thickness as a function of the web speed and the rolling force in a dynamic R2RNIL process. We also verified the characteristics of each mold separation method, parallel/perpendicular to the grating orientation, by performing mold separation analysis. Additionally, the fabrication of semi-transparent metal electrode and P3HT:PCBM polymer blend coating with enhanced crystallinity for organic solar cells have been demonstrated as applications of R2RNIL.

Chapter 4

Direct Metal Imprinting (DMI)

4.1 Introduction

Many practical applications in optics and flat-panel displays demand nano-scale metal gratings rather than that in polymers due to high electrical conductivity and typical optical properties in metal nano wires such as localized surface plasmon resonance (LSPR). However, direct patterning of submicron metal structures in a reasonably large size is very difficult because general metals have high modulus at room temperature and they require very high temperature to have enough mobility to be molded. Therefore, other alternative methods relying on lithography followed by metal depositing or electroplating have been commonly used to form metal nano structures. However, they also require many additional processing steps such as non-isotropic etching or lift-off process to finalize metal structures, which costs a great portion of a total production expense and a processing time. To overcome these drawbacks, many different approaches for direct metal patterning have been explored. Kim et. al. used "cold-welding" to add or subtract defined metal layer to/from the substrate and demonstrated organic electronic devices using this technique[70, 71]. Pre-deposited metal on the patterned stamp was transferred to other substrates by micro-contact printing (μ-CP) for organic photovoltaic devices[8, 9, 72]. More aggressively, direct imprinting of nickel substrates using a

diamond stamp has been demonstrated, which realized sub-10 nm line patterning in a simple way[73]. However, it requires very high pressure (c.a. 400 Mpa), and consequently all diamond stamps have been fractured after completing process. Moreover, this process generates very shallow indented lines rather than discrete metal gratings.

We present a simple nanopatterning technique to directly create discrete metal gratings using Si mold at relatively low pressure. Direct Metal Imprinting (DMI) uses polymer cushion layer between thin metal film and hard substrate, which enables room-temperature nanoimprinting of metal layer by overcoming troublesome hard-to-hard surfaces contact. In this work, we demonstrated direct patterning of 350 nm linewidth gold gratings on various polymers as a cushion layer.

4.2 Principle of DMI

DMI was inspired by the work on the transparent metal electrode fabrication[8] but, can be expanded to many applications requiring nanoscale metal patterning with simple and continuous process. Figure 4.1 illustrates DMI process and optional metal pattern transferring process. First, polymer cushion layer and metal layer were coated on a hard substrate. For metal patterns on flexible substrate, simply metal layer is coated on flexible plastic substrate. Second, Si mold gets in contact to the substrate and pressed. After demolding, metal gratings are generated by cutting or indenting on selectively pressed metal layer. Optionally, DMI metal gratings can be simply transferred to another hard or flexible substrates for further applications[8, 9]. Direct metal imprinting without a polymer cushion layer requires extremely high pressure, which occasionally results in the

damage of a mold[73]. In addition, it would be very difficult to achieve conformal surface-to-surface contacting between hard materials. A polymer layer used in DMI can effectively reduce imprint pressure and ensures conformal contacting when a Si mold engages.

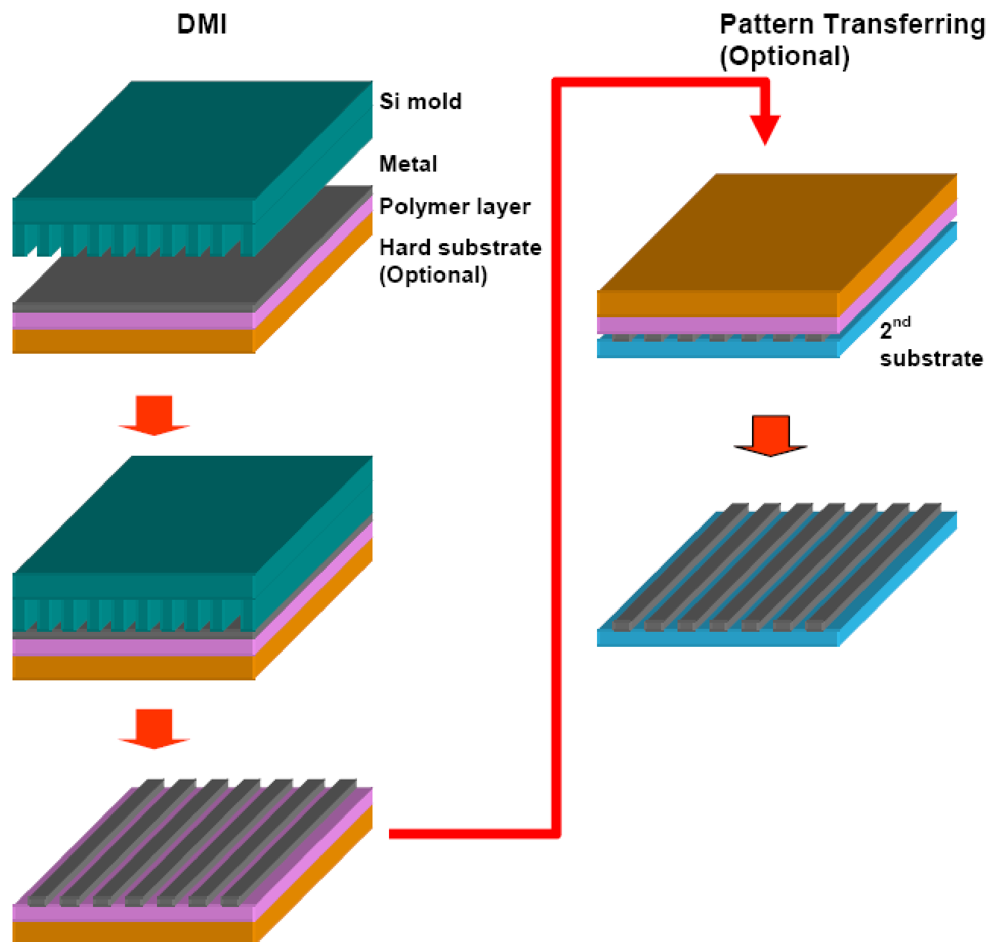

Figure 4.1 Schematics of Direct Metal Imprint (DMI) process. Optional metal transferring process to the second substrate can be done after DMI.

4.3 Results and discussion

As fore mentioned, a polymer cushion layer supporting the metal film is a key element in DMI process for successful direct metal patterning preventing mold damage. Therefore, mechanical properties of the polymer, such as modulus, affect a great deal on DMI patterning. In that sense, four polymers (Polydimethylsiloxane (PDMS, E = 2.4 MPa), Polyurethane (PU, E = 500 MPa), Polycarbonate (PC, E = 2.0 GPa) and Poly(methyl methacrylate) (PMMA, E = 3.0 GPa) have been evaluated as a cushion layer material that is sandwiched by a 50 nm gold film and a Si substrate. As shown in Figure 4.2a-d, PMMA having the higher modulus (3 GPa) provides the better gold grating formation in 700 nm period overall area (1 cm by 1cm), while a soft PDMS layer shows non-uniformly fractured metal lines. This is because too soft material such as PDMS can not support thin gold film but bulk PDMS deforms by a distributed contacting pressure from a Si mold (Figure 4.2a). On the other hand, in high modulus polymer, the pressure from the extruded part of a mold is much localized on the metal surface and, therefore, clearly discrete metal gratings can be generated as shown in Figure 4.2d.

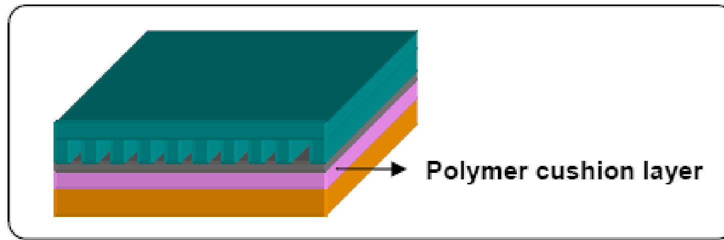

a. PDMS (E = 2.4 MPa)

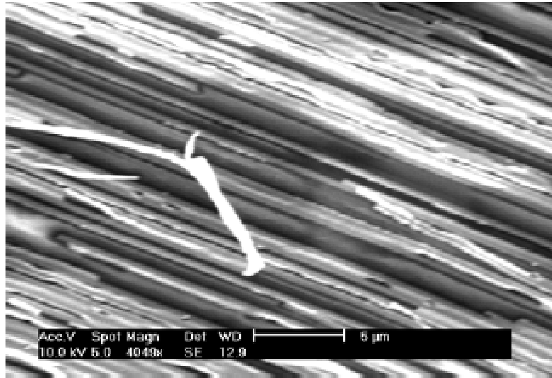

b. Polyurethane (E = 500 MPa)

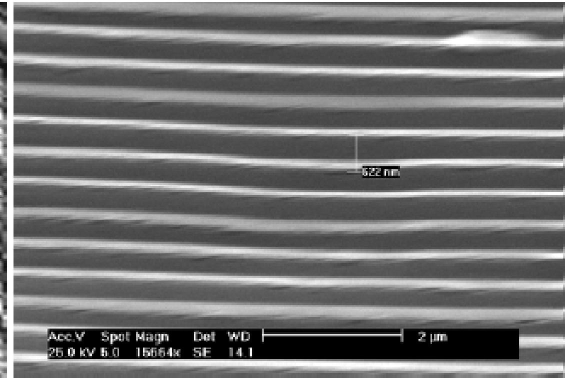

c. Polycarbonate layer (E = 2.0 GPa)

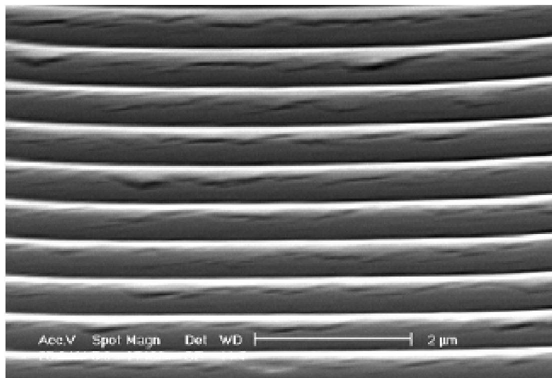

d. PMMA layer (3.0 GPa)

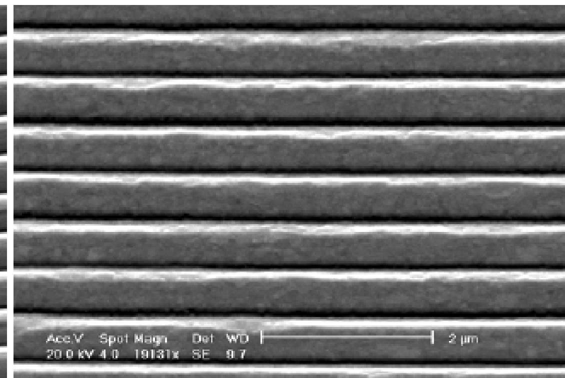

Figure 4.2 Figure 4.2 Effect of the modulus of polymer cushion layer on DMI patterning. (a) Polydimethylsiloxane (PDMS, E = 2.4 MPa), (b) Polyurethane (PU, E = 500 MPa), (c) Polycarbonate (PC, E = 2.0 GPa), (d) Poly(methyl methacrylate) (PMMA, E = 3.0 GPa) as a cushion layer, respectively. 50 nm thick gold is coated on each polymer layer on the Si substrate. 20 MPa pressure.

The shape of the metal pattern by DMI also depends on the mold geometries. DMI pattern by using a flat-end mold (Figure 4.3a) produces very shallow indentation as the tip shape of the mold (Figure 4.3a-1), while the same process using a sharp-end mold

(Figure 4.3b) results in discrete, chevron-like gold gratings (Figure 4.3b-1) under the same applied pressure, 20 MPa. As supported by a finite element simulation in Figure 4.3a-2 and b-2, actual contacting pressure in DMI using the sharp-end mold is much higher than that of the flat-end mold, and the gold film is deeply indented and cut into a polymer layer underneath to form the final structure shown in Figure 4.3b-1. Such nano wires possessing tiny gaps (c.a. 50 nm) can be used as a etching mask in an RIE process to create narrow nano metal wires as the width of original trenches. Etching the underlying polymer layer followed by a metal deposition and lift-off can create narrow metal lines.

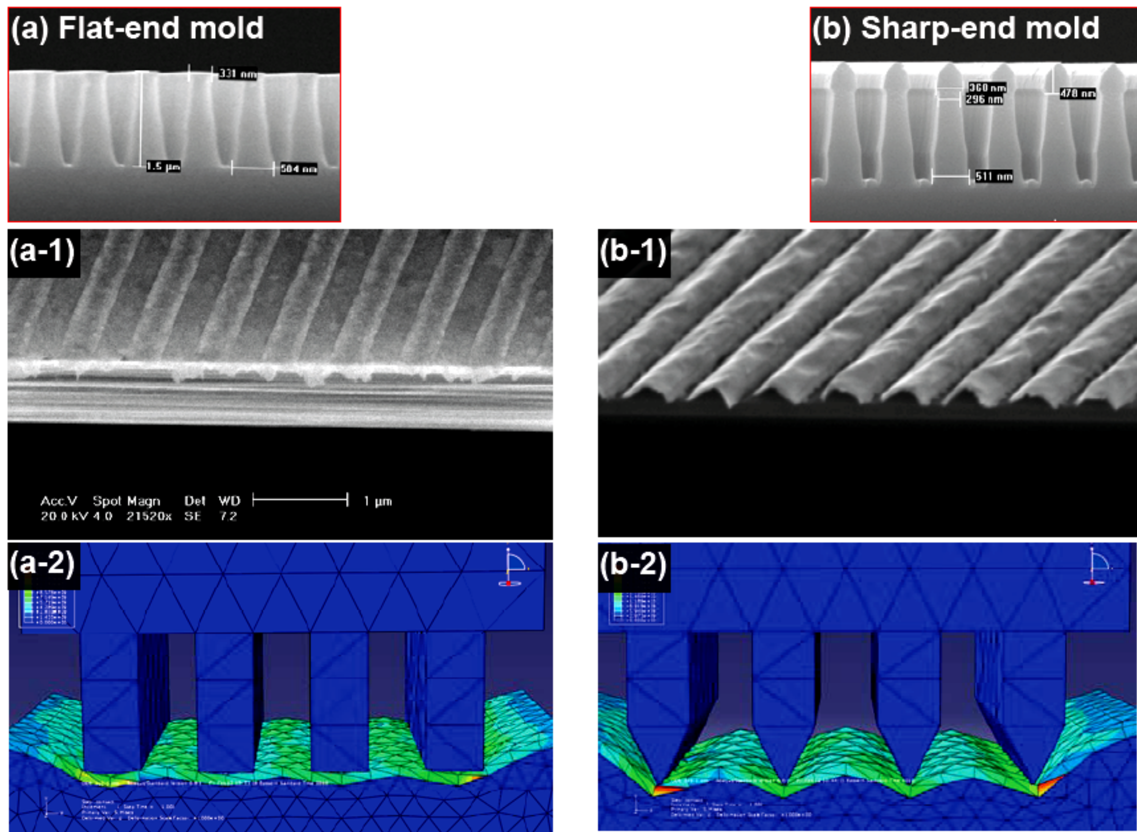

Figure 4.3 SEM images of the Si molds with different tip-geometries (a, b) and the resulting 700 nm period, 50 nm thick gold nano patterns by DMI (a-1, b-1) using each mold respectively. Applied pressure is 20 Mpa. (a-2, b-2) Finite element analysis supporting each DMI result under the same pressure condition but using different geometry of mold (a, b).

For further applications that require wide spacing between metal lines, we suggested a simple technique illustrated in Figure 4.4a. We first fabricated DMI pattern (Figure 4.3b) on flexible PET substrate (100 μm) and then, bent it perpendicular to the grating direction with heating. A convective heat air gun was used to heat up sample at 150 °C, which is higher than Tg of the cushion layer, PET. The top surface of the sample where there are metal gratings subjects to a tensile strain with respect to the neutral line when it is bent. Space increases when backing polymer stretches while keeping the metal width unchanged. Figure 4.4b shows SEM image of gold grating pattern created by this process. Initial 700 nm period gratings done by DMI have a space of 50 nm (Figure 4.3b), but after heated bending, the spacing becomes 180 nm, which is over 250 % increase. Interestingly, the increase in trench size is much larger than a theoretical value, and that increase is mostly due to the shrinkage of metal line width. This is probably because the thermal effect (heating and cooling cycle) may result in geometry change of metal gratings (i.e. folding). It needs further study for clear verification.

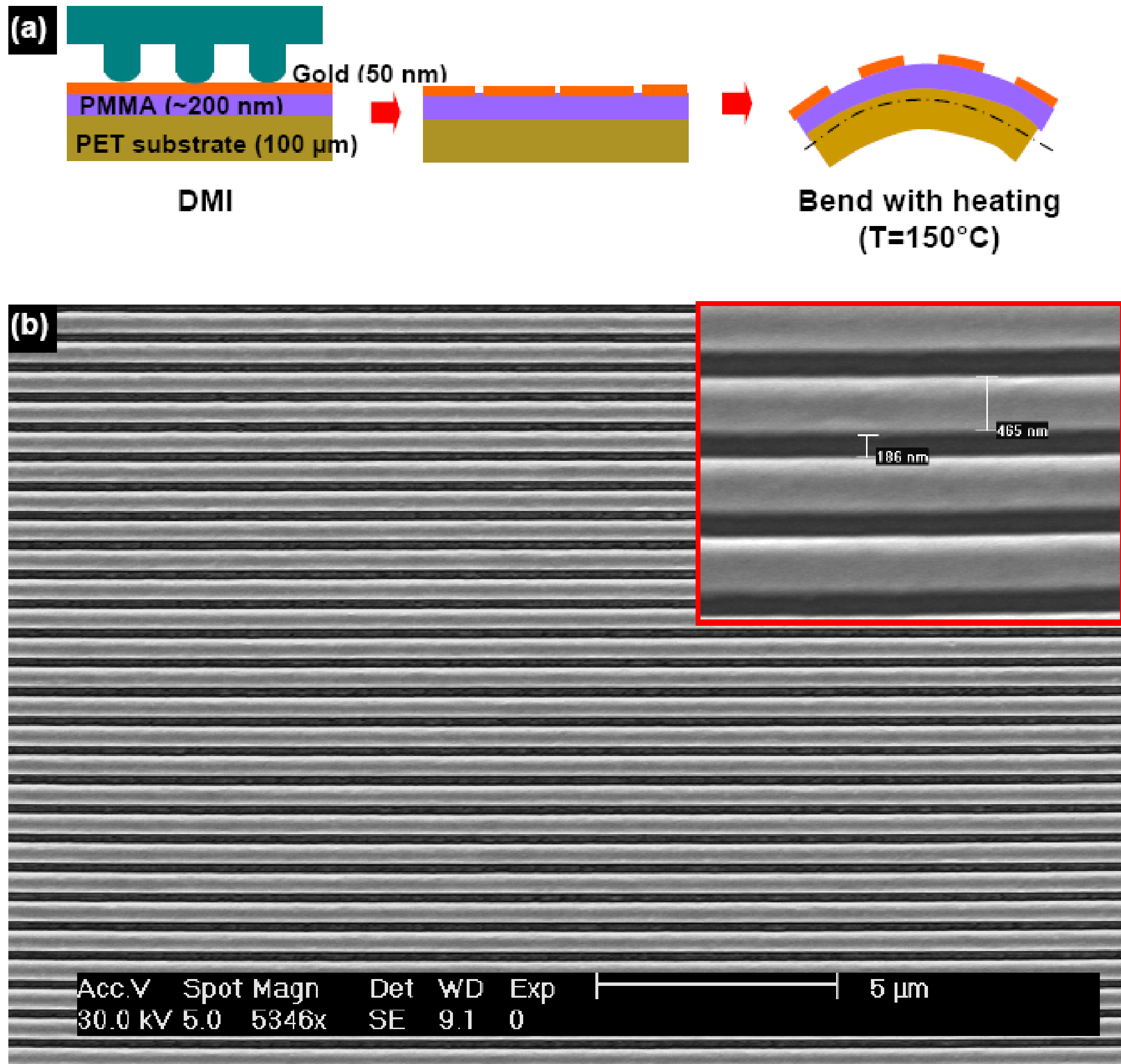

Figure 4.4 (a) Schematics of the space-enlarging process, DMI followed by bending with heating. (b) SEM image of 700 nm period DMI pattern after space-enlarging process showing 250 % increase in space (186 nm).

4.4 Summary

A simple way to directly create nano scale metal gratings has been demonstrated, which can drastically reduce processing steps compared to lithography induced processes. In DMI process, a polymer cushion layer placed under a metal film effectively reduces

imprint pressure and helps to form discrete metal gratings with conformal contact. The shape of patterned metal gratings is depending on the polymer cushion material and mold geometries. Once metal gratings with tiny space are fabricated by DMI, we can enlarge the space using a simple heat assisted stretching method. Nano metal gratings fabricated by DMI can be utilized in transparent metal electrodes, optical polarizers and biosensor applications with much simplified processing steps.

Chapter 5

Dynamic Nano-Inscribing for Continuous and Seamless Metal and Polymer Nanogratings

5.1 Introduction

The increasing demands for nano-scale grating and channel structures in optics and bio-industries have stimulated many emerging technologies such as laser interference lithography, nano-ruling and nanoimprint lithography (NIL)[17, 46, 74]. However, the current process and throughput in NIL (on the order of a few minutes per wafer) is still far from meeting the demands of many practical applications, especially in photonics, biotechnology, and organic optoelectronics. Recently R2RNIL was developed to provide much improved throughput while preserving nanoscale resolution[29, 30]. However, its UV or high temperature heating process may damage sensitive resist materials and, there is an unavoidable seam region where the two ends of the flexible mold meet on the roller, which interrupts the otherwise continuous patterns. In addition, it is very difficult to fabricate the large area original imprint molds that are used to replicate the flexible stamps for R2RNIL. We present a Dynamic Nano-Inscribing (DNI) technique for directly creating large-area, truly continuous nano-grating patterns in a variety of metal or polymer materials with feature size down to sub-50 nm and at very high speed (10 cm/sec)[75]. DNI is carried out under either ambient temperature or with a brief heating

time on the order of ten microseconds, which minimizes damage on UV or thermo-sensitive functional materials. We also demonstrated future applications of DNI process into the simple, one-step fabrication of split-ring resonator (SRR) structures for negative index materials.

5.2 Principle of DNI

In this work, we introduce a Dynamic Nano-Inscribing (DNI) technique that offers drastically increased throughput and with nanoscale resolution, while provides continuous and seamless grating patterns at ambient condition or with very short time heating. Using DNI, we demonstrated high-speed nanopatterning of metals and several important functional polymers, and also illustrate its versatile use in producing free-form array patterns and patterning over curved surfaces. Figure 5.1a illustrates the mechanism of the DNI process to create metallic nanopatterns on a polymer substrate. DNI uses the sharp edge of slightly tilted cleaved Si mold to directly inscribe on a moving substrate, thereby creating seamless micro- and nanopatterns in a continuous fashion. DNI shares similarities with room temperature nanoimprinting and relies on the plastic deformation of the inscribed material. However, contrast to nanoimprinting, the deformation in DNI takes place under gradually increased pressure over a very small contacting region where the sharp edge of tilted Si mold engages. As a result, continuous linear patterns with infinite length on various polymers, metals or even hard materials such as ITO can be successfully created by using very low applied forces (several Newtons), and with a speed drastically faster than other nanopatterning techniques. The DNI process can be separated into four sequential steps as depicted in Figure 5.1a. First, in region (1), the

mold makes the initial contact with the substrate material to be inscribed. Second, in region (2), the polymer layer is imprinted with gradually increased pressure as the Si mold moves. Third, in region (3), the sharp edge of the cleaved Si mold, is where most of the plastic deformation occurs since the pressure is the highest at this region. Finally, in the elastic recovery region, (4), the pressed polymer recovers by a certain amount and determines the final geometry. Note that throughout the whole DNI process, the metal layer still remains on top of the imprinted polymer film without being removed, which supports the plastic deformation as the pattern formation mechanism rather than material removal. There are several important properties a substrate material must possess for a successful DNI process. Since DNI relies on the plastic deformation of the polymer material, materials with lower modulus are preferred to achieve large deformation under a given applied force. Toughness is another very important property in DNI. Material having a low toughness can be easily fractured by the sharp edge of the Si mold and generates debris during the DNI process; and the accumulated debris further hampers the inscribing process. Therefore, materials with sufficiently high toughness are preferred for faithful and debris-free pattern formation. The optional elastomeric cushion layer underneath the inscribed polymer is to ensure conformal contact between the substrate and the edge of the Si mold that is not perfectly flat, but having terraces that is resulted from the cleaving step. DNI can create debris-free nanoscale gratings without causing mold damage because it employs a large negative rake angle ($\boldsymbol{\alpha<0}$) in the process, which means the mold is almost parallel to the substrate surface, like in nanoimprinting. In general mechanics, a negative rake angle has low material removal capability but provides better mechanical stability for the brittle tool materials such as ceramic or

diamond[76]. DNI utilizes both characteristics from a negative rake angle to create continuous nano gratings without generating debris nor damaging mold. The cross sectional profile of the metal nano gratings created by the DNI process depends on the end shape of the mold grating structure. As shown in Figure 5.1b, when a Si grating mold with a flat-tip is used, the metal layer deforms and follows the shape of the inscribed polymer pattern and forms continuous metal gratings. On the other hand, when the metal layer is inscribed by a mold with a sharp-tip, the metal film breaks at the midpoint where it meets the tip of the mold tip. As a result, metal lines with discrete metal caps are formed on top of the inscribed polymer gratings (Figure 5.1c).

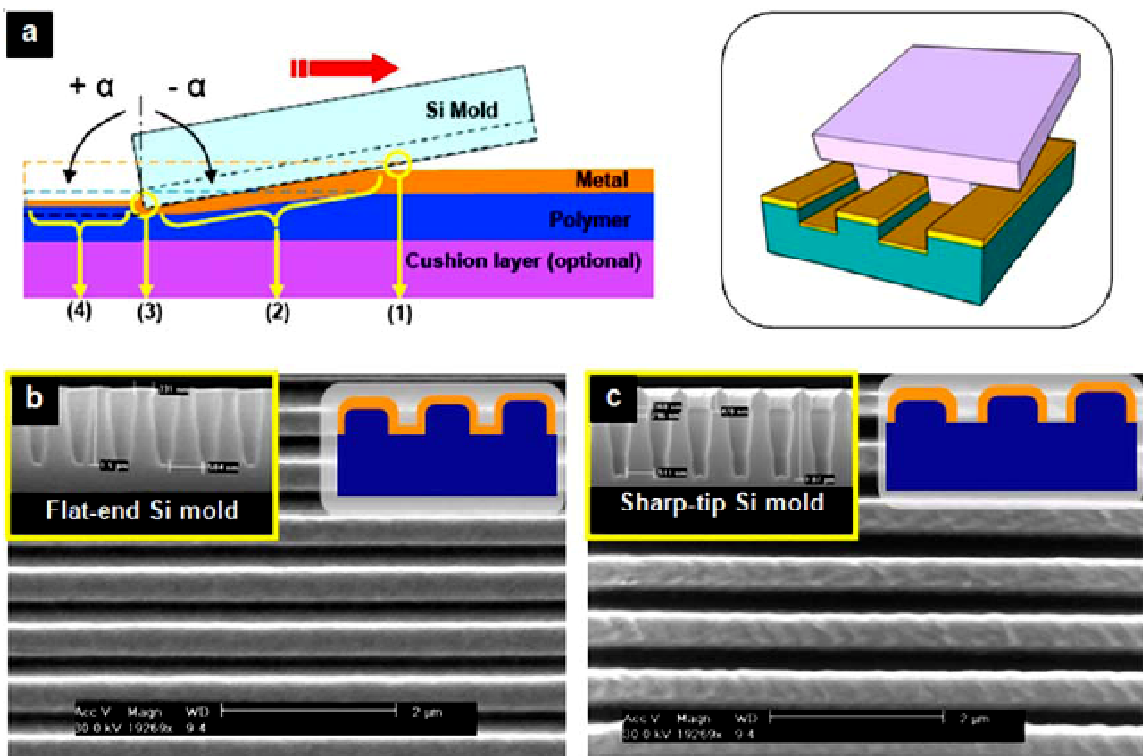

Figure 5.1 (a) Schematics of the DNI process for creating metal nano gratings. (1) Initial contacting point, (2) Gradual imprinting region, (3) Edge point responsible for plastic deformation and (4) Elastic recovery region. (b, c) SEM images of the Si molds with two different tip geometries (flat-end, sharp tip) and the resulting silver nano gratings inscribed by each mold respectively.

5.3 Experimental details

Experimental setup for DNI is shown in Figure 5.2. A slice of cleaved Si mold is mechanically clamped by a static holder that is tilted with adjustable angle to a 5-DOF stage where the substrate is placed. The contacting force between the mold and the substrate is controlled by z-direction micro-stage and monitored by a flexible force sensor (Tekscan. Inc). The substrate is inscribed as the stage moves in x-direction. For roll-to-roll DNI, the substrate is continuously inscribed at the roller surface by tilted Si mold. Web speed is controlled by an AC motor controller (Figure 5.2c). For localized heating assisted DNI (LH-DNI), the Si mold is directly heated by a heating element with temperature controller (Figure 5.2c, HOTSET Inc.) during inscription.

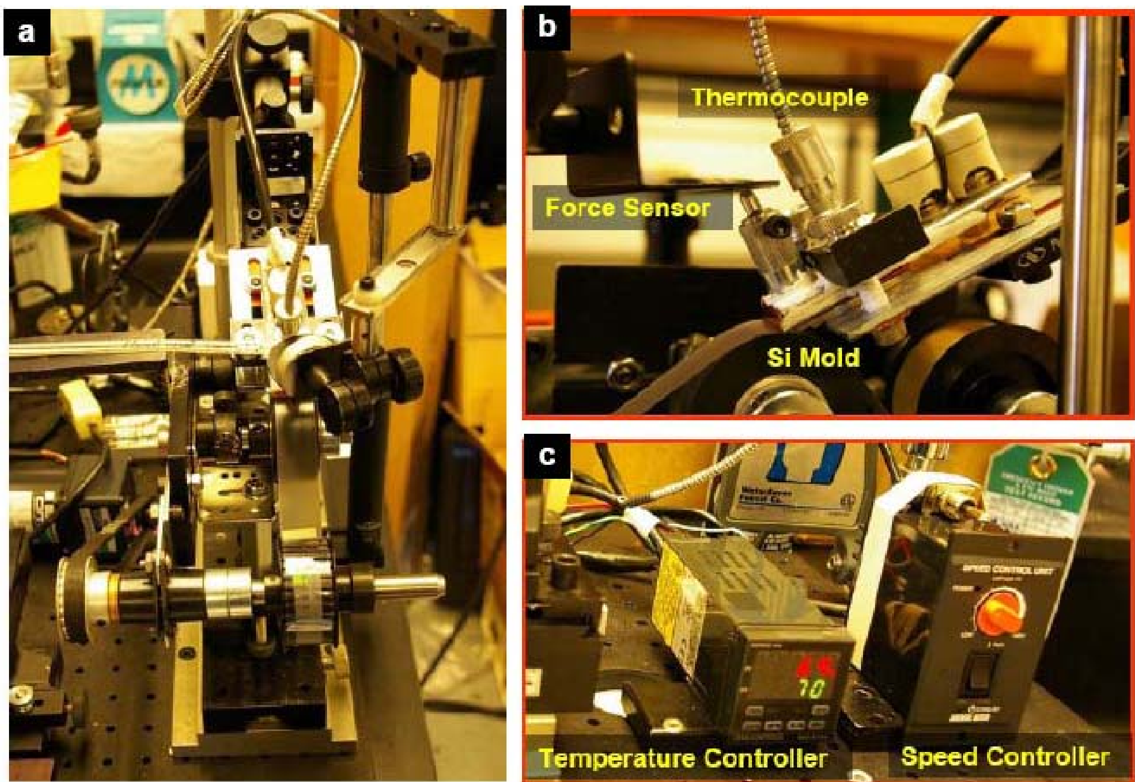

Figure 5.2 (a) Experimental setup for DNI. (b) Inscription part composed of heater attached tool holder, thermocouple and force sensor. (c) Temperature controller and web speed controller

5.4 Results and discussion

5.4.1 DNI on metals

DNI can proceed in straight linear fashion or in free forms by changing the substrate moving direction with respect to the orientation of the mold grating. Figure 5.3a shows angled but continuous 200 nm period gratings that were created by sharply turning the substrate during the room-temperature DNI process (RT-DNI). Such a feature is impossible to achieve by the regular NIL process using a linear grating mold. Figure 5.3b represents square-shaped gold nano-patterns fabricated by two consecutive DNIs carried out in orthogonal directions. DNI is not limited to only polymeric and ductile metallic materials. Direct inscribing of much harder materials, such as conductive Indium Tin Oxide, ITO, is also successfully demonstrated by RT-DNI. Figure 5.3c shows 700 nm period nano gratings directly created on an ITO-coated PET substrate. ITO is a very hard material having a modulus of 97 GPa that is slightly smaller than that of Si. Therefore, it is very difficult to directly pattern on ITO surface by conventional fabrication techniques, however, DNI provides a unique solution for ITO nano patterning.

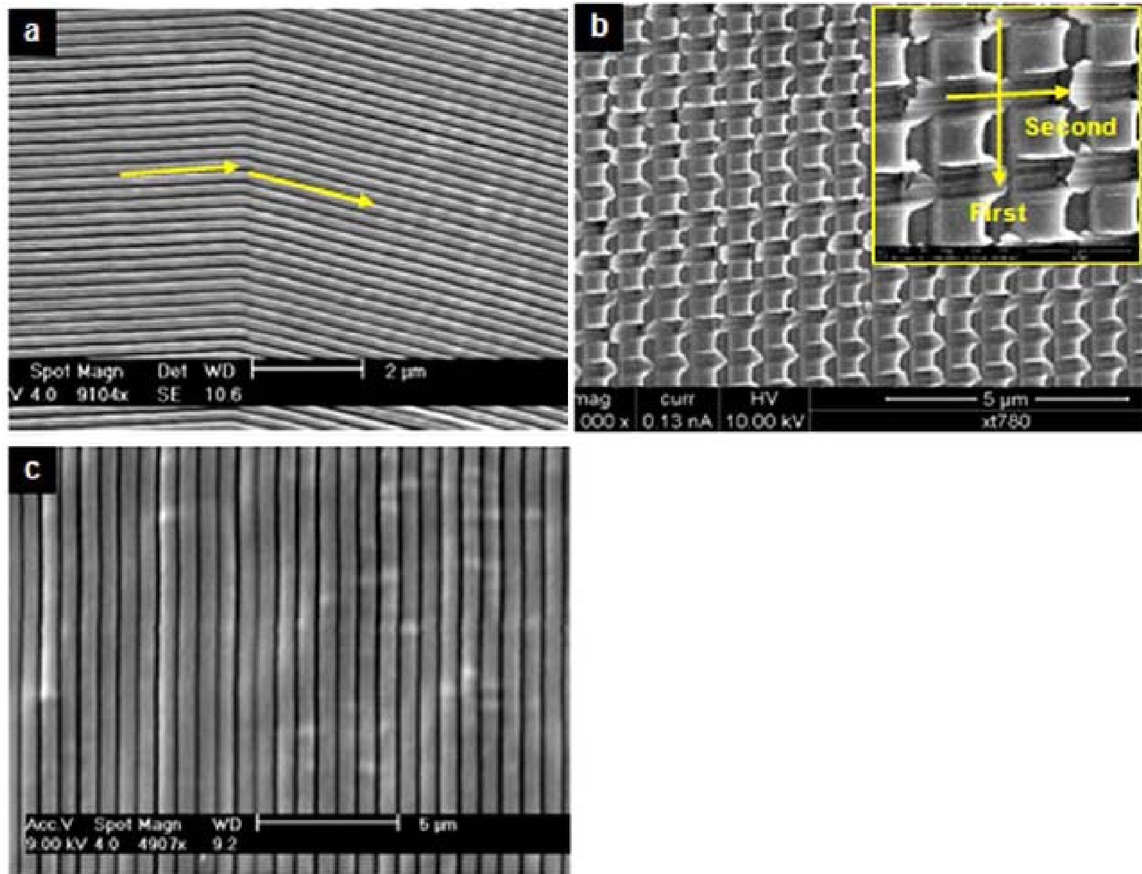

Figure 5.3 SEM images of (a) continuous 200 nm period gold gratings by DNI with sharp turns, (b) Square-shaped gold nano-patterns fabricated by two sequential DNIs in orthogonal directions, and (c) 700 nm period grating directly fabricated on ITO surface.

5.4.2 DNI on plastics

Roll-to-roll printing technique can offer high-speed patterning in a continuous fashion. But roller based printing technology generally requires a very large-area flexible mold to wrap around a roller surface, and at least one seam per revolution exists where the two ends of the flexible mold meet. However, DNI can generate essentially infinitely long and seamless grating pattern by using just a small slice of a cleaved Si mold. This feature could find potential applications, e.g. in large format displays and for creating long polymer nanofibers. In this respect, a high speed roll-to-roll process can fully take

the advantages offered by DNI. Figure 5.4a shows a 22 inch long, half inch wide, 700 nm period, seamless nano-grating pattern created on a polycarbonate strip using roll-to-roll DNI. The inset (Figure 5.4b) shows the SEM image of the grating. In this case, the web speed is 10 cm/sec, which is significantly faster than the NIL technique. We expect that the speed can be increased by at least an order of magnitude or higher in practical applications by proper tool design. Such high speeds are possible because DNI relies on the plastic deformation, which can occur on a time scale of micro-sec[77]. In comparison, regular NIL relies on the filling of the cavity features on the mold by the polymer materials, which takes much longer time (seconds to minutes, depending on the material viscosity)[18]. In addition, continuous and curved nanograting patterns over a large area is another unique capability of DNI, which is very difficult to achieve by other nanopatterning techniques. In Figure 5.4c, we demonstrated concentric circular nano-gratings on a fluoropolymer film, ethylene-tetrafluoroethylene, fabricated by a rotating DNI process. Such structures may find potential applications in magnetic data storage such as discrete track media[78]. Furthermore, since DNI only requires essentially line contact with the substrate, it offers a convenient method to pattern on curved surfaces. As an example, 700 nm period nano gratings created on a curved surface are shown in Figure 5.4d. In this result, the patterns are inscribed on a common photoresist, SU-8, which is coated on the hemi-cylindrical PDMS surface and subsequently cured by UV light. Nano-scale metal electrodes or patterned organic materials on the curved surface are potentially useful for light detection or energy generating devices[79]. Large-area nano patterning is also possible if wide mold is used. Figure 5.4e shows a 46 mm wide, 88 mm long, 700 nm period grating pattern in ETFE film.

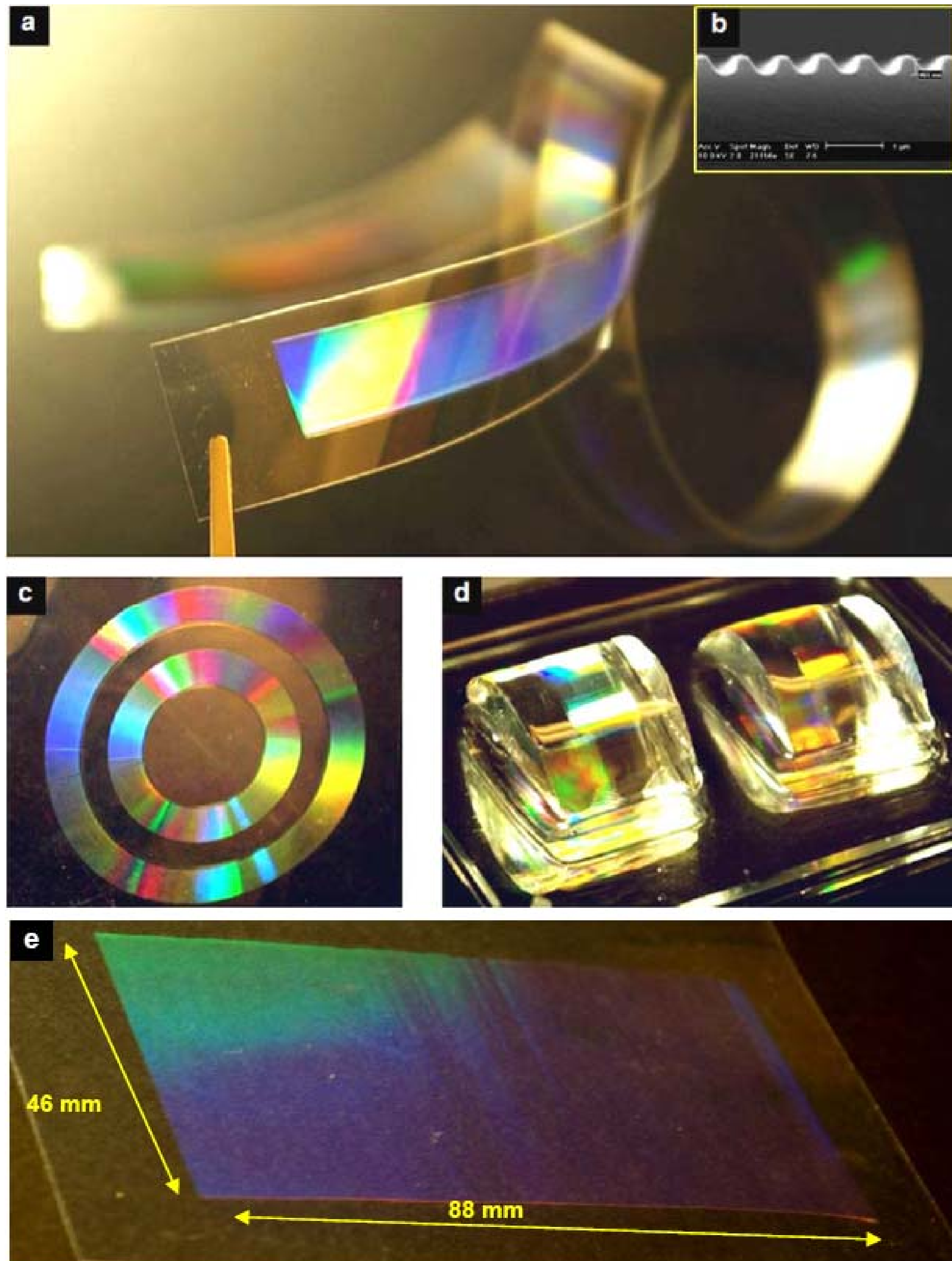

Figure 5.4 (a) A 22 inch long, half inch wide, 700 nm period, continuous nano-grating pattern directly created on a polycarbonate strip by roll-to-roll DNI process and (b) its SEM image. (c) Concentric nano-gratings on ethylene-tetrafluoroethylene (ETFE) film fabricated by a rotating DNI process. Outer diameter is 2 inch. (d) 700 nm period gratings inscribed in crosslinked photoresist SU8 on curved surfaces. (e) A 46 mm by 88 mm, large-area 700 nm period grating pattern on ETFE film fabricated by DNI.

It has been reported that in the NIL of micro-nano combined structures, defects or pattern failures in the form of incomplete pattern transfer can occur as a result of different filling speeds in varied pattern density[51]. As a solution for this problem, Cheng et. al. suggested 'combining NIL with photolithography (CNP)' method using a hybrid mold, and successfully demonstrated micro-nano combined patterns with good fidelity[80]. Contrast to NIL where patterns are defined by filling of viscous liquid resist into mold cavities, DNI relies on plastic deformation of solid, which is much faster. Therefore, DNI can successfully generate micro-nano combined features in a single inscription without need of special mold or process. Figure 5.5a shows micro-nano combined line structures in polycarbonate created by simple DNI process. Moreover, the surface is ideally smooth since there is no mechanical contact on the top surface of pattern during inscription (Figure 5.5b and inset). Such micro-scale linear rails can find applications in the optical waveguides for high Q-factor sensors that requires very smooth surface.

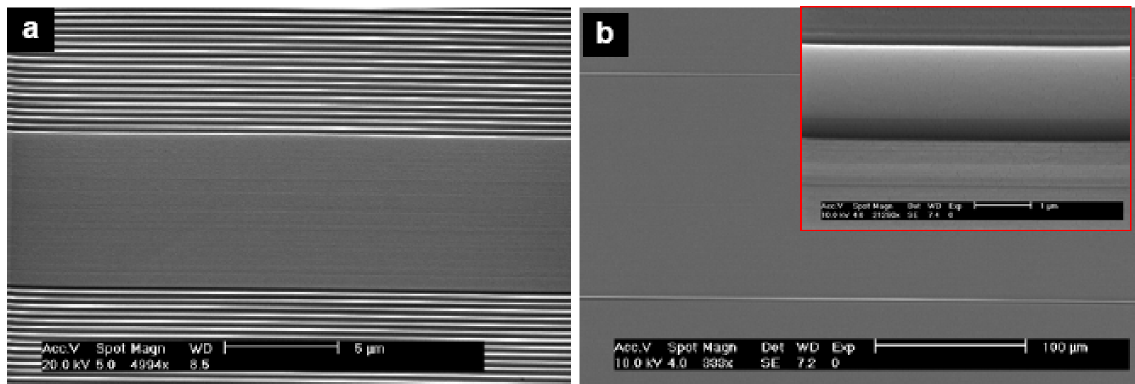

Figure 5.5 (a) Micro-nano combined structure fabricated by single-step DNI process. (b) Micro scale bumps having ideally smooth top surface fabricated by DNI.

5.4.3 Localized heating assisted DNI (LH-DNI)

Even though DNI can be performed in most cases under the ambient environment, heating of the polymer during the inscribing process can effectively reduce the modulus of the material and enhance its toughness, which can lead to more faithful polymer patterns. However, bulk heating of the whole substrate results in significant pattern deformation due to polymer flow at elevated temperatures. Therefore, we used conductive heating of the Si mold to localize the heating to only a very small region of the moving substrate where the Si mold is engaged. Such local heating allows the patterned structure to quickly cool down after the inscription, and also does not affect the inscribed structures away from the mold contact region. Figure 5.6a illustrates the localized heating assisted DNI (LH-DNI). The Si mold is directly heated by a heating element with temperature controller (HOTSET Inc.). As shown in Figure 5.6b, the pattern depth in the polycarbonate increases with temperature under the same applied force (4.2 N) and web speed (2.5 mm/sec) conditions. Polycarbonate nano gratings fabricated at room temperature (RT-DNI) show a shallow and rounded profile (Figure 5.6c), while the sample fabricated by LH-DNI at 140 °C, a temperature slightly lower than the Tg of polycarbonate (150 °C), shows much deeper trenches and sharper edges, representing a more faithful replication (Figure 5.6d) of the grating structure on the original mold (Figure 5.5e).

Since RT-DNI mostly relies on the plastic deformation of polymer, bulk deformed region by the pressure lower than material's yield stress tends to turn back its initial shape after removing loads (elastic recovery), while the region getting higher than its yield stress is permanently deformed and forms its final geometry. Contrast to the RT-

DNI using deep, high aspect ratio Si mold (Figure 5.6e) showing clear grating pattern (Figure 5.6c), the inscribed polycarbonate pattern by shallow and low aspect ratio Si mold (Figure 5.6h) at room temperature results in not clear, very shallow grooves as shown in Figure 5.6f because its initial deformation is small and most of deformed region recovers elastically due to low applied pressure below its yield strength. However, localized heating in DNI provides well-defined pattern geometry even using the same shallow mold under the same force condition (Figure 5.6g) due to the lowered modulus and the yield strength of material at elevated temperature, which makes the polymer behavior close to viscoelastic liquid.

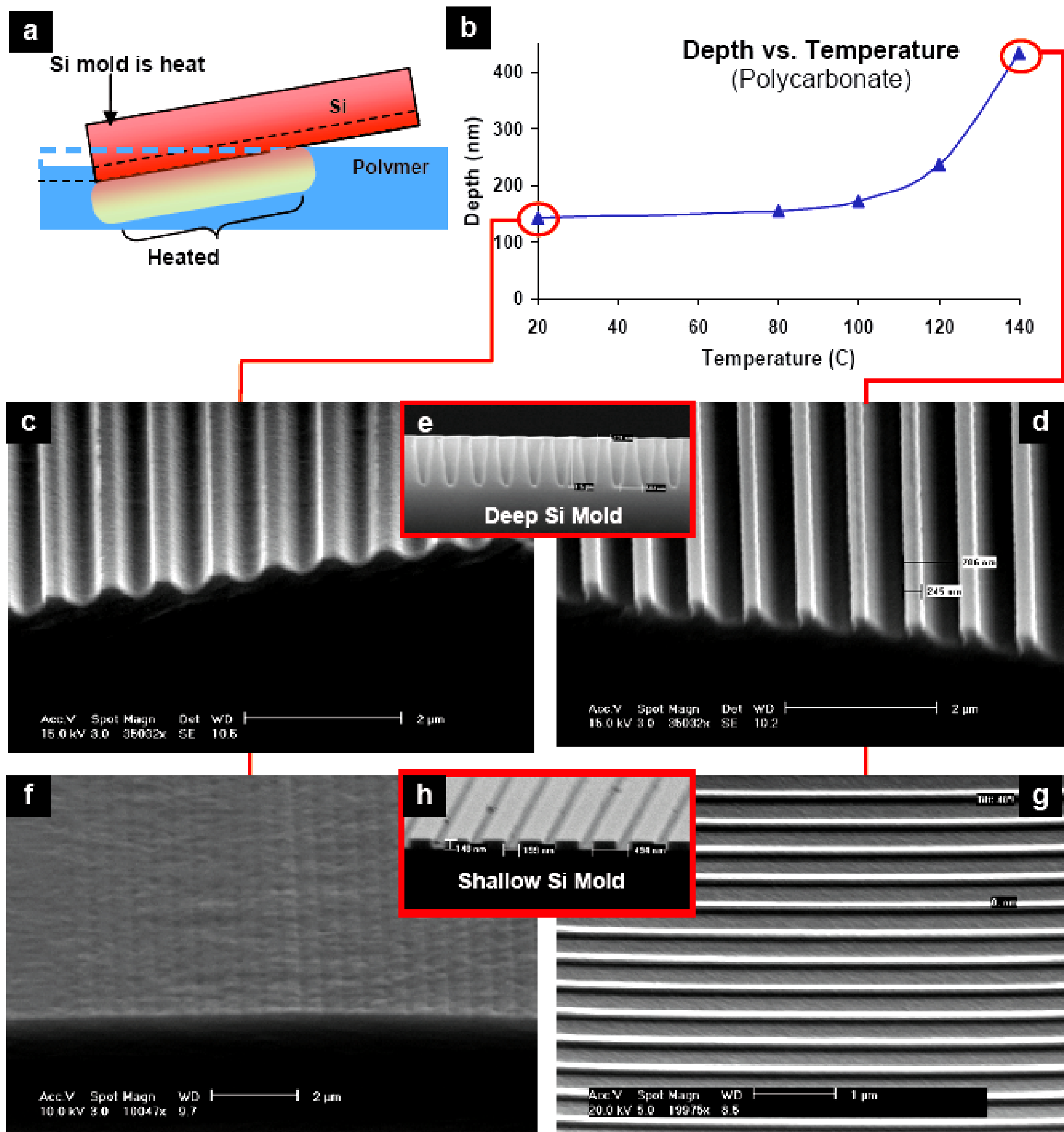

Figure 5.6 (a) A schematic of the localized heating assisted DNI (LH-DNI) process. (b) Inscribed depth in the polycarbonate film versus temperature. (c) 700 nm period polycarbonate gratings fabricated by room-temperature DNI (RT-DNI). (d) The polycarbonate sample fabricated at 140 °C showing sharper and more faithful pattern formation. The inset (e) shows the deep Si mold used to produce (c) and (d). (f) RT-DNI and (g) LH-DNI (140 °C) on polycarbonate using a low aspect-ratio (1:1, 150 nm thick), 500 nm period Si mold (h).

An interesting observation in the room-temperature DNI (RT-DNI) is that the inscribed depth is almost constant regardless of web moving speed. This means RT-DNI

can provide very high speed nano patterning without sacrificing depth and geometry of gratings. As shown in Figure 5.7a, inscribed peak-to-valley depth of polycarbonate under the same load condition (3.24 N) at room temperature shows almost constant value at the inscribing speed from 2.5 mm/s to 93.0 mm/s. This means most of plastic deformation in polymer is completed in a very short time. For example, considering typical contacting length of several microns and moving speed of 93.0 mm/s, mold engaging time is in the order of ten micro second. The time-dependent polymer deformation behavior at room temperature can be explained by famous Maxwell model combining Boltzmann superposition principle of linear viscoelasticity[81],

$$\varepsilon(t) = J_0\sigma(t) + \int_{0^-}^{t} \Delta J(t-\tau)\frac{d\sigma(\tau)}{d\tau}d\tau \qquad (5\text{-}1)$$

where $\varepsilon(t)$ is the strain, $\sigma(t)$ is the stress, $J(t)$ is the material's creep compliance, J_0 is the initial value of the compliance, and $\Delta J(t)$ is the transient component of the compliance. This equation represents the long-term polymer deformation as a function of time, creep. Since the time-dependent second term is almost constant in a short period time (several seconds or less), the strain, $\varepsilon(t)$ is constant if given stress $\sigma(t)$ is constant with time. In RT-DNI process, inscribed depth is constant regardless of contacting duration since the strain is determined by constant creep compliance and stress which are constant with time.

However, when heating is applied, the inscribed depth decrease as web speed increases (Figure 5.7a). This is because the temperature at certain depth from surface, which affects the modulus of polymer, is a function of heat transferring time while heated Si mold is engaged. A simple heat transfer model for predicting the temperature at certain depth (x) from surface as a function of contacting time, t, is shown in Figure 5.7b and the equation for transient semi-infinite heat transfer can be expressed as follows[82],

$$T(x,t) = T_s + (T_i - T_s)\cdot erf(\eta),\ \eta = x/(4\alpha t)^{\frac{1}{2}} \qquad (5\text{-}2)$$

where, T_s is the surface temperature, T_i is the initial temperature at position x, $erf()$ is Gaussian error function and α is the thermal diffusivity. Figure 5.7c is the simulated result showing the temperature of polycarbonate at the depth, x in terms of web speed, in case that T_s is 140 °C and T_i is 20 °C.

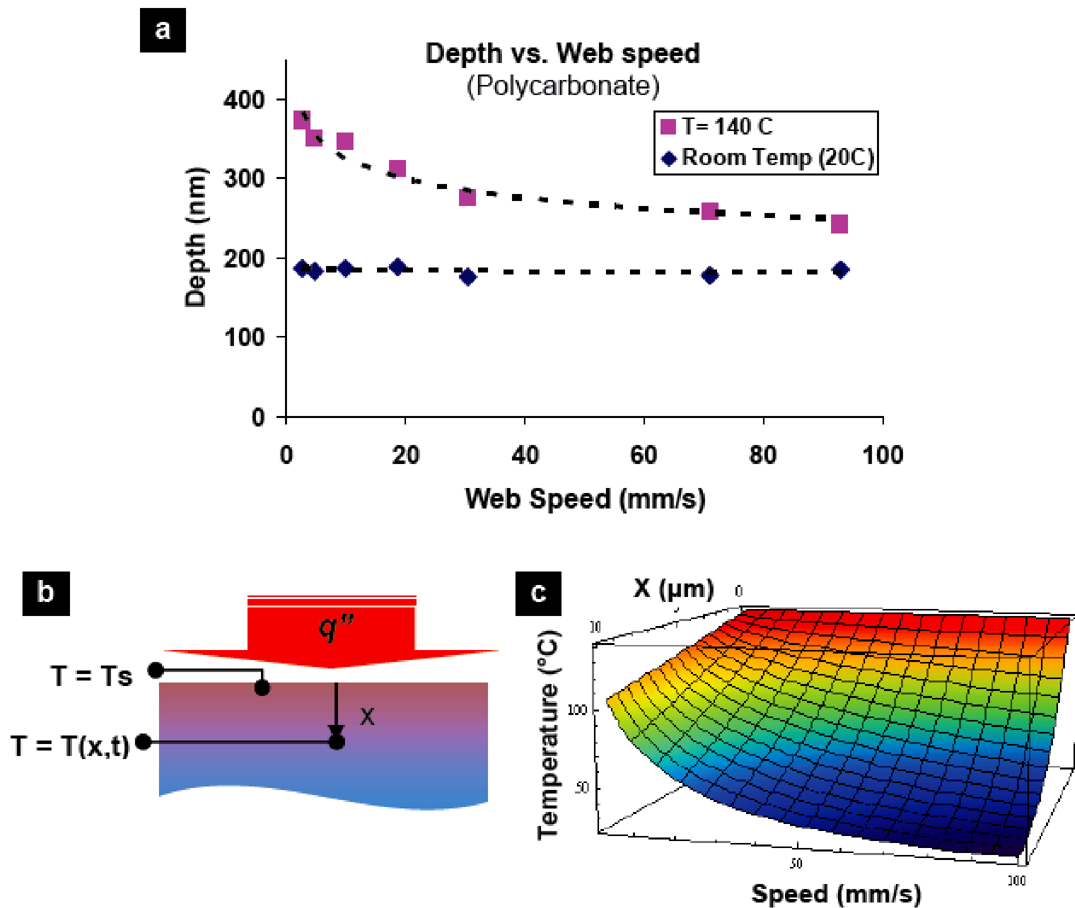

Figure 5.7 (a) Inscribed depth corresponding to the web speed for RT-DNI (20 °C) and LH-DNI (140 °C). (b) Simplified heat transfer model for LH-DNI. (c) The temperature distribution from (b) corresponding to the web speed and measured point. In this plot, the surface temperature (T_s) is 140 °C and the initial temperature (T_i) is 20 °C.

5.4.4 LH-DNI of functional materials

In LH-DNI, even though heat is applied, the actual time for heat transferring to the substrate is only on the order of tens of microseconds, which is several orders of magnitude shorter than the heating time used in a typical thermal NIL process. This can drastically minimize any potential damage to thermal sensitive materials. In this paper, we demonstrated DNI on conductive polymer, poly(3,4-ethylenedioxythiophene) (PEDOT) and an organic semiconductor—conjugated polymer poly(3-hexylthiophene) (P3HT), which are representative materials commonly used in organic electronics and organic optoelectronics. It has been reported that nano patterned P3HT in organic photovoltaics shows enhanced light absorption[83] and an increase in overall solar cell efficiency[84]. In addition, various techniques have been explored to pattern micro or nano structures on P3HT and PEDOT for applications in organic photovoltaics, organic TFTs and organic LEDs[85-88]. Compared to these referenced techniques, DNI provides superior throughput and a simple one-step process for patterning organic functional materials while minimizing possible thermal damage. Figure 5.8a and 5.8b show 700 nm period nano gratings directly created on PEDOT and P3HT coated PET respectively by LH-DNI at 90 °C. We should point out that it is also straightforward to carry out the DNI process in an oxygen-free environment to prevent the oxidation effect and further preserve the functionality of the conjugated polymers. A potential application is in the field of organic solar cells, where DNI could be used to directly inscribe conjugated polymers to produce the ordered nanoscale interface between a donor and an acceptor organic semiconductors for efficient charge separation and charge transport[89]. As another example of patterning functional polymers, Nano-inscribing of Nafion film

(DuPont), an important polymer material in electrochemistry, has been explored. Nafion film serves an important role as the ion exchange membrane in fuel cells due to its excellent proton conductivity, and its thermal and mechanical stability[90]. Recently it has been reported that nano patterning of Nafion can provide enhanced efficiency in micro-fuel cells by increasing the electrochemical active surface areas[91, 92]. In Figure 5.8c, well defined 700 nm period gratings are created in Nafion film by a simple DNI process using localized heating at 80 °C.

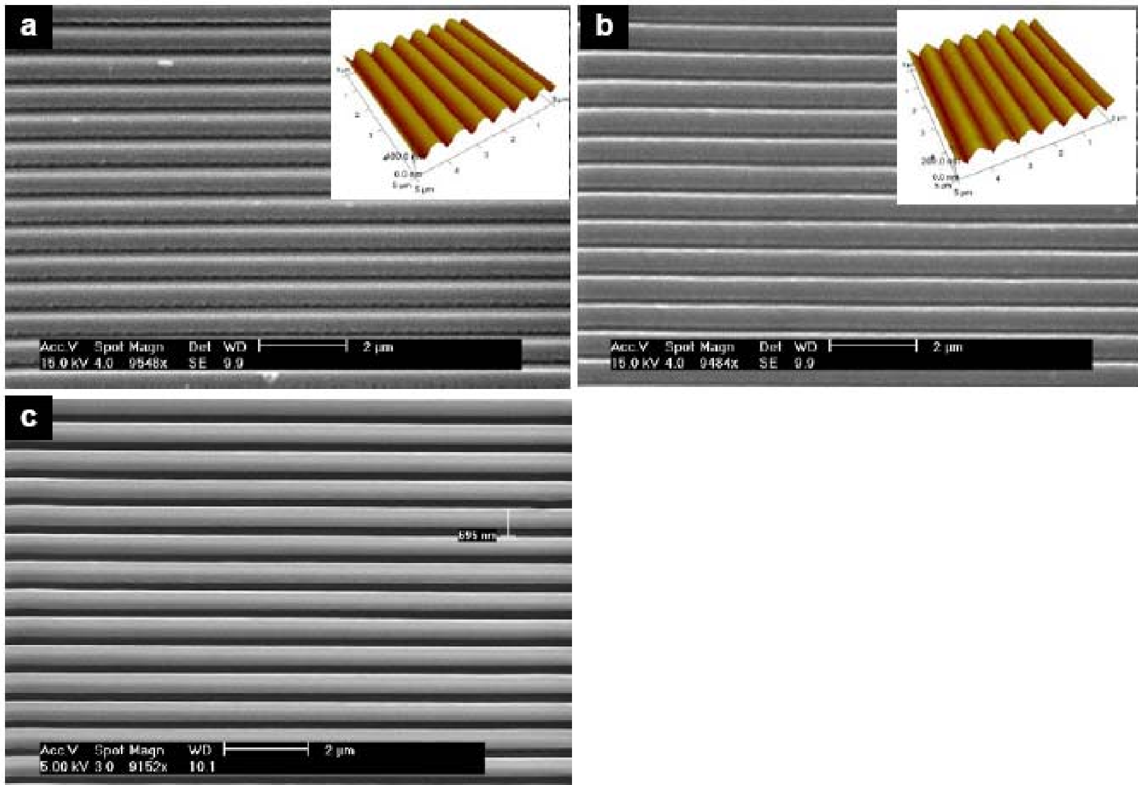

Figure 5.8 700 nm period gratings created by LH-DNI on (a) conductive polymer PEDOT and (b) semiconducting polymer P3HT coated on PET substrate (90 °C) and their corresponding AFM images shown in the insets, respectively. (c) 700 nm period gratings generated on proton exchange polymer, Nafion by LH-DNI (80 °C).

5.4.5 Fabrication of split-ring resonator (SRR) using DNI

Finally as an application in photonics, we show that a metallic grating fabricated by a one-step DNI can be used to construct negative refractive index metamaterials. Negative refraction requires a simultaneously negative permittivity and permeability. While negative permittivity is readily achievable in metallic structures due to plasmon dispersion, negative permeability can only be obtained in specially designed artificially structures. Previously several variations of the so-called split-ring resonator (SRR) structures have been exploited to produce magnetic response and negative permeability[93-95]. Recently an elongate SRR structure has been demonstrated by using direct laser writing and silver chemical vapor deposition, which offers the advantage of normal incidence[96]. To produce magnetic response and negative permeability at shorter wavelength ranges (e.g. visible band), the dimension of the subwavelength element in the structure has to be reduced accordingly. We have recently studied a Split-Ring-Resonant-Grating (SRRG) structure fabricated by nanoimprinting and metal film deposition, which shows the potential of achieving negative refraction at visible wavelengths[97]. In this work, we demonstrated the fabrication of 200 nm period (30 nm trench) SRRG structure using the DNI process (Figure 5.9a). To achieve this structure, 20 nm thick silver is thermally deposited on a polycarbonate film and simply inscribed using a 200 nm period Si mold at room temperature. Figure 5.9b shows the transmittance spectra of sample 5.9a for both TM (transverse magnetic) and TE (transverse electric) polarization, showing particularly strong TM mode transmission valleys at visible wavelength range of 430 nm and 590 nm. Based on our simulation[98], we can identify that the valley at 430 nm is due to electrical resonance while the one at 590 nm is due to magnetic resonance and

leads to negative permeability. Further optimization of the structure to demonstrate negative index at visible band is currently underway. As compared with NIL and other nano fabrication techniques[96, 99], DNI provides a very simple, single step process to create large area continuous nano metal grating patterns for negative index metamaterial applications.

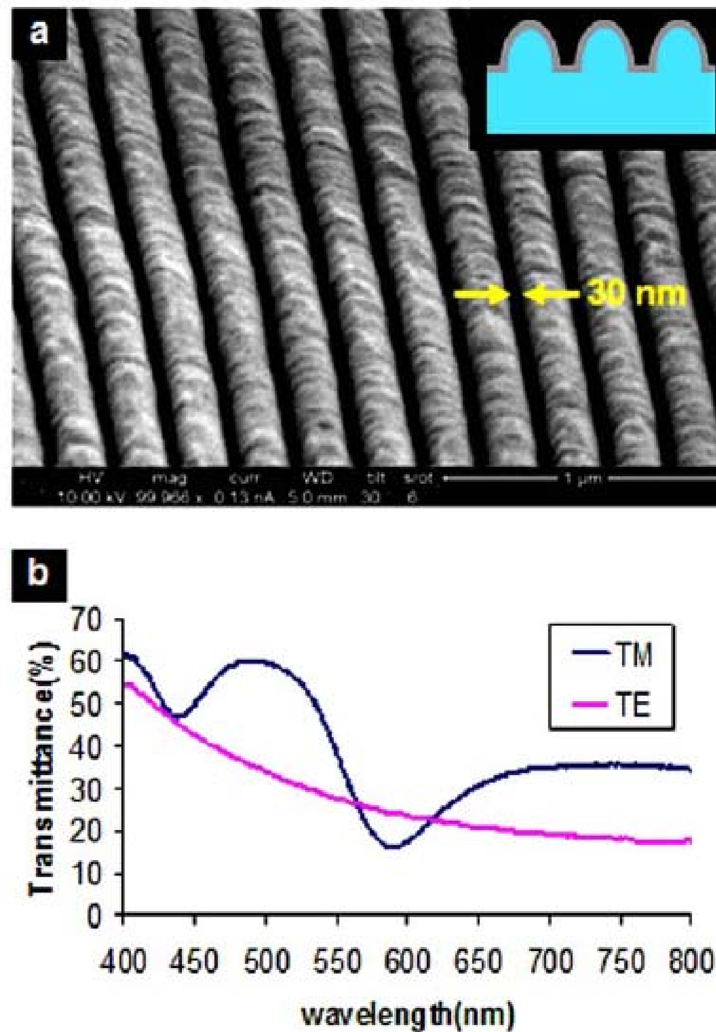

Figure 5.9 (a) 200 nm period silver gratings fabricated by DNI. 20 nm thick silver is thermally deposited on polycarbonate film and simply inscribed using a 200 nm period Si mold. (b) Transmittance spectra of sample (a) showing valleys at 430 and 590 nm which are due to electrical and magnetic resonances, respectively.

5.5 Summary

In summary, we introduced a new nano patterning technique, DNI, for directly creating truly continuous nano grating patterns in a variety of metal and polymer materials at ambient temperature or with localized heating. With a demonstrated resolution of 30 nm and a speed of 10 cm/s that can both be further improved, we can envision that DNI can be applied into many practical applications in optics, flat panel displays, and bio-industries that require a non-toxic, room temperature environment to produce well-defined nanopatterns at extremely high-speed.

Chapter 6

Continuous Formation of Nano-scale Periodic Patterns by Localized Dynamic Wrinkling

6.1 Introduction

Micro/Nano scale grating structures are widely used in display, optics and bio industries as key functional elements. In the fabrication of nano grating pattern, many emerging techniques such as electron beam lithography, laser interference lithography, and nanoimprint lithography (NIL) have been utilized[17, 34, 46, 100]. Among them, electron beam lithography, however, provides extremely low process throughput even though it has excellent dimensional resolution down to sub-10 nm with maskless free-drawing capability. Another nanofabrication technology, low-cost, high-throughput NIL always requires the same-size original stamps containing nano scale structure, which is another headache to fabricate[18].

Parallel to the development of lithographic-based nanopatterning methods, a whole different patterning approach based on ordered surface wrinkling has also been investigated in the past decade[101-104]. Wrinkling or buckling is commonly observed physical phenomenon that is the deformation under mechanical instability when membranes are exposed to compressive stresses. However, the nature of nonlinear behavior in wrinkling not only makes it difficult to analyze theoretically but also the

process difficult to control[105]. For better repeatability, most of researches on wrinkling use thin stiff layer (metal deposition, oxidation or UV exposure) under pre-stretched rather thick soft elastomeric substrate such as poly(dimethylsiloxane) (PDMS) to form spontaneous winkles by releasing the strain[101, 102, 105, 106]. Uniaxially strained membrane forms well-ordered grating patterns possessing their typical periodicity and amplitude, and they can be utilized in variety applications such as stamps for micro-contacting printing, cell alignment and surface metrology[107-109]. However, to create well-oriented wrinkles in practically large area is still challenging because experimentally it is very difficult to apply pure uniaxial strain to a large-size membrane, which is generally limited by the strain-generating device. Moreover, patterns on a soft elastomer substrate have only limited application, and need additional pattern transferring process on to a glass or a Si wafer or other hard plastic substrates for broadening its usage.

We present a novel nano patterning technique, Localized Dynamic Wrinkling (LDW), which continuously creates micro/nano-scale gratings in a thin metal film coated on a polymer substrate by simply sliding a flat edge of a cleaved Si wafer over the metal film. LDW shares the basic principle as the buckling (wrinkling) phenomenon of a thin and stiff film on a compliant substrate under uniaxial stress; but the moving edge of the tilted Si wafer exerts stress to metal coated polymer along the movement direction and sequentially generates localized winkles in the metal film in a dynamic fashion. More interestingly, the period and the geometry of patterned gratings can be controlled by several material and process parameters such as the thicknesses of the metal layer, the type of backing polymer substrate and the adhesion property between the metal and the polymer layer. Very good agreement of experimental data on the pattern period from

LDW with a theoretical model has been obtained. Furthermore, the sequential nature of the localized wrinkle formation along the Si edge movement direction makes LDW easily applicable to a high-speed, continuous roll-to-roll process. In this work, we demonstrated the fabrication of gold nano gratings with linewidth from micron scale down to 150 nm on plastic substrates.

6.2 Principle of LDW

LDW relies on the localized wrinkle formation of the thin metal film on a polymer substrate. As illustrated in Figure 6.1a, moving sharp edge sequentially creates a single winkle (or following several winkles with decaying amplitude) and finally produces metal grating pattern having typical periodicity. In our experiment, gold in various thickness (10 ~ 100 nm) is thermally deposited on two types of plastic substrates, polyethylene terephthalate (PET, 100 μm thick) and polycarbonate (PC, 100 μm thick), and scanned by well a cleaved Si wafer in proper size. In LDW process, both a gold film and underlying polymer layer plastically (permanently) deform under high enough normal and shear stress from moving Si edge. This can be checked by removing underlying polymer layer in the solvent. Results showed free-standing winkled metal layer keeping its initial period, which supports the plastic deformation of gold film. Figure 6.1b illustrates LDW process to create discrete metal gratings. While flat Si wafer slides on the metal coated substrate with proper pressure, localized wrinkle starts to be generated by shear (friction) and normal force. As the Si wafer moves further, wrinkle fully grows and defines its period (λ) and amplitude (A). Then, the Si wafer goes over the bump (wrinkle) and finalizes the pattern geometry, reduced amplitude (A') while keeping

its period (λ) constant. If friction force is higher than the fracture strength of the metal film, discrete metal gratings are generated by fracturing the metal film between bumps. Higher friction force gives larger spacing (S) between metal lines but, keeps its period almost constant. After forming a single wrinkle (or following several winkles with decayed amplitude), it starts over the initial step to sequentially create another wrinkle under the same mechanism, and finally periodic grating pattern is generated. Figure 6.1c shows the result of finite element analysis demonstrating localized winkle formation in LDW process, which is contrast to the bulk wrinkling where wrinkles simultaneously form overall surface where compressive strain is evenly applied (Figure 6.1d).

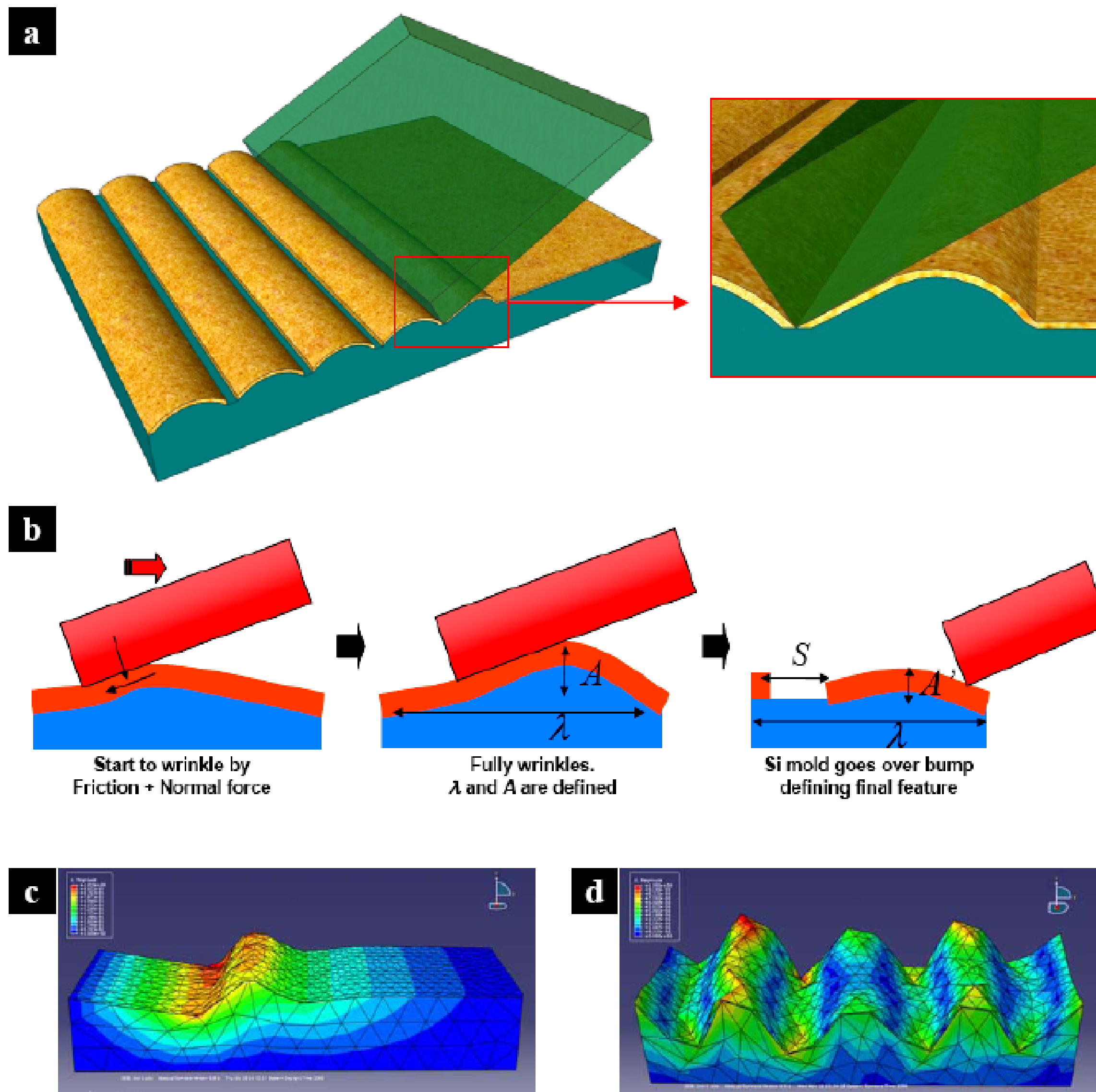

Figure 6.1 (a) Schematic of LDW system. (b) LDW process to create discrete metal gratings. (c) Finite element analysis (ABAQUS software) representing localized wrinkle formation by LDW on a thin gold film on PET substrate, which is contrast to bulk wrinkling, (d), when compressive strain is evenly distributed.

A prominent feature in LDW is its self-boundary conditioning to produce uniaxial strain without need of special device. When thin and stiff layer on the compliant substrate subjects to anisotropic compressive strain, the directional preference increases as the

strains become more anisotropic, from the labyrinths, to the herringbones, and to the stripes[110]. Therefore, to achieve well-oriented grating pattern, fixed boundary condition in lateral direction with free of longitudinal directional stretching from the specially designed strain-generation equipment is required, which also limits the size of patterned area. However, in LDW process a flat edge of Si wafer that gets in conformal line contact with substrate effectively prevents lateral strain while only allows Si tool movement directional strain, and therefore, creates well-oriented stripe winkles under the anisotropic strain condition.

6.3 Results and discussion

6.3.1 Large-area continuous grating generation by LDW

LDW provides a way to continuously generate large-area nano metal gratings with few defects. Defects including missed and non-straight lines are mostly from not perfectly cleaved Si wafer having terraces, which results in non-uniformity in the force vector when the Si edge engages, but can be technically overcome. Figure 6.2 shows 800 nm linewidth, 970 nm period grating pattern of 50 nm thick gold on PET substrate by LDW process. As seen the SEM (and inset), well oriented discrete gold gratings are fabricated on a large area. The period is very uniform overall area with the deviation of less than 5%.

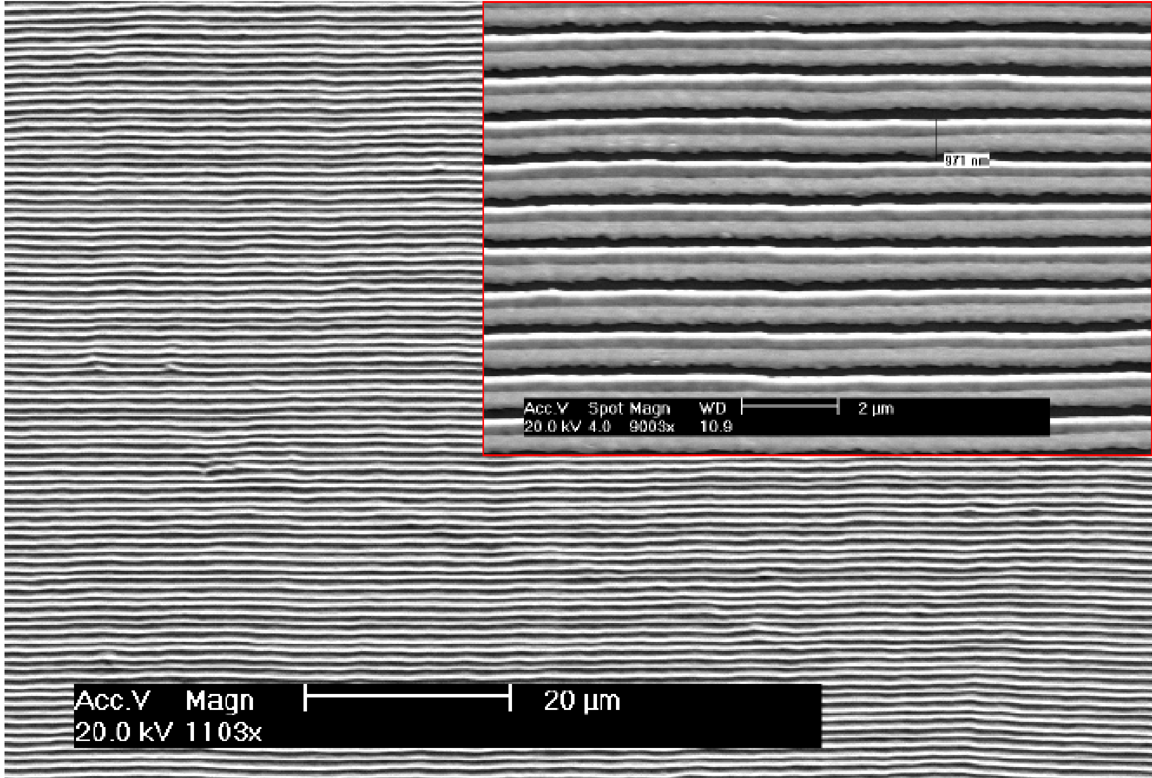

Figure 6.2 SEM image of 970 nm period gold grating pattern fabricated by LDW process

6.3.2 Controllable period and geometry in LDW patterning

An interesting characteristic in LDW is its controllable period in patterned grating. Previously, Huang et. al. performed an analytical study on the bulk wrinkling of double-layer system composed of stiff film and compliant layer underneath (Figure 6.3a) [110], which is similar to our sample used in LDW, a thin gold film on a polymer substrate. Figure 6.4b shows three representative patterns of wrinkle formed under different strain conditions. In that work, they introduced the winkle's wave length (period) at equilibrium as a function of stiff layer thickness and the moduli of substrates [110],

$$\lambda_{eq} = 2\pi h \left(\frac{\bar{E}}{3\bar{E}_s} \right)^{1/3} \qquad (6\text{-}1)$$

Where, h is the thickness of stiff layer, and $\overline{E}$ and $\overline{E}_s$ correspond to the plane strain modulus of the stiff layer and the compliant substrate, respectively.

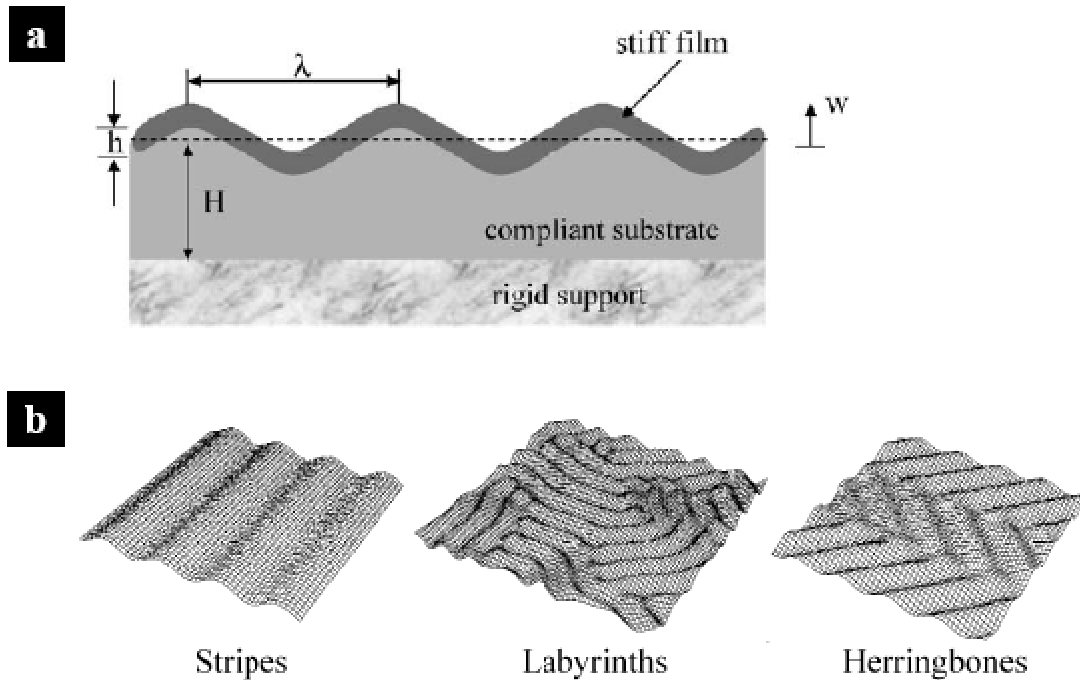

Figure 6.3 (a) A schematic of double-layer system used in winkling analysis [110]. (b) Graphical illustration of three representative patterns of wrinkles: stripes, labyrinths and herringbones. (Reprinted from Ref.[110]. Copyright 2005 ELSEVIER Publication.)

In LDW, we observed similar linear trends in the pattern period with increased metal thicknesses, which show very good agreement with equation (6-1) for the theoretical expression in bulk wrinkling. The results are summarized in Figure 6.4a. Dots represent experimental data points and lines are from the theoretical models from equation (6-1). In this plot, substrates of different Young's modulus (PC at 160 °C, PET at 100 °C, PET at room temperature) are used to check the substrate modulus dependency on pattern period. For heating process a Si wafer is heated by a conductive heating element with a temperature controller. Experimental results clearly show that harder

substrate (room temperature PET, E = 3.0 GPa) produces smaller periodic pattern, while softer one (PC at 160 °C, E = 50 MPa) results in larger periodic patterning, and each of them also follows the linearly increasing trend with metal thickness. Figure 6.4b shows the corresponding SEM images of LDW grating pattern on different gold thicknesses (10 nm, 50 nm and 100 nm) on a PET substrate at 160 °C representing different periods (200 nm, 1.2 μm and 2.3 μm, respectively). Room temperature LDW produces smaller period (900 nm) pattern for the same thickness (50 nm) of gold.

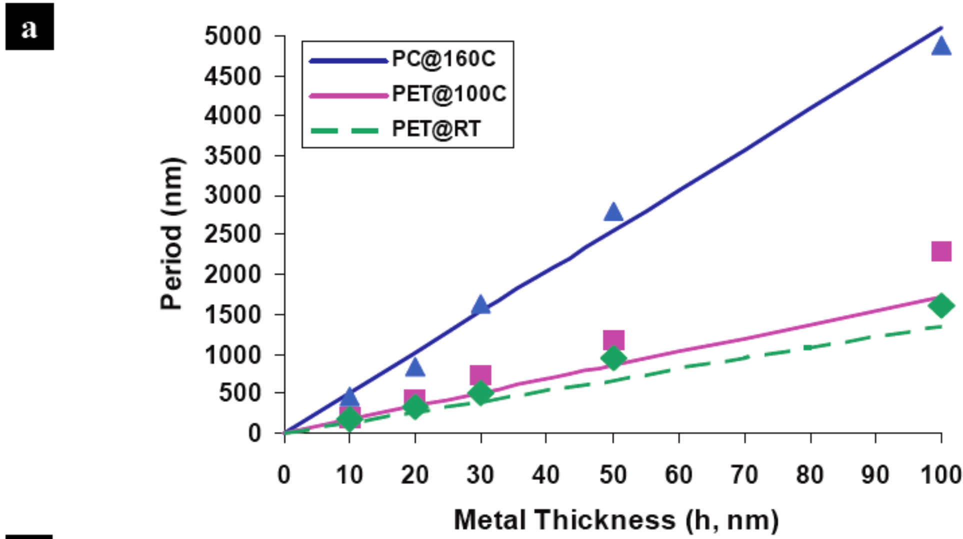

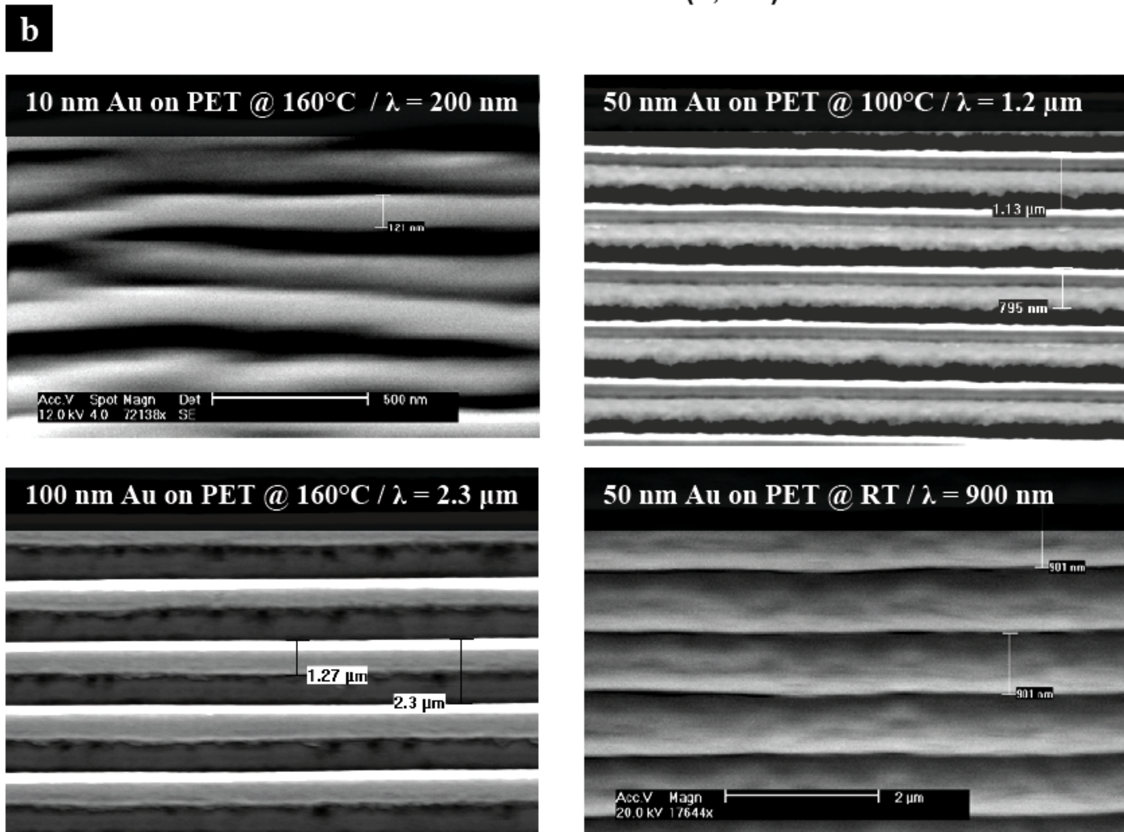

Figure 6.4 (a) Pattern period as a function of gold thickness. Solid line - theoretical model from eq. (1), Dots – experimental data from LDW process. (b) Corresponding SEM images of LDW grating pattern on different gold thicknesses (10 nm, 50 nm and 100 nm) on a PET substrate at 160 °C representing each different periods (200 nm, 1.2 µm and 2.3 µm, respectively). Room temperature LDW produces smaller period (900 nm) pattern for the same thickness (50 nm) of gold.

In addition to the metal film thickness, an adhesion property between the metal and the plastic substrate also affects the pattern period and geometry. To verify the surface energy dependency, we used surface treated (1H,1H,2H,2H-Perfluorodecyl trichlorosilane) PET having comparably lower adhesion to gold layer and compared it to bare PET. After LDW, we intentionally removed part of patterned gold layer to inspect bottom PET surface. Experimental results show clear difference on each case, the surface treated PET and the bare PET. As shown in Figure 6.5a, room-temperature LDW on 50 nm gold coated bare PET forms 900 nm periodic wrinkles on both a gold and a PET surfaces, which is as described in Figure 6.1. However, in case of using surface-treated PET (Figure 6.5b), much larger periodic patterns ($\lambda = 3$ μm) were generated only on a gold film. Moreover, the profile of the wrinkles is very different from that using a bare PET substrate (Figure 6.5a). What makes such differences? This can be explained as different wrinkling mechanism, delamination buckling. When LDW performs on gold-PET bilayer with weak interfacial energy, the gold film delaminates from PET surface and buckles under high shear force. In this step, the size of wrinkle becomes larger by further delamination toward, which means increase in period.

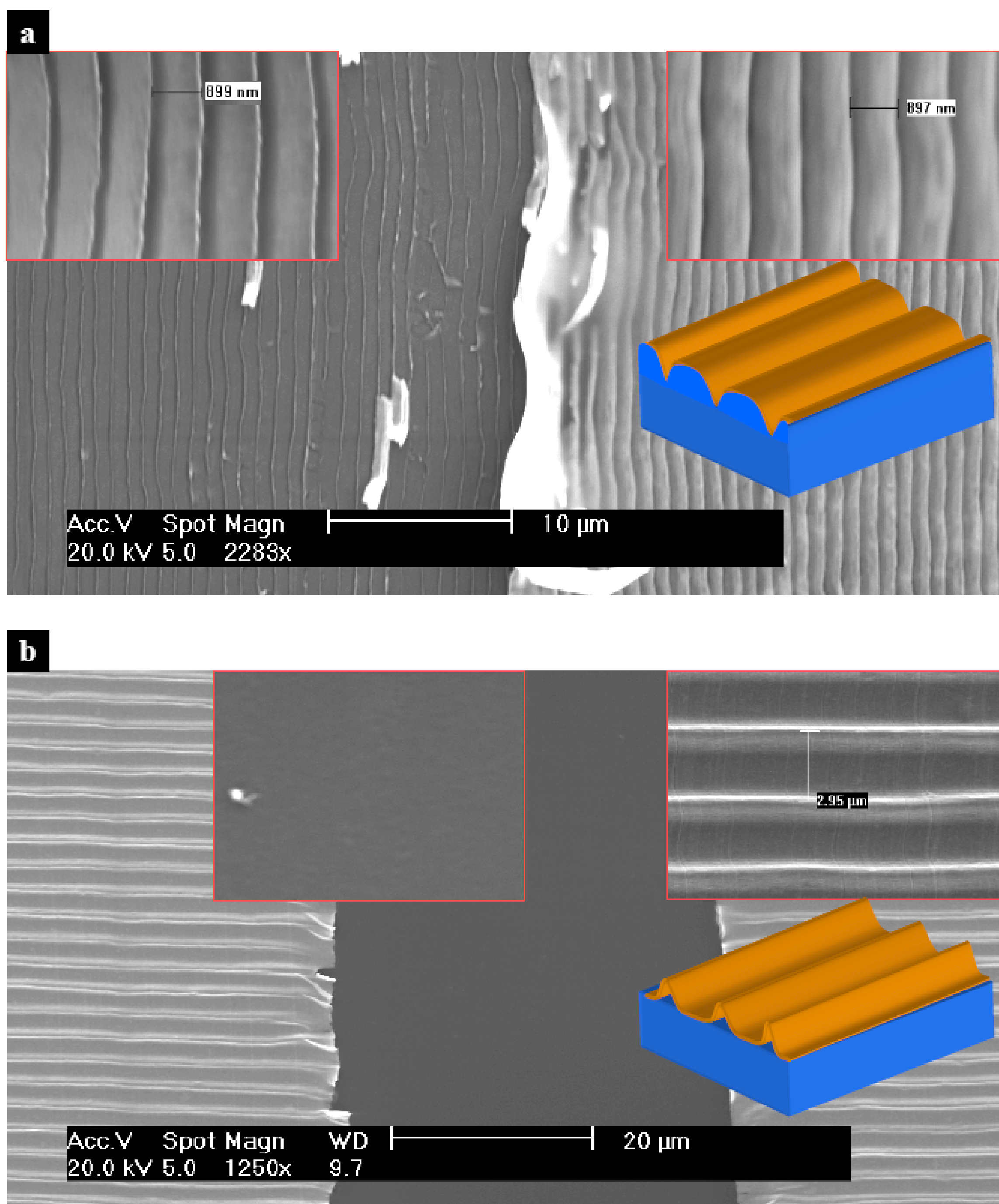

Figure 6.5 (a) Room-temperature LDW of 50 nm gold on a bare PET substrate produces 900 nm periodic patterns on both gold and PET layers, and (b) the same process but on a fluoro-silane surface treated PET shows much larger period (3 µm) and different shape.

6.3.3 Easy pattern transferring

LDW is very simple and versatile patterning technology that can directly create nano metal gratings using a flat edge of a hard material, but should be done on a plastic substrate having certain level of compliance. This may limit future applications that require hard substrates such as a Si wafer and a glass. However, here we have an alternative way to overcome this drawback; metal grating fabricated by LDW can be simply transferred to other substrates for further practical applications. Since in general, gold has low adhesion to most of hard and plastic surface, we can take this advantage in transferring gold pattern to other substrates after LDW. For even better result, we can use anti-sticking surface-treated plastic substrate as previously described. We demonstrated the transferring of LDW pattern to a glass substrate by use of UV curable epoxysilicone[44] as an adhesive layer (Figure 6.6a). Additionally, the patterned gold lines can also be transferred to a thermoplastic substrate with heating, which is explained in Ref. [8, 9]. Figure 6.6b is the SEM image of the initial gold pattern on a surface-treated PET substrate, and Figure 6.6c is the transferred pattern on a glass substrate showing an inverse profile of 6.6b and exactly same period.

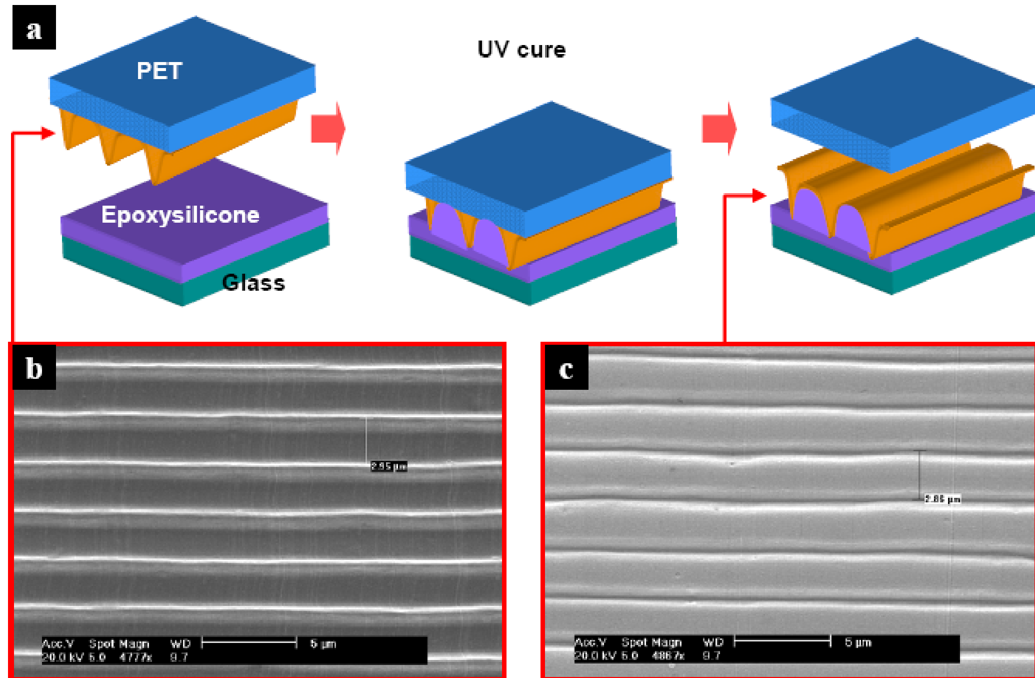

Figure 6.6 (a) Schematic of pattern transferring step after LDW using UV curable epoxysilicone as an adhesive layer (b) Initial LDW gold pattern on a fluoro-silane surface treated PET (from Figure 6.5b), (c) Transferred pattern on a glass substrate showing inverse profile of initial pattern (a).

6.3.4 High-speed patterning with constant period regardless of speed

In addition to dimensional resolution, processing speed is also very important factor in nanofabrication. LDW provides continuous formation of well ordered nano scale metal grating pattern at high speed. In the experiment we used the speed up to 50 mm/sec and could get good pattern formation. To check the sliding speed dependency on the pattern geometry and period, a PET substrate covered by 100 nm thick gold was moved with respect to a fixed Si wafer by micro linear motor that provides speed range from 24 um/sec to 266 um/sec, and also much high speed, 5 mm/sec by AC motor have been tried for comparison. Results show constant period in pattern regardless of sliding speed in that range. SEMs in Figure 6.7 show almost identical pattern period, 1.56 µm, with a standard

deviation of 0.03 μm in the speed range of 24 to 5000 μm/sec. Because the speed of elastic wave (wrinkling) is extremely high, in the order of 10^9 μm/sec [111], the localized wrinkle by LDW reaches the fully developed steady state in a very short engaging time while Si wafer scans over. This is very promising result implying repeatable formation of ordered grating pattern without taking care of one processing parameter, scanning speed. Moreover, we can even speed up to produce the same quality of nano patterns, which is what all manufacturing processes are pursuing.

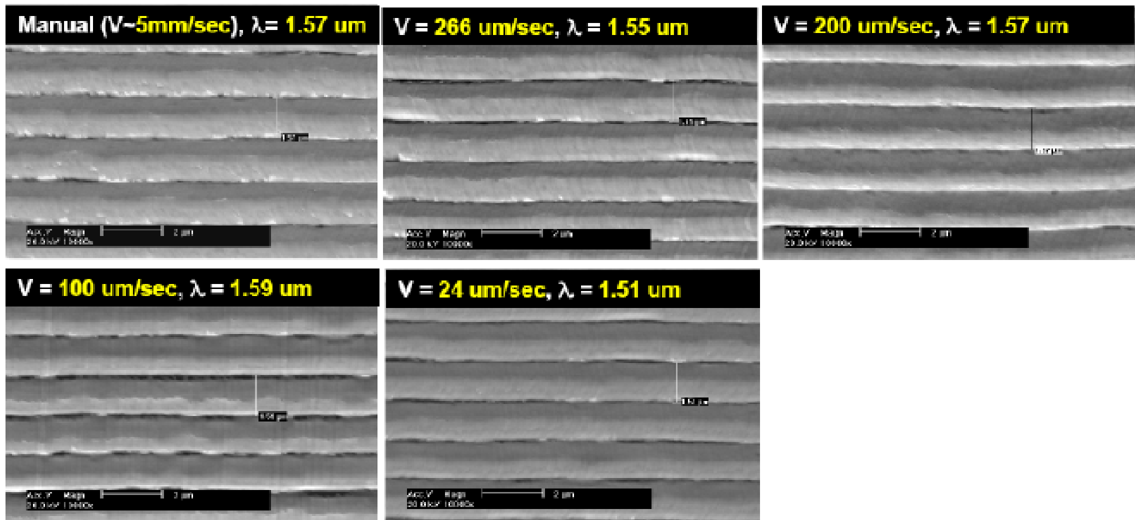

Figure 6.7 Periodic pattern by LDW at different sliding speed (from 24 μm/sec to 5 mm/sec) showing identical pattern period, 1.5~1,6 μm, regardless of speed (contacting time) for the same thickness (100 nm) of gold layer on PET at ambient temperature.

6.3.5 Large-opening nanowires for semi-transparent metal electrode application

Nano metal gratings can be utilized in transparent metal electrodes that can potentially replace current ITO electrodes in display and solarcell applications[8]. However, metal transferring technique used in Ref. [8, 9] requires PDMS template, and moreover, it needs successive metal deposition and cleaning processes for another

patterning. LDW can directly form nano metal gratings on plastic substrates without need of a template. However, since the grating pattern generally have very small trench window, it can not provide enough transparency to be utilized as transparent electrodes application. However, this drawback can be simply overcome by uniaxial stretching on LDW pattern with heating. As illustrated in Figure 6.8a, the pattern by LDW having tiny opening is stretched orthogonal to the grating direction with heat (higher than Tg of polymer substrate) to get larger openings. Figure 6.8b is the initial grating pattern fabricated by LDW on a 50 nm gold coated PET substrate with tiny openings (less than 20 nm). 20 % stretching at 200 °C results in wider opening (Figure 6.8c) and 30 % stretching produces even larger openings (Figure 6.8d). For comparison, the same thickness of a bare gold layer on a PET substrate without LDW has been strained (Figure 6.8e). Compared to strained LDW gratings, the bare gold layer with 20% stretching results in not uniformly fractured metal film in much larger dimension (~ 10 µm). Figure 6.8f is the corresponding transmittance of each sample listed. A 50 nm bare gold film on a PET substrate shows about 20 % maximum transmittance at 510 nm wavelength. LDW pattern has slightly enhanced transmittance (~ 30 %) due to tiny openings. 30 % strained LDW pattern provides up to 50 % transmittance with the resistance of 26.8 Ω for 5 mm by 5 mm pattern, which is acceptable for electrode applications. However, the strained gold film without LDW shows much lower transmittance which is similar to that of initial LDW pattern. Since our stain generating device does not provide pure uniaxial strain but there is a biaxial component, the stretched gratings are buckled due to a lateral compressive strain. We are certain that higher quality transparent metal electrodes can be produced if use improved experimental setups.

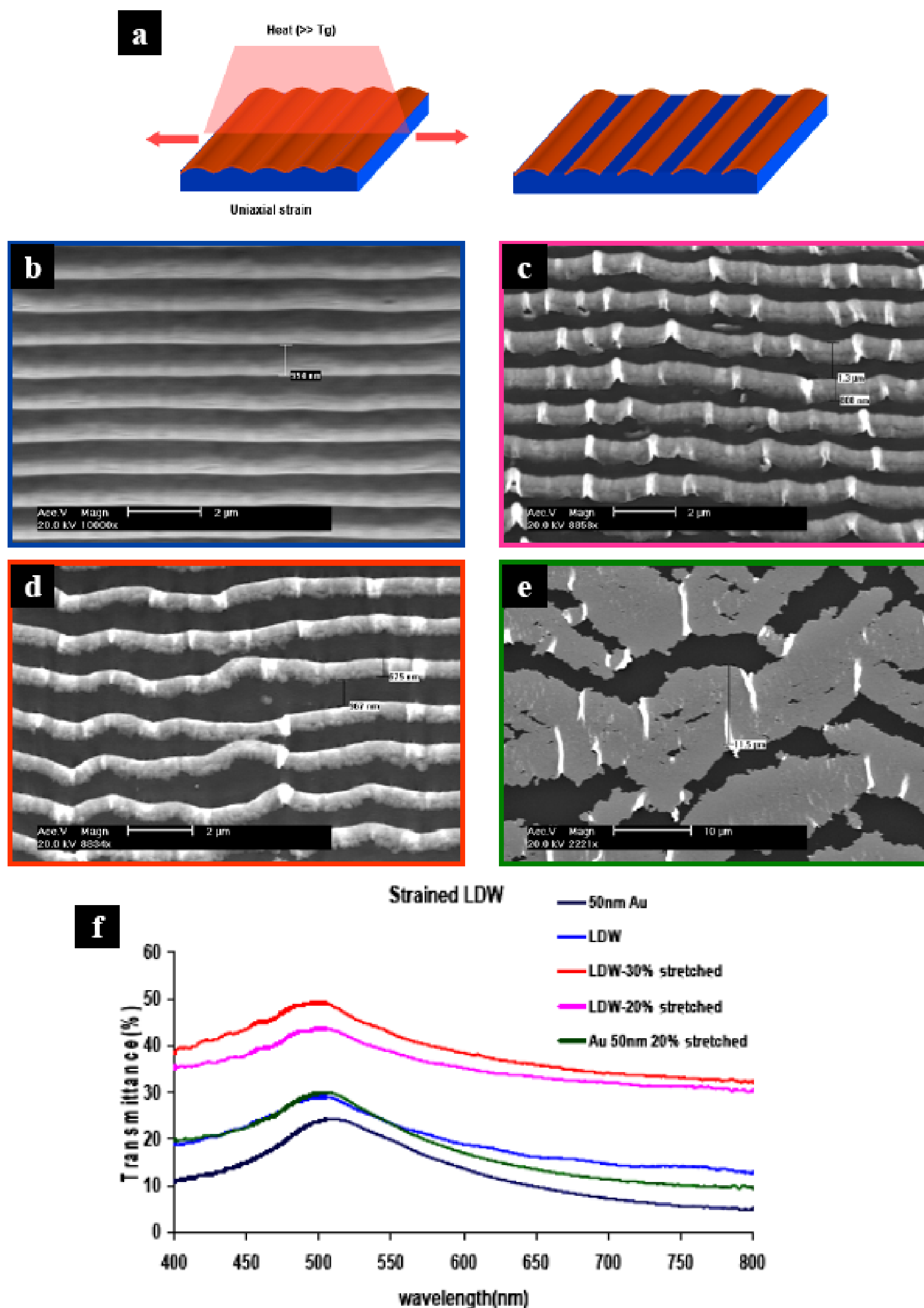

Figure 6.8 (a) Uniaxial stretching with heat (T > Tg) to enlarge openings between metal wires. (b) SEM of LDW pattern in 50 nm gold coated PET. (c) 20% strained LDW pattern. (d) 30% strained LDW pattern. (e) 20% strained bare 50nm gold coated PET without patterning (for comparison). (f) Transmittance of each listed sample.

6.4 Summary

Most of micro/ nano fabrication processes having practically high throughput, such as photo lithography or NIL, rely on “replication” scheme using pre-patterned masks or stamps. Aforementioned DNI (Dynamic Nano-Inscribing, Chapter 5) is also within the boundary of replication technologies even though it can produces infinitely long grating pattern using a small piece of Si mold. We can refer such replication processes “second generation” patterning process.

LDW is the “first generation” patterning process that can create patterns from just a flat edge of any hard material. LDW is a novel nano patterning technique based on localized wrinkling of a thin metal film on a compliant polymer layer. We demonstrated the formation of gold nano grating pattern having the linewidth down to 150 nm using LDW method. The pattern geometry and the period in LDW can be controlled by using different metal thickness and types of polymers. We also showed the adhesion property of metal-polymer interface affected the pattern geometry. Gold nano gratings fabricated by LDW can be easily transferred to other substrates for further applications. LDW is cost-effective and a powerful nano patterning technology that can be simply applied in high-speed, continuous roll-to-roll process.

Chapter 7

Continuous Fabrication of Nanogratings with Real-Time Period Modulation using High-Frequency Sequential Indentations

7.1 Introduction

Optical lithography has dominated micro/nano scale patterning in Integrated Circuit (IC) and flat panel display industries for over half century due to its excellent reproducibility and ability to stacking multiple layers of complex geometry[112]. However, the nature of light diffraction or beam scattering limits the optical lithography going down to sub-100 nm feature size patterning. Nanoimprint Lithography (NIL) that relies on physical contacting provides an unique solution to create sub-10 nm spatial resolution with reasonably high throughput[17, 18]. Newly developed Dynamic Nano-Inscribing (DNI, Chap.5) provides the fabrication of sub 50 nm, seamless metal and polymer gratings with extremely high speed[75]. However, both NIL and DNI require expensive original stamps containing nano structures, which should be fabricated by low-throughput, high-cost processes such as electron beam lithography. In the previous chapter, we demonstrated Localized Dynamic Wrinkling (LDW) to create nano metal gratings, which is not by an original stamp but using just a cleaved Si wafer. Although

LDW provides continuous fabrication of tunable-period gratings with high speed, it still has a challenge in generating perfect straight lines due to its nature of nonlinearity in wrinkle formation. In addition, LDW only works on thin stiff film (metal) on a compliant plastic substrate, and it may be a roadblock for further applications demanding broad choice of material.

Patterning by direct mechanical indentation has no limit in material if the hardness of tool is higher than that of substrate material. In that sense, nano hole arrays fabricated by successive AFM indentations have been demonstrated for biomimetic dry adhesive[113] or for ultrahigh-density data storage applications[114]. Indentation induced nano patterning was also performed on hard materials such as metals. Shin et. al. presented 3-D micro-nano hybrid patterning on an aluminum substrate using indentation process[115].

We introduce a novel nano patterning process, Dynamic Nano-Cutting (DNC) to create micro/nano gratings on various materials. Similar to LDW process (Chapter 6), DNC also uses a tilted flat edge of hard material (e.g. Si wafer) but high-frequency vibration makes sequential indentations on a moving substrate to create grating pattern continuously. DNC provides perfectly straight lines with real-time controlled grating period that LDW is not able to achieve. Since DNC relies on mechanical indentation, there is no limit in substrate materials once they are softer than tool material. Therefore, DNC is a “first generation patterning” process that does not require original stamps containing nano structures.

7.2 Principle of Dynamic Nano-Cutting (DNC)

The working principle of DNC is very simple and straightforward. Well cleaved Si wafer (or any flat edge of hard material) with proper tilting angle sequentially indents into a moving substrate by a high-frequency external vibration to generate periodic gratings (Figure 7.1). When the tool (Si wafer) vibrates at the frequency of f and indents a moving substrate at the linear speed of V, the period of pattern is simply $\lambda = V / f$. In addition, assuming perfectly cleaved Si wafer having 90 ° edge and ignoring elastic recovery of substrate material after denting, the indented trench width becomes $s = h(\tan\theta + \cot\theta)$, where h is indented depth and θ is tool tilting angle. Therefore, there are two processing parameters to control the pattern period; vibration frequency and substrate speed. Fortunately, these two parameters can be very easily controlled in real time, thus, nanograting pattern having varying period can be simply created. The trench width can also be controlled by the indenting force (vibration amplitude) and tool tinting angle. Similar to aforementioned techniques, DNI (Dynamic Nano-Inscribing) and LDW (Localized Dynamic Wrinkling) that also use tilted flat edge, faithful contacting in DNC is a key criterion for successful patterning. Therefore, polymer substrate having certain level of compliance is critical to guarantee conformal contact and preserve tool material. Stable vertical oscillations of tool with uniform and high enough amplitude are also important in DNC. To achieve uniformly indented patterns, the frequency and the amplitude need to be consistent, and at the highest point of oscillation, the tool should be away from a substrate for smooth feeding.

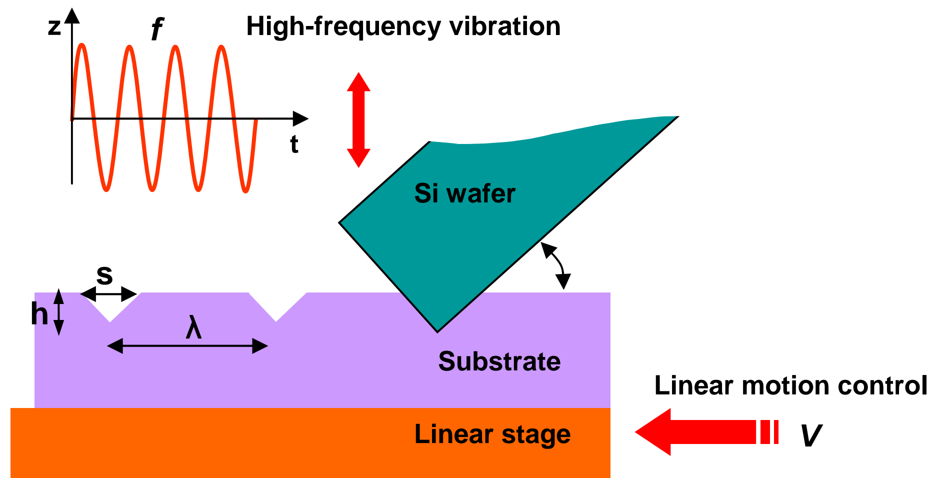

Figure 7.1 Graphical illustration of Dynamic Nano-Cutting (DNC) to generate periodic grating pattern.

7.3 Experimental details

Figure 7.2 shows the experimental setup for DNC process. High-speed DC motor (up to 24000 rpm, RadioShack) with an eccentric mass is fixed on a tool holder. A substrate on the 5-DOF stage is translated by motorized linear motor (Newport). High-frequency mechanical vibration of the tool (cleaved Si wafer) sequentially indents a moving substrate to generate periodic grating pattern. Substrate feeding speed we used was from 24 μm/sec to 266 μm/sec. Vibration force from an eccentric mass (m) with the distance from mass center, e, at rotating speed of ω, is

$$F_e(t) = me\omega^2 \cdot \sin \omega t \qquad (7\text{-}1)$$

The corresponding vertical response is

$$z(t)=\frac{m}{M}e\left(\frac{\omega}{\omega_n}\right)^2|G(i\omega)|\sin(\omega t-\phi) \qquad (7\text{-}2)$$

Where ω_n is natural frequency, ζ is damping ratio of system and

$$G(i\omega)=\frac{1}{1-(\omega/\omega_n)^2+2i\zeta\omega/\omega_n}.$$

At resonance ($\omega=\omega_n$), the amplitude is very high in "no damping" and "under damping" system, which frequently makes the vibration out of control. Therefore, for stable vibration with proper amplitude, we should avoid the resonance, or enhance damping ratio (e.g. critical damping ($\zeta=1$)). Since the vibrating motor uses single eccentric mass, there must be other components of vibrating motion rather than vertical direction. However, the tool holding setup mostly eliminates the parallel (y) vibration because of much higher stiffness in y direction, and mostly allows vertical (z-directional) vibration to realize smooth vertical indentations with less lateral perturbation.

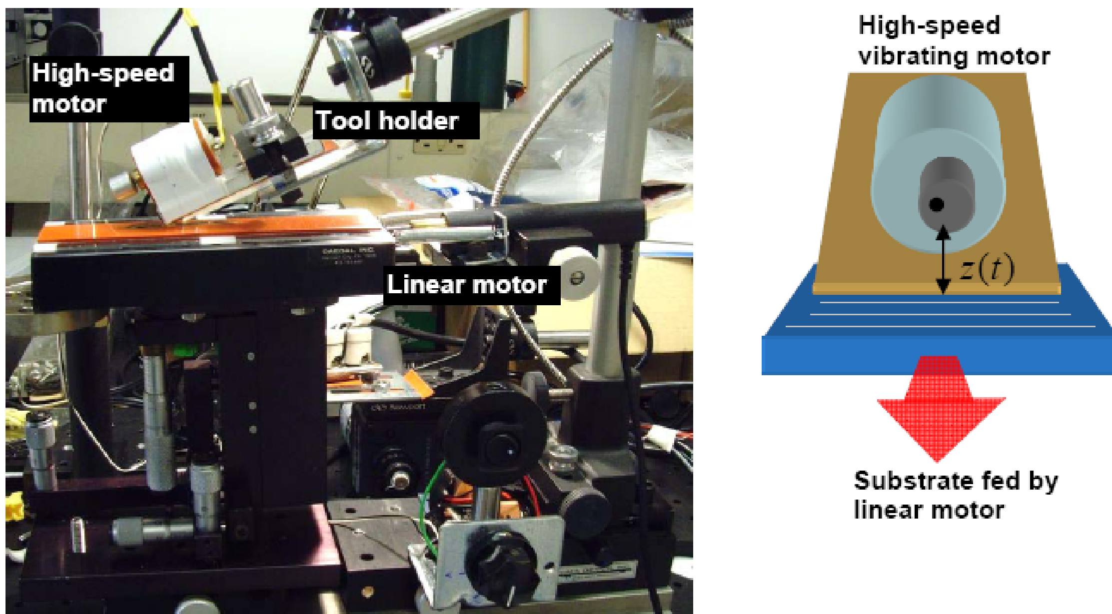

Figure 7.2 Experimental setup for Dynamic Nano-Cutting (DNC).

7.4 Results and discussion

One of the prominent features in DNC is a simple period tunability. By modulating two independent processing parameters, vibration frequency and substrate feeding speed, we can fabricate grating patterns having various periods. Trench width can also be controlled by adjusting indenting force. Micro and nano scale grating patterns in PET substrates by using different vibration frequency are shown in Figure 7.3a and 7.3b, respectively. In Figure 7.3a and inset, we used 70 Hz vibration with 250 µm/s feeding speed to generate 3.5 µm periodic pattern. The same speed with 325 Hz vibration yields 780 nm periodic pattern (Figure 7.3b). The trench width in DNC is depending on the contacting point of the oscillation cycle. When indentation occurs at the mid point of the oscillation cycle where the force is the maximum, the largest trenches can be achieved. On the other hand, if the tool (Si wafer) just touches the substrate at the lowest point of oscillation cycle, very shallow trenches are fabricated (Figure 7.3b). Since in well controlled DNC does not involves mechanical contact during feeding, the top surface of pattern is ideally smooth.

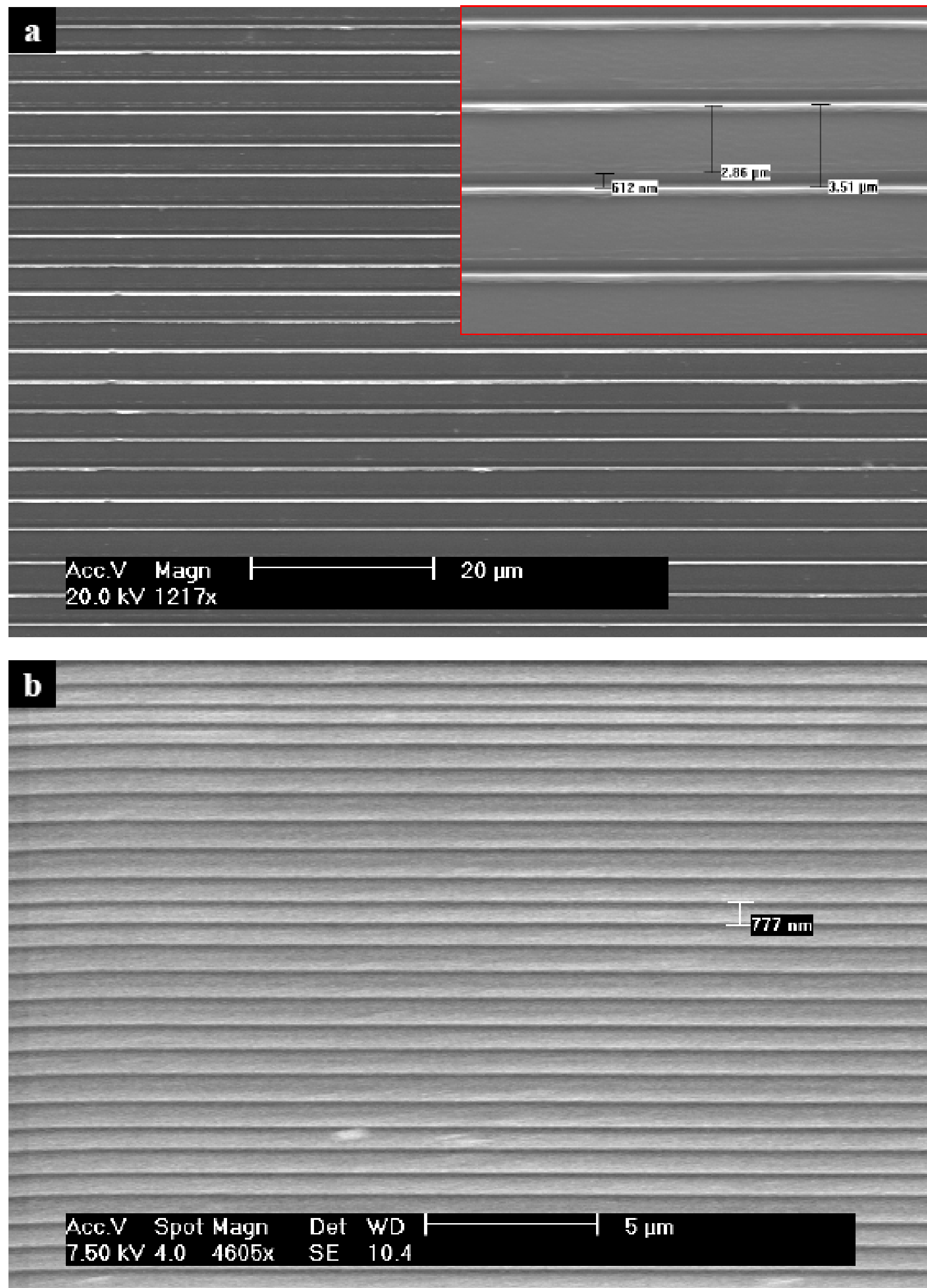

Figure 7.3 Micro / Nano gratings directly fabricated on a PET substrate by DNC using different vibration frequencies. (a) 70 Hz vibration with 250 µm/s feeding speed generates 3.5 µm period pattern. (b) The same speed with 325 Hz vibration yields 780 nm period pattern.

Basically DNC does not have a limit in substrate materials if they are softer than tool material. Using DNC, we demonstrated successful patterning on various materials. Figure 7.4a is the SEM of 1.5 μm period grating pattern performed on a 50 nm gold coated PET substrate. The gold film is cut and indented into PET to form discrete gold lines. Since aluminum has lower toughness than gold, it tends to be fractured by DNC and forms not clean patterning (Figure 7.4b). However, we can remove fractured aluminum in trenches by following cleaning process such as ultrasonic agitation. Kapton film, a commercial brand of polyimide film, is widely used in electrics and space engineering due to its excellent chemical and mechanical stability at high temperature. However, its very high Tg (over 350 °C) and low toughness make Kapton film very difficult to be patterned using conventional thermal NIL. We successfully fabricate micro gratings on Kapton film using DNC process (Figure 7.4c). Additionally, DNC provides a solution for room-temperature nano patterning of thermo-sensitive organic materials. PEDOT is a key functional material in organic lightning and organic photovoltaic applications. Previously we used localized heated Dynamic Nano-Inscribing (LH-DNI) to create nano gratings on PEDOT and P3HT[75]. However, DNI provides room-temperature patterning on thermosensitive organic material, PEDOT, as shown in Figure 7.4d. Further reduction in pattern period is possible if higher frequency vibration is used.

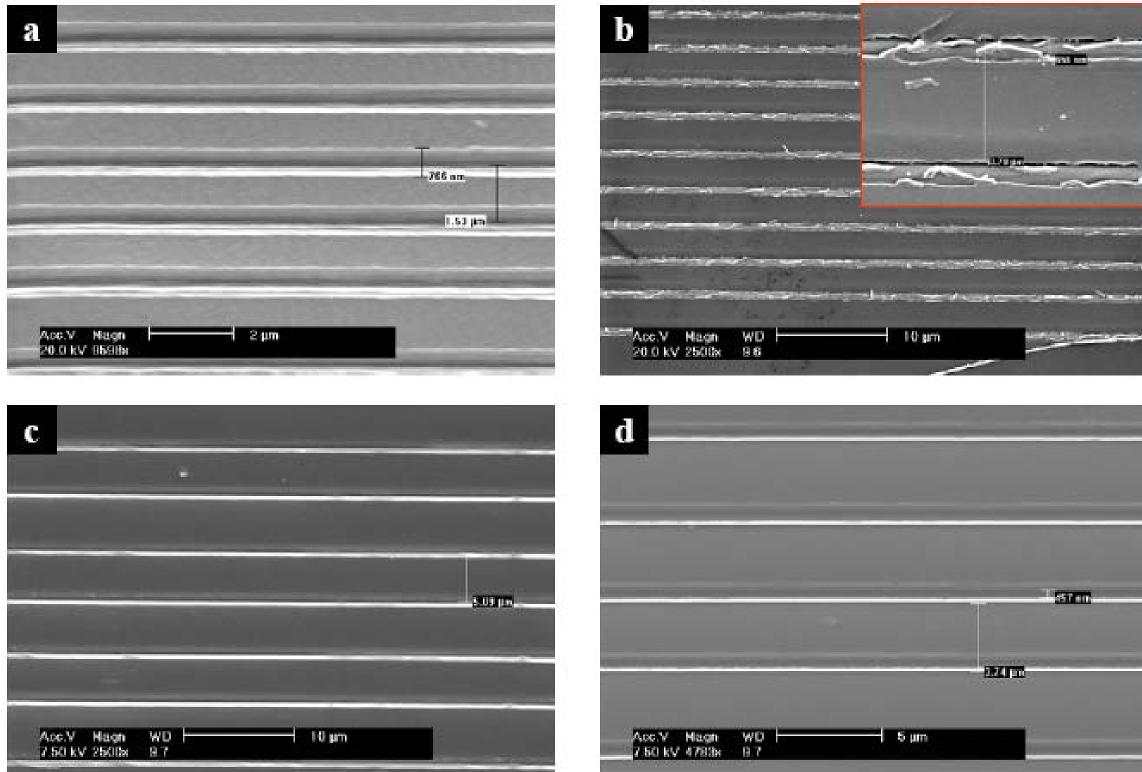

Figure 7.4 Micro-scale gratings fabricated on various substrates by DNC. (a) On 100 nm gold coated PET, (b) on 50 nm Aluminum coated Polycarbonate, (c) on Kapton film (polyimide), (d) on PEDOT coated PET.

Most of electrical and optical applications require nanogratings pattern with uniform period, and they are fabricated by many nanomanufacturing processes such as laser interference lithography. However, only few processes can produce gratings with variable period (chirp gratings) that are required in some specific optical applications such pulse shaping, bandpass filters, tunable lasers[116]. Electron-beam lithography is the most popular method used in chirp grating mask fabrication[117]. However it has a critical drawback, extremely low processing speed. Lien et. al. demonstrated a new technique to generate chirp gratings based on gradually increased surface strain from the stretched PDMS with geometric gradient[116]. This method is very simple and

straightforward, however, the precise pitch control is still challenging because it needs pre-designed PDMS stamp that cannot be modified during process.

The most attractive characteristic in DNC is its simple real-time period modulation. By changing the indenting frequency or substrate feeding speed, we can continuously generate micro/nano gratings containing varying periods. Figure 7.5 shows the examples of grating pattern with decreasing (and increasing) period fabricated by DNC. In Figure 7.5a, we used the substrate feeding speed of 100 μm/s, and increased vibration frequency from 80 Hz to 200 Hz to create varying periods from 1.2 μm to 500 nm. For Figure 7.5b, we kept the frequency 200 Hz but decreased feeding speed from 100 μm/s to 10 μm/s, and generated down to 126 nm periodic gratings. Such grating patterns having steeply varying periods can also find potential application in patterned optical color filters[118].

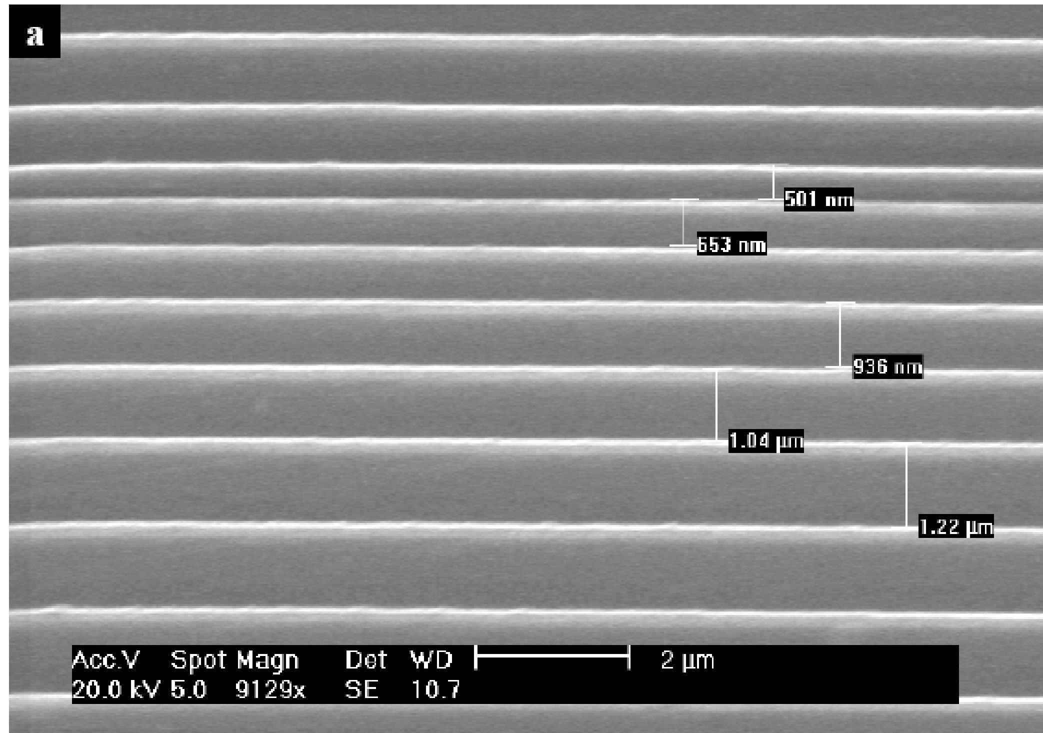

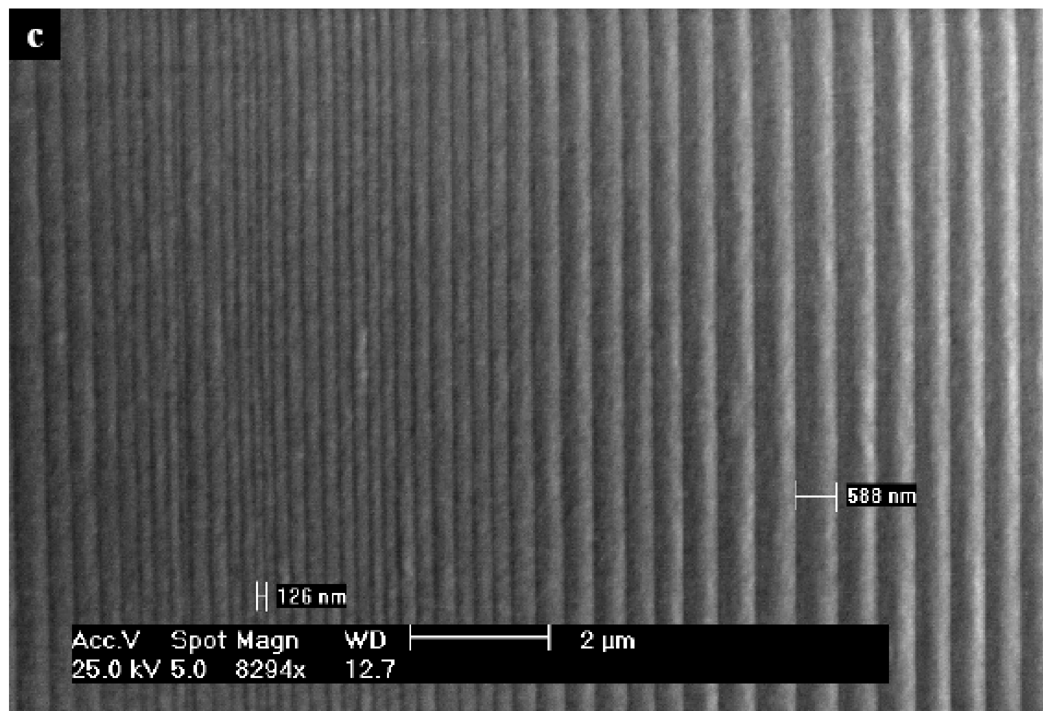

Figure 7.5 Grating patterns having decreasing (and increasing) period from micro to nano scale. (a) DNC on PET at feeding speed of 100 μm/s but increasing vibration frequency from 80 Hz to 200 Hz yielding 1.2 μm to 500 nm period. (b) Keeping the frequency 200 Hz but decreasing feeding speed from 100 μm/s to 10 μm/s generates down to 126 nm periodic gratings.

7.5 Summary

In this work, we demonstrated newly developed nanopatterning technique, Dynamic Nano-Cutting (DNC) that enables continuous fabrication of micro/nano gratings with real-time period modulation. The nature of mechanical indentation in DNC broadens the choice of substrate materials overcoming the limit in patterning resolution faced in optical lithography. In addition, its easy period modulation provides a unique way to create chirp nanogratings. Since this work is in a very early stage, we used a simple vibrating motor and manual frequency control. However, we are certain that higher frequency vibration source (e.g. ultrasonic transducer) and programmed precise control of frequency and feeding motion can produce more faithful sub-50 nm gratings in designed geometries.

Chapter 8

Conclusion

8.1 Summary of thesis

We have developed five nano patterning technologies for high-throughput, continuous fabrication of nano gratings. Utilizing the proposed techniques, we also demonstrated actual applications such as metal wire-grid polarizers and transparent metal electrodes for organic electronics. Each process relies on different mechanisms to form nanoscale periodic structures and therefore, each has different patterning characteristics. General characteristics of each process are summarized in Table 8.1. The numeric values shown in the table are roughly estimated based on our experiments. Nanoimprint Lithography (NIL) is included for comparison to the other proposed processes.

	R2RNIL	DMI	DNI	LDW	DNC	NIL
Pattern Resolution	< 50 nm	< 100 nm	< 100 nm	< 150 nm	< 100 nm	< 50 nm
Continuity	Yes, But seams exist	No	Yes. No seams exist	Yes	Yes	No
Material to be patterned	Polymer resist	Metal film on polymer	Polymer or metal film on polymer	Metal film on polymer	Any material softer than tool (Si)	Polymer resist
Types of Pattern	Any shape depending on mold	Any shape. But mostly gratings	Gratings	Gratings	Gratings	Any shape depending on mold
Grating Direction WRT Feeding Direction	Any	N/A	Parallel	Perpendicular	Perpendicular	N/A
Max. Linear Speed	> 15 mm/s	N/A	> 100mm/s	> 50mm/s	> 0.5 mm/s depending on freq.	N/A
Mold Requirement	Yes	Yes	Yes	No	No	Yes
Pattern/Mold Ratio	> 1:1	1:1	> 10^5:1	∞	∞	1:1
Defect %	< 1%	< 5%	< 5%	< 10%	< 5%	< 1%

Table 8.1 Patterning characteristics of each proposed process. NIL is for comparison.

Roll-to-roll nanoimprint lithography (R2RNIL) shares the same principle as NIL but uses a flexible mold on a roller to continuously imprint at high speeds. In this work, we demonstrated patterning of 4-inch wide and 12-inch long samples of 350 nm linewidth gratings on both flexible and hard substrates using a newly developed R2RNIL apparatus. The minimum feature size shown in this work was 50 nm but this can be

reduced if a smaller period mold is used. The maximum web speed that we used is c.a. 15 mm/s. The patterned area to mold area ratio is much higher than 1:1 since a flexible mold of limited size can continuously create large-area patterns.

Direct Metal Imprinting (DMI) enables simple formation of discrete metal wires by the same principle as NIL in an ambient environment, but it uses a polymer cushion layer under the metal film to ensure conformal contact. We demonstrated 100 nm minimum lateral feature size, but further reduction is possible.

Dynamic Nano-Inscribing (DNI) was motivated from DMI to create metal wires since we noted a moving tilted mold continuously creates seamless gratings on various materials including metals, polymers and even ITO. The nature of plastic deformation makes the patterning speed of DNI extremely high (> 100 mm/s). DNI uses only a very small edge region (c.a. 2μm) of a Si mold to generate very long patterns (e.g. 22 inch), thereby the pattern to mold area ratio is extremely high ($>10^5$).

As compared to the above mentioned techniques, Localized Dynamic Wrinkling (LDW) and Dynamic Nano-Cutting (DNC) do not require a mold containing nanogratings but use any flat edge of a hard material (e.g. Si wafer). Both technologies generate gratings perpendicular to the substrate feeding direction but rely on different principles. LDW is done by sequential formation of localized nano wrinkles in a thin metal film on a plastic substrate, while in DNC, high-frequency indentations generate nano-trenches on a moving substrate. Additionally, DNC provides real-time period modulation to realize grating patterns containing various periods.

8.2 Summary of specific achievements

A R2RNIL/R2PNIL apparatus that enables 6" wide continuous nanopatterning on either flexible substrates (R2RNIL) or hard substrates (R2PNIL) has been developed. All processes including coating, pressing and demolding take place in a continuous manner synchronized by a precisely designed pulley/belt system. High-speed processing is possible because low viscosity epoxysilicone resist quickly fills the non-sticking ETFE flexible mold on the rollers with good fidelity, and is quickly cured within a second in a dynamic situation. We demonstrated the fabrication of high extinction-ratio (up to 2500) metal wire-grid polarizers that can potentially be used in many optical and display applications. In addition, utilizing R2R processing, large-area transparent metal electrodes have been produced. Analytical models to estimate residual layer thicknesses in R2R processing have also been newly developed. Before our work, a very limited amount of research had been done on R2RNIL, and to the best of our knowledge, the apparatus that we have developed is the first one that can provide sub-100 nm resolution nanoimprinting with commercially acceptable size and speed.

Direct Metal Imprint (DMI) has been demonstrated, which enables a simple fabrication of nano metal gratings through conventional imprinting by using a polymer cushion layer under the metal film to ensure conformal contact even at low pressure. DMI reduces the time for many processing steps which would otherwise require several additional vacuum processes to fabricate the same structures if done by photolithography or traditional NIL.

We developed a novel Dynamic Nano-Inscribing (DNI) technology. Rather than surface-to-surface contact used in regular NIL, DNI relies on line contact from the sharp

edge of a tilted mold. DNI creates a seamless and essentially infinitely long nano grating patterns at very high speeds (10 cm/sec), which cannot be achieved by other existing processes. As a future application of DNI, we demonstrated the fabrication of Sprit Ring Resonators (SRR).

Localized Dynamic Wrinkling (LDW) relying on sequential nano-wrinkle generation has been developed. Compared to “second generation” processes that require original stamps containing the same features as the final patterns, LDW does not need a stamp but simply a flat edge of hard material to fabricate metal nano gratings. We also showed period modulation by adjusting the metal layer thickness, types of substrate and adhesion properties at the metal/polymer interface. LDW is a novel nanofabrication technology that has never been introduced in academia or industries, and may have a huge impact on many future engineering applications that require nano metal gratings.

Additionally, we introduced another continuous nano patterning technique, Dynamic Nano-Cutting (DNC), to create micro/nano scale gratings using sequential high-frequency indentations. Its unique features and real-time period modulation allow periodic patterns having various pitches and designed linewidths, which can be realized by only a few nanopatterning processes such as electron-beam lithography, but with much higher throughput.

All of the proposed technologies (R2RNIL, DMI, DNI, LDW and DNC) addressed in the work are targeting high-throughput, continuous processes that provide nanoscale resolution at low production cost. We believe nanoscale structures can be produced as fast as newspaper printing in the near future for many practical applications,

and the addressed new technologies can play a significant role in the realization of that dream.

8.3 Future works

8.3.1 Multiple-layer DNI

In addition to Dynamic Nano-Inscribing (DNI) of a single layer, we can also try multiple-layer DNI to fabricate functional stacked structures with nano-scale grating or dot arrays in a very simple way. A detailed process is shown in Figure 8.1. Materials with proper thicknesses are sequentially coated on the substrate by either spin-coating or deposition. The total thickness of the stacked layer should be within the range of inscribing depth and the modulus of each material should be taken into account. DNI on the stacked layer forms gratings composed of multiple layers. Each layer can be continuous or discrete depending on material properties or force conditions. Stacked nano structures can be utilized in some specific applications such as multilayer meta-materials[119] but through a much simpler process compared to conventional lithography technology.

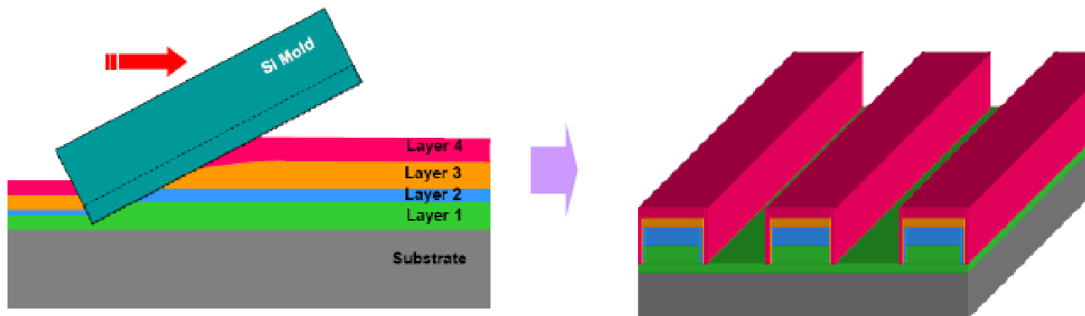

Figure 8.1 Schematic of multilayer DNI.

8.3.2 Nanowire/ nano particle fabrication by DNI

Free-standing nano-wires or nano-particles in a high volume can be simply achieved using DNI followed by lift-off process. Functional nano particles can find applications in drug delivery[120] and ordered metal particles or wires can be applied to SPR applications. Figure 8.2 describes the process to fabricate free-standing metal wires and particles. A metal film is deposited on a solvent soluble sacrificial layer (e.g. PMMA). Single DNI is performed followed by a lift-off step to remove sacrificial layer can create nano wires. Two consecutive DNIs in orthogonal directions followed by lift-off produce square (or rectangular)-shaped particles in with controlled sizes. An additional harvesting process may be required.

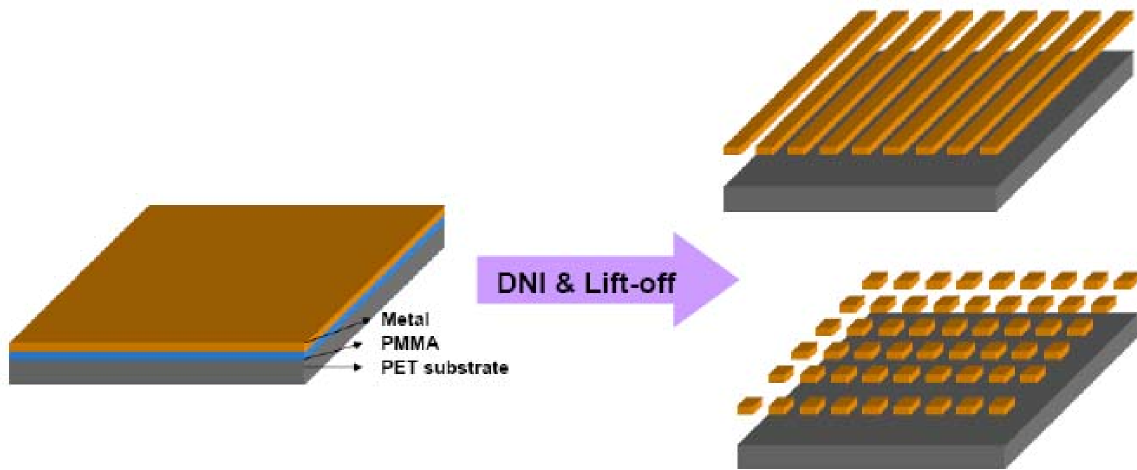

Figure 8.2 DNI followed by lift-off (polymer layer removal) can produce nano metal wires (single DNI) or dot arrays (double DNI).

8.3.3 DNI on a free-curved surface

In Chapter 5, we demonstrated nano patterning on a cylindrical surface using DNI. However, nano patterning on a spherical surface or a free-curved surface is extremely

challenging for other existing patterning processes. DNI may provide a solution for nano grating patterning on a free curved surface. To realize this process, specially designed molds are required. To follow the contour of a free-curved surface faithfully, each grating line of a Si mold should be independently moved. Embedded Si “fingers” in a PDMS cushion layer may be a good solution as a mold for this process. Figure 8.3a illustrates the mold fabrication process. A Si stamp containing a grating is molded into a thick PDMS layer. Anisotropic etching can remove the backside of the Si stamp to finalize the Si fingers embedded in the PDMS layer where each can independently move with the contour of the surface during DNI (Figure 8.3b). Close-loop force control may be required to inscribe a free-curved surface. Nano/micro gratings on a curved surface can find applications in the optics and energy industry. For example, Ko et. al. demonstrated an artificial eye camera by building an integrated circuit on a hemispherical surface using a pattern transferring technique[121].

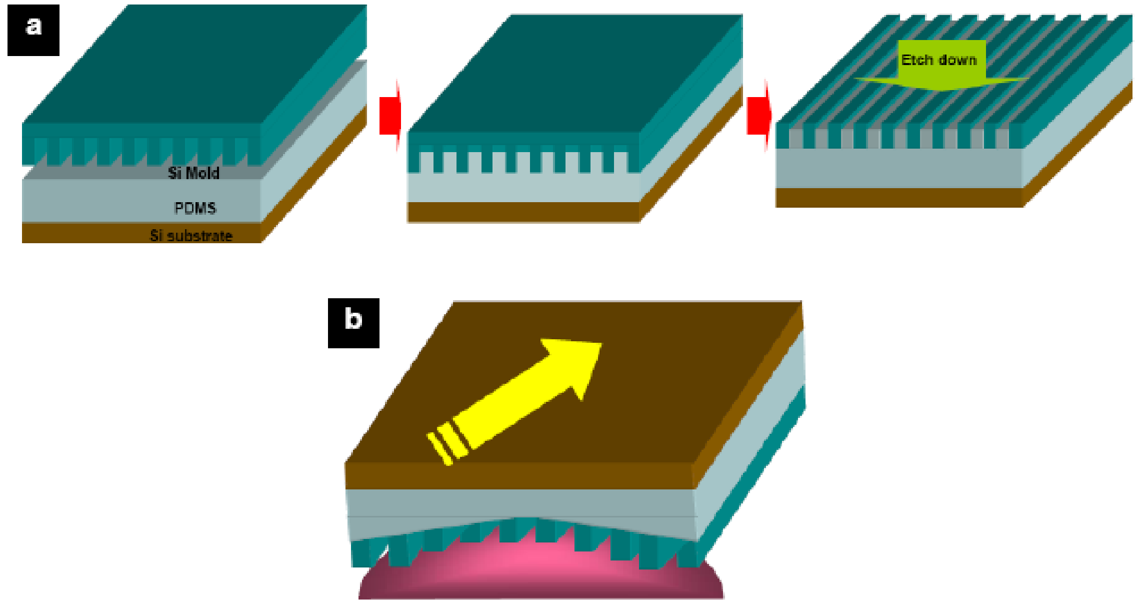

Figure 8.3 (a) Tool fabrication steps for free-surface DNI. A Si stamp is molded into PDMS/Si substrate and backside of the stamp is etched away to fabricate Si fingers. (b) DNI on any free-curved surface including spherical surface.

8.3.4 Pattern writing based on liquid DNI

DNI is a top-down process that gradually imprints material using a moving stamp. It may be possible to draw nano wires by adding material through a bottom-up DNI process. As illustrated in Figure 8.4, low viscosity UV curable liquid resist flows through the channels (grating trenches) by capillary action and continuously transfers to a moving substrate. This is the same mechanism as ink writing in fountain pen. Just after transferring, resist is crosslinked by UV exposure to form solid lines. This method may provide residual-free grating patterns which can be directly used as an etching mask without the need for a reactive ion etching process to remove the residual layer.

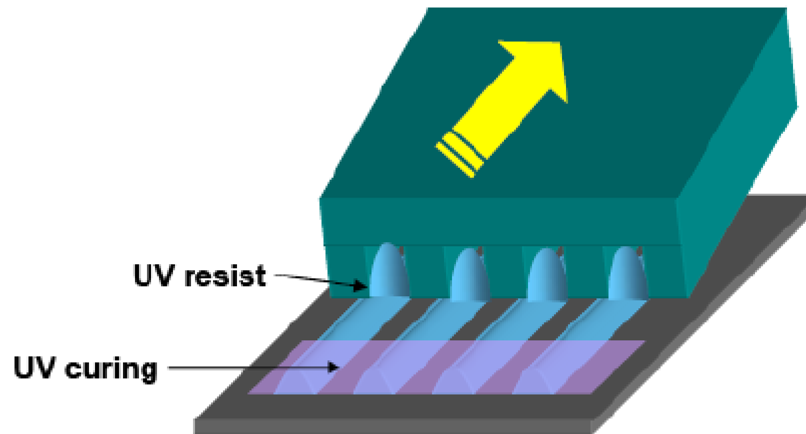

Figure 8.4 Schematic of pattern writing based on DNI

8.3.5 Si mold fabrication using LDW process

Localized Dynamic Wrinkling (LDW) generates metal nanogratings with controlled period on flexible substrates. By transferring them to hard substrates such as a Si wafer, we can fabricate a hard mold containing nano gratings. A detailed process is shown in Figure 8.5. First, LDW is performed to generate metal gratings on a plastic substrate. Second, the metal gratings are transferred to a Si substrate using UV curable resist as an adhesion layer. One can then etch down to the Si substrate using the metal as an etch mask. Lift-off can then be performed to remove the metal/resist layer to finalize a Si mold containing nano gratings. LDW can be a cost-effective solution for mold fabrication since it does not require expensive optical settings to fabricate a large size mold.

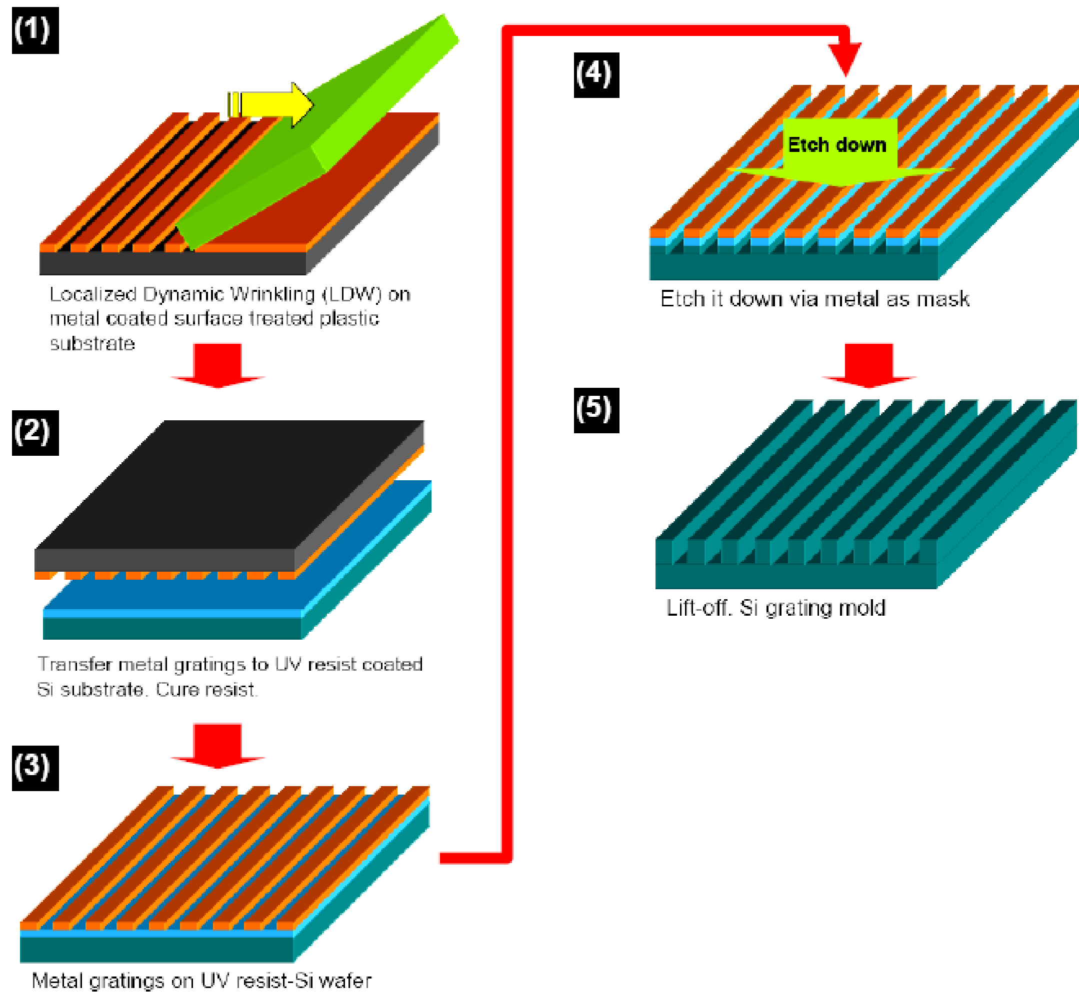

Figure 8.5 Schematics of a hard mold fabrication process from LDW pattern on a flexible substrate. (1) LDW to generate metal gratings on plastic substrate. (2-3) Transfer metal gratings to a Si substrate using adhesion layer (e.g. UV curable resist) (4) Etch down to the Si substrate. (5) Lift-off to remove metal/resist layer.

8.3.6 LDW combined with DNI

LDW and DNI have a similarity; grating patterns are continuously generated by a tilted tool (a flat edge for LDW and a Si mold for DNI) in a dynamic situation. We can combine the two processes to fabricate ordered nano dot arrays in a single step. DNI produces gratings along the direction of the mold movement while LDW takes part in a periodic cutting action perpendicular to the mold's movement direction (Figure 8.5).

Therefore, using a tool shown in Figure 8.5, which is basically a cleaved Si wafer attached to a Si grating mold, we can generate metal nano dot arrays in a simple single scanning step.

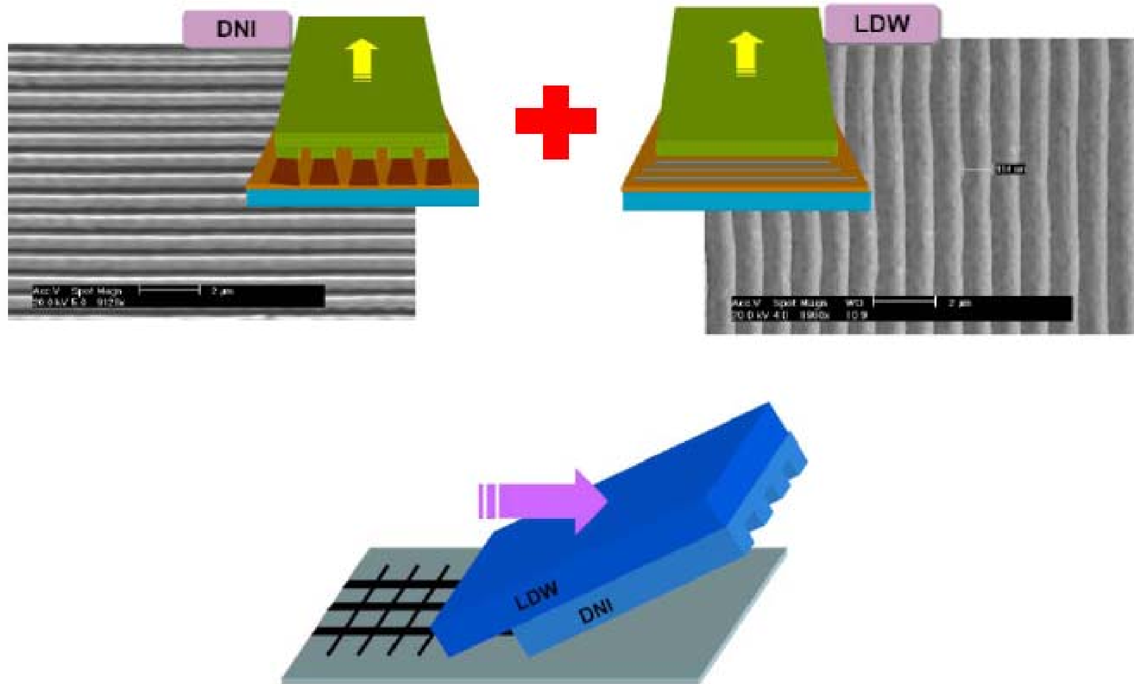

Figure 8.6 Combination of DNI and LDW can produce nanoscale metal dot arrays in a simple single step.

Bibliography

[1] Y. Martin, F. Zenhausern, and H. K. Wickramasinghe, "Scattering Spectroscopy of Molecules at Nanometer Resolution," *Appl. Phys. Lett.,* vol. 68, pp. 2475-2477, 1996.

[2] R. J. Heaton, A. W. Peterson, and R. M. Georgiadis, "Electrostatic surface plasmon resonance: Direct electric field-induced hybridization and denaturation in monolayer nucleic acid films and label-free discrimination of base mismatches," *PNAS,* vol. 98, pp. 3701-3704, 2001.

[3] K. R. Catchpole and S. Pillai, "Surface plasmons for enhanced silicon light-emitting diodes and solar cells," *J. Luminescence,* vol. 121, pp. 315-318, 2006.

[4] M. Auslender, D. Levy, and S. Hava, "One-dimensional antireflection gratings in (100) silicon: a numerical study," *Appl. Opt.,* vol. 37, pp. 369-373, 1998.

[5] M. Xu, H. P. Urbach, D. K. G. d. Bore, and H. J. Cornelissen, "Wire-grid diffraction grating used as polarizing beam splitter for visible light and applied in liquid crystal on silicon," *Opt. Express,* vol. 13, pp. 2303–2320, 2005.

[6] Y. Ekinci, H. H. Solak, C. David, and H. Sigg, "Bilayer Al wire-grids as broadband and high-performance polarizers," *Opt. Express,* vol. 14, pp. 2323-2334 2006.

[7] S. H. Ahn, J.-S. Kim, and L. J. Guo, "Bilayer Metal Wire-grid Polarizer Fabricated by Roll-to-Roll Nanoimprint Lithography on Flexible Plastic Substrate," *J. Vac. Sci. Technol. B* vol. 25, pp. 2388-2391, 2007.

[8] M. G. Kang and L. J. Guo, "Nanoimprinted Semi-Transparent Metal Electrode and its Application in OLED," *Adv. Mater.,* vol. 19, pp. 1391-1396, 2007.

[9] M.-G. Kang and L. J. Guo, "Semitransparent Cu electrode on a flexible substrate and its application in organic light emitting diodes," *J. Vac. Sci. Technol. B,* vol. 25, pp. 2637-2641, 2007.

[10] X. D. Hoa, A. G. Kirk, and M. Tabriziana, "Enhanced SPR response from patterned immobilization of surface bioreceptors on nano-gratings," *Biosensors and Bioelectronics,* vol. 24, pp. 3043–3048, 2009.

[11] B. D. Lucas, J.-S. Kim, C. Chin, and L. J. Guo, "Nanoimprint Lithography Based Approach for the Fabrication of Large-Area, Uniformly Oriented Plasmonic Arrays," *Adv. Mater.,* vol. 20, pp. 1129–1134, 2008.

[12] X. D. Hoa, M. Martin, A. Jimenez, J. Beauvais, P. Charette, A. Kirkc, and M. Tabrizian, "Fabrication and characterization of patterned immobilization of quantum dots on metallic nano-gratings," *Biosen. Bioelectron.,* vol. 24, pp. 970–975, 2008.

[13] B. Li, X. Tang, H. Xie, and X. Zhang, "Strain analysis in MEMS/NEMS structures and devices by using focused ion beam system," *Sensors and Actuators A,* vol. 111, pp. 57–62, 2004.

[14] P. Mukherjee, M.-G. Kang, T. H. Zurbuchen, L. J. Guo, and F. A. Herrero, "Fabrication of high aspect ratio Si nanogratings with smooth sidewalls for a deep UV-blocking particle filter," *J. Vac. Sci. Technol. B,* vol. 25, pp. 2645-2648, 2007.
[15] K. EFIMENKO, M. RACKAITIS, E. MANIAS, A. VAZIRI, L. MAHADEVAN, and J. GENZER, "Nested self-similar wrinkling patterns in skins," *Nat. Mater.,* vol. 4, pp. 293-297, 2005.
[16] S. Y. Chou, P. R. Krauss, and P. J. Renstrom, "Imprint of sub-25 nm vias and trenches in polymers," *Appl. Phys. Lett.,* vol. 67, pp. 3114-3116, 1995.
[17] S. Y. Chou, P. R. Krauss, and P. J. Renstrom, "Imprint Lithography with 25-Nanometer Resolution " *Science,* vol. 272, pp. 85-87, 1996.
[18] L. J. Guo, "Nanoimprint Lithography: Methods and Material Requirements," *Adv. Mater.,* vol. 19, pp. 495-513, 2007.
[19] W. Zhang and S. Y. Chou, "Fabrication of 60-nm transistors on 4-in. wafer using nanoimprint at all lithography levels," *Appl. Phys. Lett.,* vol. 83, pp. 1632-1634, 2003.
[20] D. Pisignano, L. Persano, M. F. Raganato, P. Visconti, R. Cingolani, G. Barbarella, L. Favaretto, and G. Gigli, "Room-Temperature Nanoimprint Lithography of Non-thermoplastic Organic Films," *Adv. Mater.,* vol. 16, pp. 525-529, 2004.
[21] M.-S. Kim, J.-S. Kim, J. Cho, M. Stein, L. J. Guo, and J. Kim, "Flexible conjugated polymer photovoltaic cells with controlled heterojunctions fabricated using nanoimprint lithography," *Appl. Phys. Lett.,* vol. 90, p. 123113, 2007.
[22] W. Wu, B. Cui, X. Sun, W. Zhang, L. Zhuang, L. Kong, and S. Y. Chou, "Large area high density quantized magnetic disks fabricated using nanoimprint lithography," *J. Vac. Sci. and Technol. B,* vol. 16, pp. 3825-3829, 1998.
[23] J. I. Martin, J. Nogues, K. Liu, J. L. Vicent, and I. K. Schuller, "Ordered magnetic nanostructures: fabrication and properties," *J. Magn. Magn. Mater.,* vol. 256, pp. 449-501, 2003.
[24] H. Cao, Z. N. Yu, J. Wang, J. O. Tegenfeldt, R. H. Austin, E. Chen, W. Wu, and S. Y. Chou, "Fabrication of 10 nm enclosed nanofluidic channels," *Appl. Phys. Lett.,* vol. 81, pp. 174-176, 2002.
[25] L. J. Guo, X. Cheng, and C. F. Chou, "Fabrication of Size-Controllable Nanofluidic Channels by Nanoimprinting and Its Application for DNA Stretching " *Nano Lett.,* vol. 4, p. 69, 2004.
[26] D. Falconnet, D. Pasqui, S. Park, R. Eckert, H. Schift, J. Gobrecht, R. Barbucci, and M. Textor, "A Novel Approach to Produce Protein Nanopatterns by Combining Nanoimprint Lithography and Molecular Self-Assembly " *Nano Lett.,* vol. 4, pp. 1909-1914, 2004.
[27] J. D. Hoff, L. J. Cheng, E. Meyhofer, L. J. Guo, and A. J. Hunt, "Nanoscale Protein Patterning by Imprint Lithography," *Nano Lett.,* vol. 4, pp. 853-857, 2004.
[28] M. Colburn, S. C. Johnson, M. D. Stewart, S. Damle, T. C. Bailey, B. Choi, M. Wedlake, T. B. Michaelson, S. V. Sreenivasan, J. G. Ekerdt, and C. G. Willson, "Step and flash imprint lithography: a new approach to high-resolution patterning," *Proc. SPIE,* vol. 3676, pp. 379-389, 1999.
[29] S. H. Ahn and L. J. Guo, "High-Speed Roll-to-Roll Nanoimprint Lithography on Flexible Plastic Substrate," *Adv. Mater.,* vol. 20, pp. 2044-2049, 2008.

[30] S. H. Ahn and L. J. Guo, "Large-area roll-to-roll and roll-to-plate nanoimprint lithography -a step toward high-throughput application of continuous nanoimprinting-," *ACS Nano,* 2009, In press.
[31] L.-R. Bao, X. Cheng, X. D. Huang, L. J. Guo, S. W. Pang, and A. F. Yee, "Nanoimprinting over topography and multilayer three-dimensional printing," *J. Vac. Sci. Technol. B,* vol. 20, pp. 2881-2886, 2002.
[32] K.-D. Kim, A. Altun, D.-G. Choi, and J.-H. Jeong, "A 4-in.-based single-step UV-NIL tool using a low vacuum environment and additive air pressure," *Microelec. Eng.,* vol. 85, pp. 2304–2308, 2008.
[33] Q. Xia, W. Robinett, M. W. Cumbie, N. Banerjee, T. J. Cardinali, J. J. Yang, W. Wu, X. Li, W. M. Tong, D. B. Strukov, G. S. Snider, G. Medeiros-Ribeiro, and R. S. Williams, "Memristor-CMOS Hybrid Integrated Circuits for Reconfigurable Logic," *Nano Lett.,* vol. 9, pp. 3640-3645, 2009.
[34] A. d. Campo and E. Arzt, "Fabrication Approaches for Generating Complex Micro- and Nanopatterns on Polymeric Surfaces," *Chem. Rev.,* vol. 108, pp. 911-945, 2008.
[35] M. Campbell, D. N. Sharp, M. T. Harrison, R. G. Denning, and A. J. Turberfield, "Fabrication of photonic crystals for the visible spectrum by holographic lithography," *Nature,* vol. 404, pp. 53-56 2000.
[36] C. K. Malek, F. T. Hartley, and J. Neogi, "Fast prototyping of high-aspect ratio, high-resolution X-ray masks by gas-assisted focused ion beam," *Microsystem Technol.,* vol. 9, pp. 409-412, 2003.
[37] A.-V. Ruzette and L. Leibler, "Block copolymers in tomorrow's plastics " *Nat. Mater.,* vol. 4, pp. 19-31, 2005.
[38] H. Tan, A. Gilbertson, and S. Y. Chou, "Roller nanoimprint lithography," *J. Vac. Sci. and Technol. B,* vol. 16, pp. 3926-3928, 1998.
[39] J. Zaumseil, M. A. Meitl, J. W. P. Hsu, B. R. Acharya, K. W. Baldwin, Y.-L. Loo, and J. A. Rogers, "Three-Dimensional and Multilayer Nanostructures Formed by Nanotransfer Printing " *Nano Lett.,* vol. 3, pp. 1223-1227, 2003.
[40] D. Suh, S.-J. Choi, and H. H. Lee, "Rigiflex Lithography for Nanostructure Transfer," *Adv. Mater.,* vol. 17, pp. 1554-1560, 2005.
[41] G. B. Onoa, T. B. O'Reilly, M. E. Walsh, and H. I. Smith, "Bulk production of singly dispersed carbon nanotubes with prescribed lengths," *Nanotechnol.,* vol. 12, pp. 2799-2803, 2005.
[42] S. Ahn, K. Lee, J. Kim, S. H. Kim, J. Park, S. H. Lee, and P. Yoon, "Fabrication of subwavelength aluminum wire grating using nanoimprint lithography and reactive ion etching," *Microelectron. Eng.,* vol. 78-79, pp. 314-318, 2005.
[43] C. P.-Hernandez, J.-S. Kim, L. J. Guo, and P.-F. Fu, "High throughput and etch selective nanoimprinting and stamping based on fast thermal-curable polydimethysiloxanes," *Adv. Mater.,* vol. 19, pp. 1222-1227, 2007.
[44] X. Cheng, L. J. Guo, and P.-F. Fu, "Room-Temperature, Low-Pressure Nanoimprinting Based on Cationic Photopolymerization of Novel Epoxysilicone Monomers," *Adv. Mater.,* vol. 17, pp. 1419-1424, 2005.
[45] X. J. Yu and H. S. Kwok, "Optical wire-grid polarizers at oblique angles of incidence," *Journal of Applied Physics,* vol. 93, pp. 4407-4412, 2003.

[46] T. A. Savas, M. L. Schattenburg, J. M. Carter, and H. I. Smith, "Large-area achromatic interferometric lithography for 100 nm period gratings and grids," in *The 40th international conference on electron, ion, and photon beam technology and nanofabrication*, Atlanta, Georgia (USA), 1996, pp. 4167-4170.

[47] S. Y. Chou, P. R. Krauss, and P. J. Renstrom, "Nanoimprint lithography," in *J. Vac. Sci. Technol. B 14(6)*, 1996, pp. 4129-4133.

[48] L. Chen., J. Wang, F. Walters, X. Deng, M. Buonanno, S. Tai, and X. Liu, "Large flexible nanowire grid visible polarizer made by nanoimprint lithography," *Appl. Phys. Lett.,* vol. 90, pp. 063111-3, 2007.

[49] H.-J. Lee, H. W. Ro, C. L. Soles, R. L. Jones, E. K. Lin, and W.-L. Wu, "Effect of initial resist thickness on residual layer thickness of nanoimprinted structures," *J. Vac. Sci and Technol. B,* vol. 23, pp. 3023-3027, 2005.

[50] H. Lee, "Effect of imprinting pressure on residual layer thickness in ultraviolet nanoimprint lithography," *J. Vac. Sci and Technol. B,* vol. 23, pp. 1102-1106, 2005.

[51] H.-C. Scheer and H. Schulz, "A contribution to the flow behaviour of thin polymer films during hot embossing lithography," *Microelectron. Eng.,* vol. 56, pp. 311-332, 2001.

[52] W.-B. Young, "Analysis of the nanoimprint lithography with a viscous model," *Microelectron. Eng.,* vol. 77, pp. 405-411, 2005.

[53] L. J. Heydermana, H. Schifta, C. Davida, J. Gobrechta, and T. Schweizerb, "Flow behaviour of thin polymer films used for hot embossing lithography," *Microelectron. Eng.,* vol. 54, pp. 229-245, 2000.

[54] Y. Hirai, T. Konishi, T. Yoshikawa, and S. Yoshida, "Simulation and experimental study of polymer deformation in nanoimprint lithography," *J. Vac. Sci and Technol. B,* vol. 22, pp. 3288-3293, 2004.

[55] H. Schulz, M. Wissen, N. Bogdanski, H.-C. Scheer, K. Mattes, and C. Friedrich, "Impact of molecular weight of polymers and shear rate effects for nanoimprint lithography," *Microelectron. Eng.,* vol. 83, pp. 259-280, 2006.

[56] H. D. Rowland, A. C. Sun, P. R. Schunk, and W. P. King, "Impact of polymer film thickness and cavity size on polymer flow during embossing: toward process design rules for nanoimprint lithography," *J. Micromech. Microeng.,* vol. 15, pp. 2414-2425, 2005.

[57] S.-M. Seo, T.-I. Kim, and H. H. Lee, "Simple fabrication of nanostructure by continuous rigiflex imprinting," *Microelectron. Eng.,* vol. 84, pp. 567-572, 2006.

[58] M. M. Denn and G. Marrucci, "Squeeze flow between finite plates," *J. Non-Newtonian Fluid Mech.,* vol. 87, pp. 175-178, 1999.

[59] M. D. Pascovici and T. Cicone, "Squeeze-film of unconformal, compliant and layered contacts," *Tribology International,* vol. 36, pp. 791-799, 2003.

[60] S. Hao and L. M. Keer, "Rolling Contact Between Rigid Cylinder and Semi-Infinite Elastic Body With Sliding and Adhesion," *J. of Tribol.,* vol. 129, pp. 481-494, 2007.

[61] B. N. J. Persson and F. Mugele, "Squeeze-out and wear: fundamental principles and applications," *J. Phys.: Condens. Matter,* vol. 16, pp. 295-355, 2004.

[62] S.-M. Seo, T.-I. Kim, and H. H. Lee, "Simple fabrication of nanostructure by continuous rigiflex imprinting," *Microelectron. Eng.,* vol. 84, pp. 567-572, 2007.

[63] K. L. Johnson, *Contact Mechanics*: Cambridge University Press, 1987.
[64] A. V. Pocius, *Adhesion and adhesives technology : an introduction* Hanser/Gardner Publications, 1997.
[65] M.-G. Kang, H. J. Park, S. H. Ahn, and L. J. Guo, "Transparent Cu nanowire mesh electrode on flexible substrates fabricated by transfer printing and its application in organic solar cell," *Solar Energy Materials & Solar Cells,* 2010, Submitted.
[66] H. J. Park, M.-G. Kang, S. H. Ahn, and L. J. Guo, "Facile route to polymer solar cells with optimum morphology applicable to roll-to-roll process," *Adv. Mater.,* 2010 submitted.
[67] M.-G. Kang, H. J. Park, S. H. Ahn, and L. J. Guo, "Towards Low-Cost, High Efficiency, and Scalable Organic Solar Cells with Transparent Metal Electrode and Improved Domain Morphology," *JSTQE,* 2010, In press.
[68] G. Li, V. Shrotriya, J. Huang, Y. Yao, T. Moriarty, K. Emery, and Y. Yang, "High-efficiency solution processable polymer photovoltaic cells by self-organization of polymer blends," *Nat. Mater.,* vol. 4, pp. 864-868, 2005.
[69] W. Ma, C. Yang, X. Gong, K. Lee, and A. J. Heeger, "Thermally Stable, Efficient Polymer Solar Cells with Nanoscale Control of the Interpenetrating Network Morphology," *Adv. Funct. Mater.,* vol. 15, pp. 1617-1622, 2005.
[70] C. Kim, P. E. Burrows, and S. R. Forrest, "Micropatterning of Organic Electronic Devices by Cold-Welding," *Science,* vol. 288, pp. 831-833, 2000.
[71] C. Kim, M. Shtein, and S. R. Forrest, "Nanolithography based on patterned metal transfer and its application to organic electronic devices," *Appl. Phys. Lett.,* vol. 80, pp. 4051-4053, 2002.
[72] C.-H. Chen and Y.-C. Lee, "Contact printing for direct metallic pattern transfer based on pulsed infrared laser heating," *J. Micromech. Microeng.,* vol. 17, pp. 1252–1256, 2007.
[73] K. A. Lister, S.Thoms, D. S. Macintyre, C. D. W. Wilkinson, J. M. R. Weaver, and B. G. Casey, "Direct imprint of sub-10 nm features into metal using diamond and SiC stamps," *J. Vac. Sci. Technol. B,* vol. 22, pp. 3257-3259, 2004.
[74] G. R. Harrison, "The production of diffraction gratings I. Development of the ruling art," *J. Opt. Soc. Am.,* vol. 39, pp. 413-426, 1949.
[75] S. H. Ahn and L. J. Guo, "Dynamic Nanoinscribing for Continuous and Seamless Metal and Polymer Nanogratings," *Nano Lett.,* vol. 9, pp. 4392-4397, 2009.
[76] S. Kalpakjian and S. R. Schmid, *manufacturing processes for engineering materials*, 4th ed.: Prentice Hall, 2003.
[77] L. Aretxabaleta, J. Aurrekoetxea, I. Urrutibeascoa, and M. Sa´nchez-Soto, "Characterisation of the impact behaviour of polymer thermoplastics," *J. Polymertesting,* vol. 24, pp. 145–151, 2005.
[78] K. Hattori, K. Ito, Y. Soeno, M. Takai, and M. Matsuzaki, "Fabrication of Discrete Track Perpendicular Media for High Recording Density," *IEEE TRANSACTIONS ON MAGNETICS,* vol. 40, pp. 2510-2515, 2004.
[79] M. Meitl, Z.-T. Zhu, V. Kumar, K. J. Lee, X. Feng, Y. Y. Huang, I. Adesida, R. G. Nuzzo, and J. A. Rogers, "Transfer printing by kinetic control of adhesion to an elastomeric stamp," *Nat. Mater.,* vol. 5, pp. 33-38, 2006.

[80] X. Cheng and L. J. Guo, "One-step lithography for various size patterns with a hybrid mask-mold," *Microelec. Eng.,* vol. 71, pp. 288-293, 2004.

[81] W. Luo, S. Jazouli, and T. Vu-Khanh, "Modeling of Nonlinear Viscoelastic Creep of Polycarbonate," *e-Polymers (http://www.e-polymers.org),* p. no. 017, 2007.

[82] F. P. Incropera and D. P. DeWitt, *Fundamentals of heat and mass transfer*, 5 ed.: John Wiley & Sons, Inc, 2002.

[83] J. R. Tumblestona, D.-H. Kob, R. Lopeza, and E. T. Samulskib, "Characterizing enhanced performance of nanopatterned bulk heterojunction organic photovoltaics," *Proc. of SPIE,* vol. 7047, 2008.

[84] M. Aryal, F. Buyukserin, K. Mielczarek, X.-M. Zhao, J. Gao, A. Zakhidov, and W. Hu, "Imprinted large-scale high density polymer nanopillars for organic solar cells," *J. Vac. Sci. Technol. B,* vol. 26, pp. 2562-2566, 2008.

[85] X. Yu, R. Xing, S. Luan, Z. Wang, and Y. Han, "Direct micropatterning of polymer materials by ice mold," *Applied Surface Science,* vol. 252, pp. 8544–8548, 2006.

[86] A. Takakuwa, M. Ikawa, M. Fujita, and K. Yase, "Micropatterning of Electrodes by Microcontact Printing Method and Application to Thin Film Transistor Devices," *Jpn. J. Appl. Phys.,* vol. 46, pp. 5960–5963, 2007.

[87] J. R. Chan, X. Q. Huang, and A. M. Song, "Nondestructive photolithography of conducting polymer structures," *J. App. Phys.,* vol. 99, 2006.

[88] J. R. Chan, X. Q. Huang, and A. M. Song, "Scanning Probe Microscope Based Nanolithography on Conducting Polymer Films," *Jpn. J. Appl. Phys,* vol. 45, pp. 2095–2098, 2006.

[89] M.-S. Kim, M.-G. Kang, L. J. Guo, and J. Kim, "Choice of electrode geometry for accurate measurement of organic photovoltaic cell performance," *Appl. Phys. Lett.,* vol. 92, 2008.

[90] B. C. H. Steele and A. Heinzel, "Materials for fuel-cell technologies," *Nature,* vol. 414, pp. 345-352, 2001.

[91] Y. Zhang, J. Lu, S. Shimano, H. Zhou, and R. Maeda, "Effects of the nanoimprint pattern on the performance of a MEMS-based micro direct methanol fuel cell," *J. Micromech. Microeng.,* vol. 19, pp. 1-6, 2007.

[92] A. D. Taylor, B. D. Lucas, L. J. Guo, and L. T. Thompson, "Nanoimprinted electrodes for micro-fuel cell applications," *J. Power Sources,* vol. 171, pp. 218-223, 2007.

[93] J. B. Pendry, A. J. Holden, D. J. Robbins, and W. J. Stewart, "Magnetism from Conductors, and Enhanced Non-Linear Phenomena," *IEEE Trans. Microwave Theory Tech.,* vol. 47, p. 2075, 1999.

[94] S. Linden, C. Enkrich, M. Wegener, J. Zhou, T. Koschny, and C. M. Soukoulis, "Magnetic response of metamaterials at 100 terahertz," *Science,* vol. 306, pp. 1351-1353, 2004.

[95] M. W. Klein, C. Enkrich, M. Wegener, C. M. Soukoulis, and S. Linden, "Single-slit split-ring resonators at optical frequencies: limits of size scaling," *Optics Letters,* vol. 31, pp. 1259-1261 2006.

[96] M. S. Rill, C. Plry, M. Thirl, I. Staude, G. V. Freymann, S. Linden, and M. Wegener, "Photonic metamaterials by direct laser writing and silver chemical vapour deposition," *nature materials,* vol. 7, pp. 543-546, 2008.

[97] A. F. Kaplan, M.-G. Kang, L. J. Guo, T. Xu, and X.-G. Luo, "Large Area Negative Refractive Index Structures at Optical Frequencies Using Nanoimprint Lithography," in *53nd International Conference on Electron, Ion, and Photon Beam Technology and Nanofabrication* Marco Island, FL., 2009.

[98] A. F. Kaplan, M.-G. Kang, L. J. Guo, T. Xu, and X. Luo, "Negative Refractive Index Structures at Optical Frequencies Fabricated by Nanoimprint Lithography for Large Area Applications," *J. Vac. Sci. Technol. B,* vol. 27, pp. 3175-3179, 2009.

[99] W. Wu, Z. Yu, S.-Y. Wang, and R. S. Williams, "Midinfrared metamaterials fabricated by nanoimprint lithography," *Appl. Phys. Lett.,* vol. 90, pp. 063107-1-3, 2007.

[100] M. D. Fischbein and M. Drndic, "Sub-10 nm Device Fabrication in a Transmission Electron Microscope," *Nano Lett.,* vol. 7, pp. 1329-1337, 2007.

[101] N. Bowden, S. Brittain, A. G. Evans, J. W. Hutchinson, and G. M. Whitesides, "Spontaneous formation of ordered structures in thin films of metals supported on an elastomeric polymer," *Nature,* vol. 393, 1998.

[102] W. T. S. Huck, N. Bowden, P. Onck, T. Pardoen, J. W. Hutchinson, and G. M. Whitesides, "Ordering of Spontaneously Formed Buckles on Planar Surfaces," *Langmuir,* vol. 16, pp. 3497–3501, 2000.

[103] E. Cerda, K. Ravi-Chandar, and L. Mahadevan, "Thin films: Wrinkling of an elastic sheet under tension," *Nature,* vol. 419, pp. 579-580 2002.

[104] C.-C. Fu, A. Grimes, M. Long, C. G. L. Ferri, B. D. Rich, S. Ghosh, S. Ghosh, L. P. Lee, A. Gopinathan, and M. Khine, "Tunable Nanowrinkles on Shape Memory Polymer Sheets," *Adv. Mater.,* vol. 21, pp. 1-5, 2009.

[105] A. Schweikart and A. Fery, "Controlled wrinkling as a novel method for the fabrication of patterned surfaces," *Microchim Acta,* vol. 165, pp. 249–263, 2009.

[106] J. Genzer and J. Groenewold, "Soft matter with hard skin: From skin wrinkles to templating and material characterization," *Soft Matter,* vol. 2, pp. 310-323, 2006.

[107] M. Pretzl, A. Schweikart, C. Hanske, A. Chiche, U. Zettl, A. Horn, A. Bker, and A. Fery, "A Lithography-Free Pathway for Chemical Microstructuring of Macromolecules from Aqueous Solution Based on Wrinkling," *Langmuir,* vol. 24, pp. 12748-12753, 2008.

[108] X. Jiang, S. Takayama, X. Qian, E. Ostuni, H. Wu, N. Bowden, P. LeDuc, D. E. Ingber, and G. M. Whitesides, "Controlling Mammalian Cell Spreading and Cytoskeletal Arrangement with Conveniently Fabricated Continuous Wavy Features on Poly(dimethylsiloxane)," *Langmuir,* vol. 18, pp. 3273–3280, 2002.

[109] C. M. Stafford, C. Harrison, K. L. Beers, A. Karim, E. J. Amis, M. R. VanLandingham, H.-C. Kim, W. Volksen, R. D. Miller, and E. E. Simonyi, "A buckling-based metrology for measuring the elastic moduli of polymeric thin films," *Nat. Mater.,* vol. 3, pp. 545-550, 2004.

[110] Z. Y. Huang, W. Hong, and Z. Suo, "Nonlinear analyses of wrinkles in a film bonded to a compliant substrate," *J. Mech. Phys. Solids,* vol. 53, pp. 2101–2118, 2005.

[111] B. K. Sinha, E.Şimşek, and Q.-H. Liu, "Elastic-wave propagation in deviated wells in anisotropic formations," *GEOPHYSICS,* vol. 71, pp. D191-D202, 2006.

[112] J. D. Plummer, M. D. Deal, and P. B. Griffin, *Silicone VLSI Technology*. Upper Saddle River, NJ: Prentice Hall, 2000.
[113] M. Sitti, "High Aspect Ratio Polymer Micro/Nano-Structure Manufacturing using Nanoembossing, Nanomolding and Directed Self-Assembly," in *IEEE/ASME Advanced Mechatronics Conference* Kobe, Japan, 2003.
[114] A. Jo, W. Joo, W.-H. Jin, H. Nam, and J. K. Kim, "Ultrahigh-density phase-change data storage without the use of heating," *Nat. Nanotech.,* vol. 4, pp. 727-731, 2009.
[115] H. G. Shin, J. T. Kwon, Y. H. Seo, and B. H. Kim, "Development of 3d micro–nano hybrid patterns using anodized aluminum and micro-indentation," *Thin Solid Films,* vol. 516, pp. 6438–6443, 2008.
[116] V. Lien, Y. Wu, D. Zhang, Y. Berdichevsky, J. Choi, and Y.-H. Lo, "A Novel Technology for Fabricating Gratings of Any Chirp Characteristics by Design," *IEEE PHOTONICS TECHNOLOGY LETTERS,* vol. 15, pp. 712-714, 2003.
[117] R. Steingruber, M. Mohrle, A. Sigmund, and W. Furst, "Continuously chirped gratings for DFB-lasers fabricated by direct write electron-beam lithography," *Microelec. Eng.,* vol. 61-62, pp. 331–335, 2002.
[118] Y.-T. Yoon, H.-S. Lee, S.-S. Lee, S. H. Kim, J.-D. Park, and K.-D. Lee, "Color filter incorporating a subwavelength patterned grating in poly silicon," *OPTICS EXPRESS,* vol. 16, pp. 2374-2380, 2008.
[119] N. Liu, H. Guo, L. Fu, S. Kaiser, H. Schweizer, and H. Giessen, "Plasmon Hybridization in Stacked Cut-Wire Metamaterials," *Adv. Mater.,* vol. 19, pp. 3628–3632, 2007.
[120] P. Kallinteri, S. Higgins, G. A. Hutcheon, C. B. S. Pourcüain, and M. C. Garnett, "Novel Functionalized Biodegradable Polymers for Nanoparticle Drug Delivery Systems," *Biomacromolecules,* vol. 6, pp. 1885-1894, 2005.
[121] H. C. Ko, M. P. Stoykovich, J. Song, V. Malyarchuk, W. M. Choi, C.-J. Yu, J. B. G. III, J. Xiao, S. Wang, Y. Huang, and J. A. Rogers, "A hemispherical electronic eye camera based on compressible silicon optoelectronics," *Nature,* vol. 454, pp. 748-753, 2008.